Interrogating Light-Initiated Dynamics in Metal-Organic Frameworks with Time-Resolved Spectroscopy

Brian Pattengale, Sarah Ostresh, Charles A. Schmuttenmaer, Jens Neu*

Table of Content

Abstract

Time-resolved spectroscopy is an essential part of both fundamental and applied chemical research. Such techniques access light-initiated dynamics on timescale ranging from femtosecond to microsecond. Many techniques falling under this description have been applied to gain significant insight into metal-organic frameworks (MOFs), a diverse class of porous coordination polymers. MOFs are highly tunable, both compositionally and structurally, and unique challenges are encountered in applying time-resolved spectroscopy to interrogate their light-initiated properties. These properties involve various excited state mechanisms such as crystallographically-defined energy transfer, charge transfer and localization within the framework, photoconductivity, and structural dynamics. The field of time-resolved MOF spectroscopic studies is quite nascent - each original report cited in this review was published within the past decade. As such, this review is a timely and comprehensive summary of the most significant contributions in this emerging field, with focuses on the overarching spectroscopic concepts applied, and on identifying key challenges and future outlooks moving forward.

1. Introduction

Metal-organic frameworks (MOFs) entered the spotlight as an important class of functional materials in 1999 with the development of the first MOF structure capable of remaining stable without supporting guest molecules (such as solvent molecules) in their highly porous structure.[1] MOFs are generally constructed from an inorganic node and a multidentate organic linker capable of coordinating multiple inorganic nodes.[2,3] Depending on the connectivity of these two components, MOFs can have 2-dimensional structure as sheets, forming layered

structures relying upon van der Waals interactions, or 3-dimensional structure. The guiding principle behind their structural design is the concept of reticular chemistry, wherein the synthetic chemist has control (and even predictive capability) of the crystalline structure of the material by altering the structure of the secondary building units (SBUs) that are used to construct the material, i.e. the multidentate linker and the inorganic node.[4,5] As a result, there are profound efforts to construct diverse MOF structures and understand their properties, with an eye toward both fundamentals and functional applications.[6]

One of the main advantages of MOFs compared to more traditional heterogeneous materials, such as semiconductors, is their degree of structural tunability which, in turn, makes their properties highly tunable. Their tunable properties, including porosity, internal surface area, thermal/chemical stability, and light absorption, have led to numerous applications. These applications include gas separation and storage, sensing, electronics, optics, light absorption, and heterogeneous catalysis.[7-10] An important aspect of several of these applications is light-initiated dynamics, both fundamentally and as they relate to light harvesting and photocatalytic applications, among others.[11,12] As a result, a sizeable amount of research has emerged, largely within the past five years, applying time-resolved spectroscopic techniques to investigate photoinduced dynamics in MOFs.

This review will mainly focus on insight gained from the application of time-resolved techniques to MOFs in the femtosecond – microsecond time regime including femtosecond and nanosecond visible/NIR transient absorption, time-resolved photoluminescence, transient IR, X-ray transient absorption spectroscopy (XTA), time-resolved microwave conductivity (TRMC), and time-resolved terahertz (THz) spectroscopy (TRTS). In addition to highlighting the unique

capabilities and challenges surrounding the application of each technique to MOFs, there will also be a focus on examples that combine two or more of these techniques to gain deeper understanding than provided by each technique individually. Some examples in the literature utilizing these techniques, especially transient absorption (TA) and time-resolved photoluminescence (TR-PL), have investigated charge transfer or energy transfer between a MOF and another chromophore species. While these examples are important to the field, they will not be included in this review as such studies are often focused on the light-initiated dynamics of the chromophore, which dominates the signal due to its large extinction coefficient relative to the MOF. Rather, the focus herein will be placed on studies of light-initiated dynamics within the MOF or structural components thereof.

In the following, concepts relating to light absorption and electronic structure in MOFs will be introduced (Section 2), followed by an overview of the time-resolved techniques discussed highlighting the applicability and limitations of each technique to metal-organic frameworks (Section 3). The relevant primary research is then organized by the phenomena observed, namely exciton transport in the framework via energy transfer (Section 4), photoinduced dynamics, charge transfer, and localization (section 5), photoconductivity (Section 6), and structural dynamics (Section 8). We will also highlight combined studies exploring the interplay between carrier localization and delocalization (Section 7). As a whole, it is observed that the collective insights gained using time-resolved techniques to-date begs for further application of these techniques to this emerging class of materials to more fully understand their properties especially as they relate to functional applications.

2. Light Harvesting in Metal-Organic Frameworks

Metal-organic frameworks share light absorbing characteristics with both molecules and semiconductors, as they are composed of repeating units referred to herein as ligands and nodes. Excitations can, as a result, be ligand-centered, node-centered, or mixed. Therefore, care must be taken to fully understand the nature of UV-Visible transitions in MOFs by performing any necessary control measurements (such as measurement of isolated ligands, control clusters representing the inorganic node, or unmodified vs. modified MOF structures) and by bringing in theoretical chemistry, i.e. computational techniques such as density functional theory (DFT). Furthermore, time-resolved spectroscopy can investigate the photoinduced dynamics of the isolated units in order to provide additional insights on the interaction of the assembled node-ligand structure. In most cases, the UV-visible absorption of the assembled MOF is not equivalent to the sum of its individual components, and localized and/or band-like transitions can be identified in MOFs. Their energetic alignment to other excitations in the MOF is essential toward understanding the overall picture of light harvesting in a particular MOF structure. It is worth noting that authors sometimes favor terminology such as HOCO and LUCO (highest occupied and lowest unoccupied crystalline orbitals, respectively) over valence/conduction band terminology to confer that, due to the alternating polymeric structure of MOFs, such states may not be as continuous as those described in band theory.[11] Herein, we use these terms interchangeably, understanding that the level of continuity in a given band would be highly dependent on the electronic structure of the particular MOF. This point will be further raised in Section 6, which involves a subclass of MOFs having well-defined bands, i.e., conductive or photoconductive MOFs.

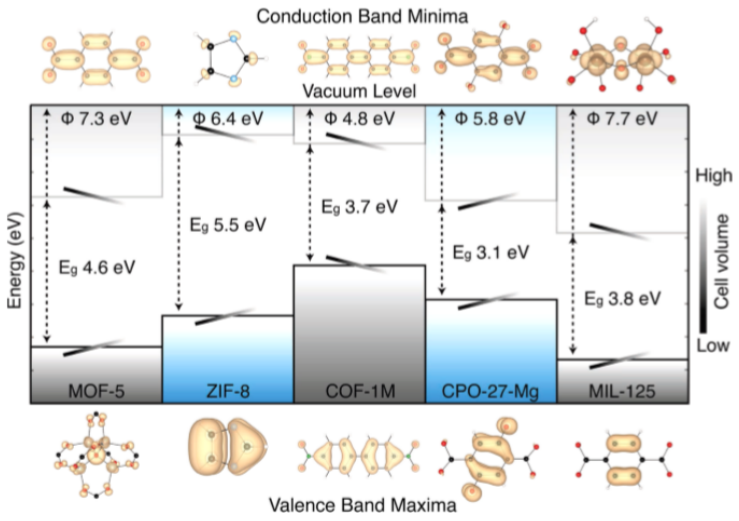

Figure 1. Calculated (DFT-HSE06) valence and conduction band energy levels of five representative MOFs. Inset in the band gap of each material are shaded lines indicating changes in the valence and conduction band positions as the volume (external pressure) is varied. Above and below each material is the electron density associated with the band edge wave functions; note that the density is associated with organic ligands, with the exception of MOF-5 (valence band, ZnO units) and MIL-125 (conduction band, TiO_2 units). Adapted from Butler et al.[13], Copyright 2014 ACS.

As mentioned, MOFs tend to feature UV or UV-Visible absorption unique from the absorption of the individual components that the MOF is constructed from. Several prototypical MOFs are discussed briefly herein, and further discussions at length are referenced in the appropriate sections of this review. A computational work by Butler et al. investigated the band structures of several prototypical MOFs (Figure 1).[13] Included in the study were MOF-5 (which is non-coincidentally the first air stable MOF ever reported by the Yaghi group in 1999),[1] ZIF-8 (where ZIF stands for Zeolitic Imidazolate Framework and shares structural homology to

traditional Zeolites),[14] and MIL-125 (MIL stands for Materials of Institut Lavoisier, as it is somewhat customary to designate a newly-discovered MOF by research institution).[15] These three MOF structures are initially discussed as representative examples followed by more applicable visible light harvesting MOFs.

MOF-5 is composed of Zn_4O tetrahedra capped with $-CO_2$ groups of the benzene dicarboxylate linkers in a cubic structure.[1] The calculated electron densities shown in Figure 1 indicate that the valence band is localized primarily on the Zn-containing nodes of the structure while the conduction band is localized primarily on the ligands, including the carboxylate moieties that form the node. Therefore, the excitation falls more under a mixed description. Further studies have investigated band gap engineering by modification of the metal nodes (i.e. replacement of Zn)[16] or even further modifications such as halogenation of the benzene dicarboxylate ligands.[17] Clearly, there is an importance of garnering understanding of the effect of such modifications on the band structure and light absorbing properties of the MOF.

ZIF-8 is based upon Zn^{2+} ions tetrahedrally coordinated to 2-methylimidazolate linkers to give a structure that is homologous to traditional zeolite materials. Uniquely, ZIFs do not contain carboxylate-anchored linkers that result in metal-oxygen clustered nodes and rather have a single N-coordinated metal ion, typically Zn^{2+} or Co^{2+}.[18] The result in Figure 1 demonstrates that the valence and conduction bands are both localized primarily on the 2-methylimidazolate linker rather than involving the node portion of the structure. This is in stark contrast to MOF-5, for instance. Band engineering has been proposed by mixing linkers in ZIFs and by substitution of the metal nodes.[19] By replacing Zn^{2+} with Co^{2+}, the bandgap of the resulting isostructural MOF, ZIF-67, becomes significantly smaller owing to a ligand-to-metal charge transfer (LMCT) state that

inherently does involve both the 2-methylimidazolate linker and Co^{2+} metal ion.[19-21] In addition to this LMCT transition in ZIF-67, there is a lower-energy transition fully-separated from the LMCT transition that is within the Co^{2+} d-manifold, i.e. a node-localized excitation that does not (formally) involve the linker; however this is a point of further discussion in Section 5.3.

MIL-125 is composed of Ti(IV) and benzenedicarboxylate in a quasi-cubic tetragonal structure.[15] The calculated valence and conduction bands in Figure 1 indicate that the valence band is localized on the linkers while the conduction band is localized on the titanium oxo nodes. Note that this is the opposite trend observed from MOF-5, even though the linker is identical. Experimentally, it was observed that while a stable Ti(III) species could not be generated with steady-state UV irradiation via ESR, a stable Ti(III) species could be observed in the presence of benzyl alcohol under UV irradiation.[15] Upon exposure to oxygen, the Ti(IV) species reformed. This experimental result suggests that added electron density localized on Ti, in agreement with the calculations by Butler et al. MIL-125 has been modified to impart visible light absorption with an amine functional group on the benzene of the linker[22] and further modifications have been investigated, experimentally and computationally.[23,24]

Further strategies have been utilized to alter the light absorption properties of metal-organic frameworks without modifying the structural units, including encapsulation of chromophores or nanoparticles[25,26] and anchoring chromophores to nodes or linkers.[27,28] However, one widely used strategy is the incorporation of a chromophore species *as a linker of the MOF*, thereby constructing the MOF using chromophores or a mixture of chromophore and non-chromophore linkers. One prime example is UIO-67 (referring to University of Oslo) doped with a $[Ru^{II}(bpy)_2(dcbpy)]Cl_2$ linker, where dcbpy is 2,2'-bipyridine (bpy) with *para*-carboxylate

groups to replace the *para*-biphenyldicarboxylate linkers of the parent structure.[29] As a result, chromophore moieties very similar to $[Ru(bpy)_3]Cl_2$ may be incorporated into the MOF structure. Further examples incorporating $Ru(bpy)_3$-based chromophores into MOFs will be discussed further in Sections 4 and 5. Another prime example is selected structures within the PCN series of MOFs (PCN stands for porous coordination network) which have porphyrin molecules as the linkers, such as PCN-222 and PCN-224.[30,31] These and other porphyrin-based MOFs will also be discussed further in Sections 4 and 5.

3. Overview of Time-resolved Techniques

Spectroscopic techniques ranging from those relying on low energy GHz waves to high energy hard X-Rays provide detailed insight into novel materials. However, to understand light-driven effects, a light-driven experiment is needed. These experiments commonly use a well-defined pump beam and a time delayed read-out. We will present several techniques spanning many orders of magnitude (fs - μs) that have been applied to understand light-driven processes in MOFs, and will point out the main technical considerations for each.

No spectroscopic technique will be able to explore all properties of a material simultaneously. Therefore, we will present the energy range exploited by a given technique and motivate what insight can be gained at these energies. While probe-energy is an important parameter, it is intuitively clear that for time-resolved techniques, the time resolution is a figure of merit. Furthermore, the excitation (pump) wavelength will define how the system is perturbed and what transitions are excited. We will first discuss the pump beam, then we will explain how

time resolved data is collected and what limitations apply, concluding this section with a comparison of probe energy regimes.

3.1 Pump Beam

Time resolved measurements utilize a pump pulse to promote the sample into an excited state. This, of course, implies that the pump beam is resonantly absorbed by the sample to some extent. Hence, every pump-probe measurement starts with a static measurement that identifies wavelengths that exhibit resonant transitions to be excited. The choice of exciting a specific transition is typically guided by some degree of understanding of the system that constitutes an experimental hypothesis to be investigated, rather than resorting to indiscriminately exciting the sample wherever it absorbs; although, the latter may be necessary in relatively unexplored MOFs in which case pump wavelength and power dependence are key parameters to obtain a baseline understanding for forming coherent hypotheses in further experiments. The experimental hypothesis can then be used to choose the proper excitation wavelength(s) to study light driven processes, thereby fostering fundamental understanding and benchmarking potential photo-performance.

After such a wavelength is identified the next challenge is to selectively excite these transitions. For this purpose, most pump-probe spectrometers use non-linear optics to transform the "monochromatic" fundamental laser output pulse into a selection of tunable pump wavelengths. The most common system in the UV-Visible-NIR range is based on optical parametric amplification (OPA),[32] either in collinear or non-collinear geometry. In an OPA system, the original laser input beam is used to generate a white light source in a supercontinuum. From

the short white-light pulse, a certain wavelength is selected which is then non-linearly mixed with the original input pulse. If performed correctly, this geometry transfers energy from the original wavelength to the generated wavelength, while preserving or even reducing the temporal envelope of the output pulse. This technique can be applied to ultrafast (subpicosecond) spectroscopy as well as nanosecond techniques.

3.2 Time Resolution

The aforementioned pump-pulse combination presents a lower limit for the time resolution achievable. However, the detection, also has a limiting effect on the time resolution. In simple terms, the time scales can be separated in direct electrical detection (“slow”) and laser-gated detection (ultrafast). The first approach is limited by the speed of electronics. The astonishing improvements in semiconductor techniques in the second half of the past century are approaching physical limitations and electronics with sub-nanosecond rise and fall times are extraordinarily challenging to fabricate. In these experiments, the probe pulse triggers the electronics and a well-defined and adjustable time delay gates the detector. The maximum time delay is basically unlimited, as the only limitation is the possible electrical delay and the repetition rate of the used pump-source. However, the shortest achievable time resolution is in the nanosecond range, making this technique unsuitable for studying ultrafast processes.

Femtosecond (fs) and sub-fs resolution is achieved by replacing the direct electrical detection by a laser-based measurement. For femtosecond resolution, the pump-pulse and the detection-pulse need to be on a femtosecond time scale, as the convolution of both defines the temporal resolution. Additionally, the interaction between the two pulses also results in a

temporal broadening of the measured value. As an example, detecting the sum frequency of a probe signal mixed with a read-out pulse will be limited by the size of the used non-linear crystal and the phase-mismatch between both pulses. While a larger crystal might yield a stronger signal, it will also reduce the temporal resolution. The temporal width of pump and probe pulse combined with the temporal broadening in the measurement and sample material will result in a temporally stretched signal. It is common to lump all these effects together into a so-called instrument response function (IRF). It is worth mentioning that the IRF will vary between different instruments, will depend on the detected wavelength, and will depend on the sample itself. It should also be noted that amplifiers used to generate high-flux femtosecond pulses are sensitive instruments, and the compression of the pulse used to generate both the pump and probe may change day-to-day; necessitating reevaluation of the IRF for studies that aim to understand processes near the IRF limit.

Direct time adjustments on a fs timescale are challenging. This issue however can easily be avoided by leveraging the correlation between travel length and the speed of light. Changing the timing between femtosecond laser pulses is typically achieved by adjusting the travel distance of one of the beams, while keeping the other path fixed. In other words, the issue of measuring fs times becomes the task of adjusting travel distance accurately and precisely on the micrometer scale, which can be achieved using commercial micro-positioning stages.

The superior time resolution achieved with mechanical delay lines comes with a limitation on the total time delay. Namely, the mechanical length of the delay line, which is typically a few hundred mm in length. With multi-passing beam guidance, the maximum delay is on the order of 10 ns. Some limited work overcoming this issue (for THz instrumentation) has been performed

by Neu et al., in which additionally to mechanical delay, electronical laser synchronization was used.[33] Similar techniques are used for TA instrumentation.[34] The electrical delay allowed for super-nanosecond time steps, while the mechanical delay maintained the desired fs-resolution.

3.3 Overview of Probed Energy Regimes

Similarly to choosing the proper pump wavelength, the probe technique and wavelength also need to be chosen careful to interrogate the effects of interest. Figure 2 presents a simplified overview depicting the different states and transitions that have been investigated in MOFs thus far.

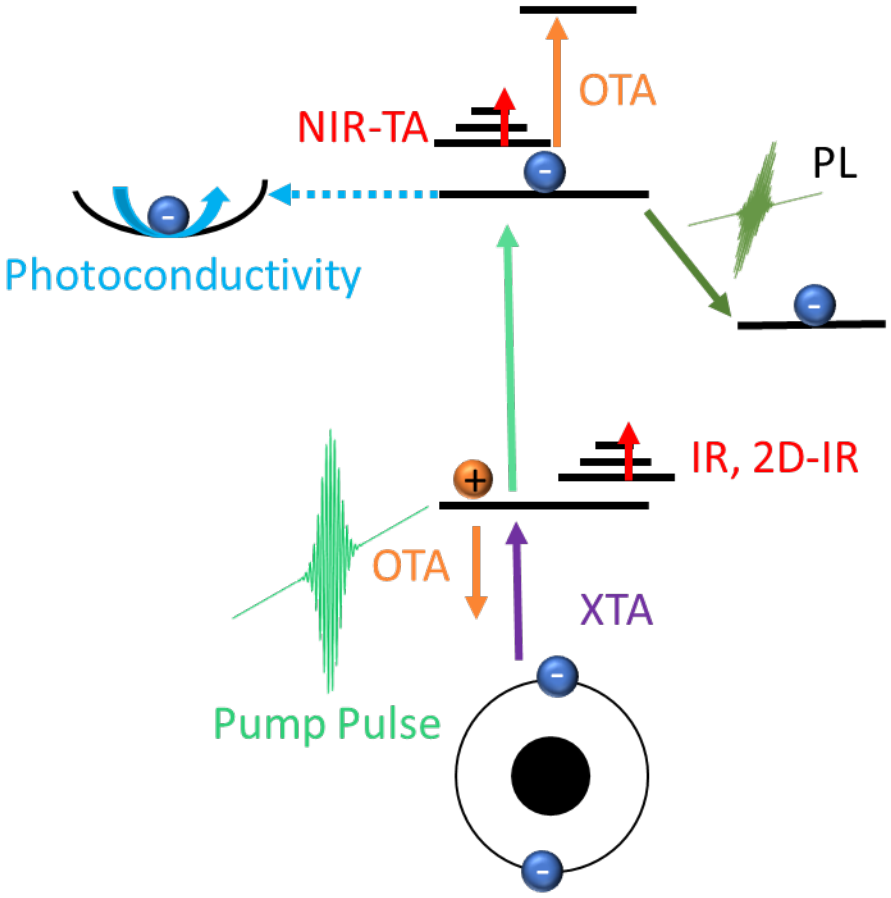

Figure 2. Simplified depiction of the energetic states in MOFs that have been probed with time-resolved techniques. OTA = Optical Transient Absorption, NIR-TA = Near-Infrared Transient Absorption, PL = Photoluminescence, IR = Time-resolved Infrared, XTA = X-ray Transient Absorption, 2D-IR = two-dimensional infrared spectroscopy.

The UV-Visible range of the spectrum is mainly dominated by dipole-excitations driving optical transitions between outer-shell electronic states. Therefore, these techniques are suited to follow an excited electron through different excited (bound) states. Hence optical transient techniques that probe localized electrons are excellently suited to understand lifetime and energetics of outer-shell electronic perturbations. Time-resolved fluorescence, or photoluminescence, is highly complementary to TA measurements. Instead of measuring occupied states, fluorescence directly detects the radiative decay of these states. It can therefore, in combination with TA, separate non-radiative and radiative decay.

The lower frequency range, namely IR, is sensitive to vibrational and rotational transitions. These modes can be used as a proxy to understand heat/energy transfer, and also to understand structural changes which strongly alter vibrational modes.

The microwave and terahertz range of the electromagnetic spectrum is too low in energy to drive electronic transitions and most vibrational modes. As a result, they tend to probe aggregate properties of the material such as the permittivity or dielectric constant, each of which are influenced by charge mobility/conductivity. Therefore, THz and microwave experiments are sensitive to mobile charges and the conductivity of them. This provides an excellent tool to understand whether an excitation created a bound state or if the charges are separated and contribute to conductivity.

Finally, the high energy range of the spectrum, namely X-Ray, is sensitive to transitions from core-shell electrons into LUCO and conduction/valence band states and continuum (ionized) states. The large energy of these transitions makes them rather robust and allows a clear element specificity. Minor changes in the transition energies can provide local electronic information for the probed atom. Fourier-transform methods can also be employed to obtain ground-state local structure information and changes in local structure due to photoexcitation. All previous techniques are focused on molecules or the crystal itself, in contrast X-Ray is atom-specific providing means to experimentally observe localization of the excitation.

3.4 Time-resolved Fluorescence spectroscopy

Fluorescence occurs due to an optical recombination of an excited state. The energy difference between the excited state and the ground state defines the available energy for an emitted photon. Fluorescence transitions are commonly competing with non-radiative transitions. For example, if an excited state electron is transferred from one location to another (donor-acceptor) this charge transfer process commonly does not involve fluorescence in the UV-Visible-NIR energy regime. However, the recombination of the charge-separated state can potentially be radiative and therefore detected. In general, the time-resolved fluorescence dynamics can provide information on excited state lifetime and can be performed in a full spectral mode using a CCD or equivalent detector to observe different emitting species that may be implicated in the excited state relaxation process.

Time resolution in time-resolved fluorescence measurements is either achieved via non-linear laser interaction or using fast electronics. In both cases, a short excitation of the system is

created using a well-defined laser pump pulse. Following this excitation, the detector is gated. For nanosecond and microsecond resolution, this gating can be performed electronically using a trigger synchronized to the pump beam. The detector collects the time resolved fluorescence, and the trigger assigns these datapoints to the measurement time axis.

Achieving fs resolutions typically utilizes a non-linear mixing of the probe beam and the fluorescence signal in a non-linear crystal.[35] The ultrashort probe pulse mixes with the signal only at the time frame in which both are present in the non-linear material. The simplest case would be a sum frequency generation between pump beam and fluorescence radiation. The big advantage is that the measured signal carries the femtosecond resolution of the pump beam, at a different wavelength. The detector itself only measures the time-integrated (slow) signal at the new wavelength which only carriers the information at a given pump-probe delay time. Changing the delay time between pump and gate pulse provides an ultrafast fluorescence trace (Figure 3).

3.5 Transient Absorption (TA) Spectroscopy

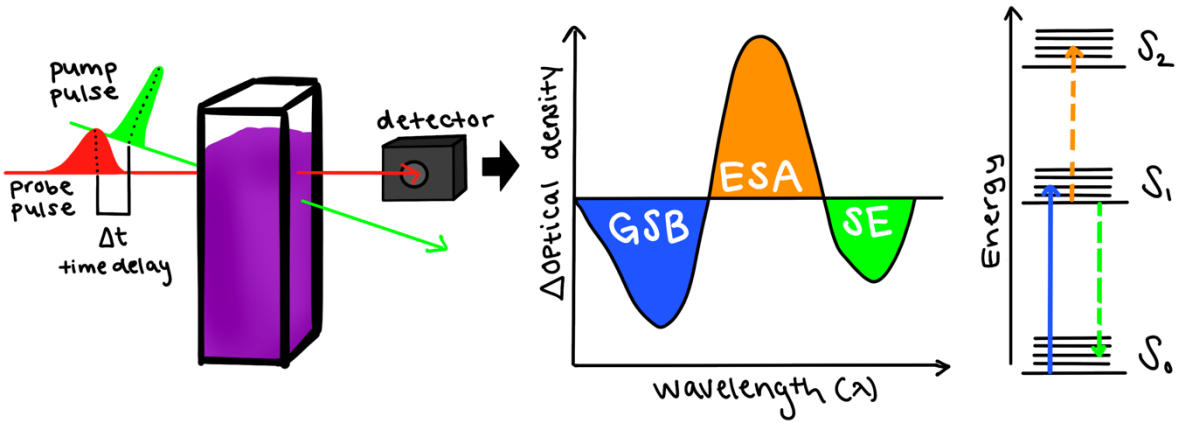

Figure 3. Example transient absorption measurement. The pump pulse and probe pulse are varied at different time delays (Δt) to capture changes in sample absorption milliseconds to

femtoseconds post-photoexcitation. A ground state bleach (GSB) can form as electrons are excited and depopulate the ground state. Excited state absorption (ESA) is due to transitions observable in the excited state electronic configuration. Changes in absorption due to stimulated emission (SE) where photon interaction causes the emission of a secondary photon in the excited state relaxing back to the ground state. Alternatively, this emission along with spontaneous emission is often explored in fluorescence experiments.

Transient absorption (TA) is complementary to fluorescence spectroscopy, but often provides more detailed and comprehensive information.[36] Fluorescence is sensitive to specific radiative transitions between states, while TA provides information of the excited state occupations directly. TA therefore provides a way to track an excitation evolving through optically excitable states, while fluorescence can monitor the decay of certain states. In the explanation of TA we will first focus on optical (UV-Vis-NIR) techniques and then present X-Ray techniques.

3.5.1 UV-Vis-NIR TA

The core concept of TA is to measure a difference spectrum between the ground state (non-excited) system and the time resolved transient spectrum at each pump-probe delay. The plural term “spectra” is used hereafter in view of a typical experiment providing a TA spectrum at each pump-probe delay time. More specifically, many experiments generate a 3-dimensional contour plot with pump-probe delay time, wavelength, and ΔA as the dimensions. An example of a TA spectrum at a single pump-probe delay time is illustrated in Figure 3. The most prominent feature

in TA spectra is, in many but not all cases, the ground state bleach (GSB) which monitors, in the simplest sense the time scale in which the system returns to the ground state. When charge transfer is involved, the interpretation of the GSB becomes more nuanced because the system (or in most measurements, only a portion of the system, because charge transfer efficiency is rarely unity) returns to a ground state with a different oxidation state with, potentially, intervening intermediate processes that may deplete or alter the feature. Thus, the experimenter must not jump to conclusions based upon a single feature unless the system is well understood. Further information can typically be gained by monitoring the occurrence of other transient features, provided that their extinction coefficient is suitable for measurement (typically > 1 mO.D. for practical purposes). This information then provides insight into the characteristics and lifetime of the excited state. Combined with other techniques, the identities of intermediate states can often be deduced, and their formation/decay lifetimes can be determined if they fall within the experimental time window.

Depending on the desired probe wavelength, different nonlinear techniques can be chosen to generate the probe. For the visible range, white light sources are used, as described below. For the NIR and IR range, OPA is commonly used to create an idler and signal pulse, longer in wavelength than the original fundamental pulse. These signals can either be used directly as NIR probe, or the difference frequency of both is generated (for example in $AgGaS_2$). This technique provides a large range of tunability at the cost of bandwidth which, in turn, forces the experimentalist to consider carefully what wavelength to probe, or to commit a significant amount of time to measure the full spectral range.

For ultrafast and ns-TA the pump beam is supplied by a laser pulse, which commonly undergoes OPA to tune the pump-wavelength. The probe could be purely electrical but commonly uses a synchronized broad band optical pulse. The detector, typically a CCD or CMOS capable of measuring the broadband probe, itself does not need to be ultrafast. The time resolution (IRF) is achieved via the time length of the pump/probe and the signal is integrated over a defined number of repetitions to build the spectral data.

For ns resolution, pulsed white light is generated in a flash discharge lamp, for example a Xenon lamp. For fs resolution, white light is typically generated from an ultrafast fundamental pulse in a supercontinuum.[37,38] While the exact mechanism is still under investigation, in practice the output of the amplifier (typically ca. 800 nm from a Ti:Sapphire amplifier, 100 fs FWHM) is focused onto a non-linear crystal (such as sapphire or CaF_2). The focal point and incident power can be adjusted to generate a stable white-light continuum to use as the probe beam. It should be noted that this process leads to dispersion that ultimately determines the IRF in most cases. Shorter incident pulses can be used at the expense of supercontinuum stability.

3.5.2 X-ray Transient Absorption (XTA)

The previous TA techniques are all table-top experiments, using lasers and laser amplifiers. These beam sources can be transformed into X-ray radiation using higher harmonic generation;[39] however, this technique is challenging and has not yet been applied to MOFs to the best of our knowledge. Bright X-Ray beams are typically generated using large facilities: free electron lasers (FEL)[40,41] or synchrotron beams.[42] While FEL can provide sub-100 fs time

resolution, no MOF system has been measured yet in this time resolution via XTA. Several MOFs have been measured using synchrotron beams (approximately 100 ps resolution).

For time resolved X-Ray spectroscopy an electron bunch in a synchrotron is synchronized with an additional optical laser pulse. This laser pulse provides the pump for the TA experiment, while the X-Ray provides a probe sensitive to inner shell electrons. X-ray absorption spectroscopy (in both steady-state and time-resolved experiments) is element-specific and is sensitive to both electronics and structure of the sample.[43] The electronic aspects can be interpreted based upon the transitions observed near the absorption edge (for instance, the K edge corresponding to a transition from a 1S core state); however the interpretation is not always straightforward because the transition has partial continuum characteristics due to ionization. Despite this, one clear signature that can be relied upon is an edge shift corresponding to a change in binding energy or oxidation state of the probed atom. Further information can be gathered above the transition edge where interference patterns between the probed atom and its neighbors can be analyzed using Fourier-transform techniques to provide excited state local structure information.[44] In practice, the X-ray absorption spectrum is collected at discrete energies with and without laser excitation, and a difference spectrum is generated by subtracting laser on – laser off spectra.[45]

3.5.3 IR TA

Infrared TA utilizes a narrowband tunable probe beam in the infrared range. This beam is generated by nonlinear mixing processes in an OPA. In contrast to visible OPA, $AgGaS_2$ is used to down convert near-IR radiation. This technique provides a large tuning range, at the cost of

bandwidth. Hence in contrast to the previous techniques the experimentalist needs to have a better understanding of the probed mechanism or invest a significant amount of time to scan the full spectral range.

IR radiation is sensitive to vibrational (and rotational) transitions. These transitions are defined by the structure and binding energies of the organic components of the MOF. If the optical excitation alters these modes, the change reveals itself in IR TA. As such, IR TA is therefore sensitive to laser driven perturbations of the structure, similar to the aforementioned X-ray techniques. The core difference is that the IR signal is not associated with an atom but sensitive to the crystal in general, probing either phonon modes or vibrational modes of the organic linkers or inorganic nodes.

3.5.4 2D IR Spectroscopy

2D infrared spectra are commonly collected using either double resonance or photon echo techniques, the former of which is highly similar to previously discussed TA techniques.[46] Double resonance 2D IR uses a spectrally narrow IR pump pulse and a broad band ultrafast IR probe pulse. The pump pulse excites vibrational modes while the probe pulse detects the difference spectrum. Analogously to TA, ground state bleaches are observed, together with coupled vibrational modes. For example, if the same ground state is involved in two transitions, linear FTIR would only provide the spectrum of these transitions, while 2D-IR also provides insight into the coupling between the states involved in this transition. Furthermore, the known pump and probe polarization provides insight into anisotropy of IR modes. The big disadvantage of this technique is the limited frequency/time resolution. Intrinsically, the pump pulse should be as spectrally narrow as possible to provide a clean excitation of the system. At the same time,

spectrally narrow IR-pulses are broad in time due to Heisenberg's uncertainty principle. As such, this technique comes with a trade-off between temporal and spectral resolution. This technique was not applied to the here reviewed MOF-work, however it is of potential interest for MOF research.

The aforementioned trade-off can be overcome using the more sophisticated photon echo technique.[47] Instead of the previously presented two beam scheme, three excitation beams and potentially a fourth read-out gate are used. All pulses are broad band and the spectral information is achieved leveraging the Fourier correlation between time and frequency information, similar to time-domain terahertz spectroscopy, which is described in the following section. As the timing between the pulses is scanned, the signal is detected heterodyne, and the time signals are then transformed into frequency space via Fourier transformation. Both 2D-IR techniques are probing an originally unperturbed system. The techniques can however be combined with an additional excitation pulse, in particular an IR pump. This additional pump pulse drives the system into a well-defined excited state, in which the 2D-IR spectra of the excited system are collected. The waiting times between the different beams can be adjusted to determine coherence and lifetimes of the prepared states, shedding light on coupling mechanisms.

3.6 Time-Resolved THz Spectroscopy (TRTS)

All previous examples of TA used well-known optical techniques in the X-ray to IR range. In this subsection we will take a brief look at the low energy terahertz (THz) spectral range, 10-300 cm^{-1}. At this energy range non-conductive solids are rather transparent. However, some

materials, including MOFs, have resonant transitions due to collective motions of many atoms in this energy range.[48] THz waves are also sensitive to mobile carriers, such as those implicated in electrical conductivity. The electrical field at THz frequencies alternates significantly slower than in the visible range, hence mobile charges can more easily respond to this alternating field. As a result, electromagnetic energy is transferred to mobile carriers, resulting in a broadband attenuation of the THz field propagating through the sample.

Terahertz spectroscopy is unique from the previous techniques because it is a purely time-domain technique. THz time-domain spectroscopy (THz-TDS) is a spectroscopic technique in which short THz pulses are generated and detected in the time domain.[49] In a typical experiment, an ultrafast pulse is split into a THz generation pulse with fixed path length and an delayed optical detection pulse that gates a detector. The collected signal is detected time and sign resolved, providing the full spectral information of the electro-magnetic wave, including spectral amplitude and phase.

Time resolved THz spectroscopy (TRTS) combines the THz spectral amplitude and phase information with an optical excitation pulse. [50] The timing between the THz probe pulse and the optical pump pulse is adjusted with fs resolution, thereby providing an outstanding view on mobile carriers upon excitation. The time resolution is mainly limited by the temporal length of the THz pulse which is usually on the 100 fs order. The maximum delay is limited by the mechanical delay line to approximately 10-20 ns. The measured TRTS time-traces are proportional to the mobile carrier density. The onset of the TRTS signal provides information on injection dynamics and efficiency. The term “injection” is colloquially used to describe a mechanism by which a conductive state is populated, whether it be from a bandgap transition or

from another mechanism such as charge transfer from a separate light-activated material. These two mechanisms can be distinguished by their injection dynamics, in which charge transfer events exhibit a finite time constant delaying the onset of conductivity, observable if shorter than the IRF. The decay of photoconductivity, on the other hand, sheds light on the recombination of the electron-hole pair and/or the trapping of mobile charges. Both effects are crucial for light driven electrochemical and photovoltaic applications. Furthermore, due to the short THz pulse traces, this technique is very sensitive to intra-grain mobility in contrast to the latter discussed TRMC which is more sensitive to inter-grain mobility. Separating these effects paves the way towards a more conclusive understanding of the physical origin of effects limiting the conductivity and provides an angle to enhance device performance. While the area is relatively new, there are a few examples of using TRTS to investigate MOF photoconductivity, presented in section 6.3.

3.7 Time-resolved Microwave Conductivity (TRMC)

Microwave conductivity measurements utilize fast electronics and resonant cavities. The sample material is mounted in the cavity, and a fixed but tunable microwave interacts with the material. This measurement can provide the static complex permittivity of the sample material, which carriers information on the intrinsic conductance of the sample. The technique can be combined with an optical pump pulse, providing time resolved microwave conductivity (TRMC).[51] Similar to ns-fluorescence techniques, the pump pulse creates a synchronized trigger which is collected in combination with the microwave transmission through the sample. The data collection is limited by the speed of the used electronics, usually in the µs range. Microwave

experiments have the intrinsic advantage that they measure low frequency photo-conductance providing an excellent proxy for DC-conductivity which is a figure of merit for many photo-electrical applications. Compared to THz photoconductivity, microwave measurements present several shortcomings. The temporal resolution is limited by the electronics, as well as fundamentally by the probe wavelength. Therefore, sub-ns information cannot be achieved, and most TRMC systems have a temporal resolution in the 100 ns range. Also, the spectrally accessible range is limited by the used electronics and cavity, commonly restrained to a couple of GHz, while THz measurements span thousands of GHz range. THz systems therefore combine larger bandwidth and better time resolution, however often demand more sophisticated, sensitive, and expensive equipment, and are further less comparable to DC measurements. In general, both experiments could be applied to a given material to give a thorough characterization of the conductivity, in particular to separate grain boundary effects and intra grain defects.

3.8. Sample Preparation Considerations

The best sample for any spectroscopical investigation is a pure, defect free single crystal. This is, of course, a grave challenge for most emerging materials and, in particular, for MOFs. Many, but not all, MOFs are air stable or stable without a solvent, and only a very small subsection can be grown into single crystals having a size comparable to or larger than the beam spot size. Furthermore, MOFs typically have defects or, at the very least, non-negligible surface states due to the termination of the crystal lattice. As-prepared, MOFs typically comprise guest molecules, often a coordinating solvent such as DMF or another used during the synthesis or preparation of the MOF. This adds a significant layer of complexity, but also intrigue, because MOFs may be

investigated in an as-prepared state, exchanged with different solvents or guest molecules, or in an “activated” state where solvent/guest molecules are removed.

Most MOF syntheses provide a bulk powder having nano- to micrometer sized crystallites. Some time-resolved experimental techniques are capable of measuring a bulk powder, including, at the lower energy range of the spectrum, TRMC, THz, and potentially IR. As the frequency increases, resonant features tend to dominate the interaction of light with matter and, as a result, their bulk properties in the NIR, visible, and UV ranges typically differ from air or solvent surrounding the MOF to an extend that radiation cannot transmit through the sample for the purposes of spectroscopic measurement. Limited experiments, as further described in Section 5, have been performed using diffuse reflectance to overcome this transmission limitation. As implied in the previous sentence, dispersion of the MOF in solvent may provide better refractive index matching for transmission mode measurement, however solvent effects need to be accounted for. At the high energy end of the spectrum, X-ray measurements can be reliably performed using an X-ray fluorescence detection scheme, overcoming the need for transmission. However, MOFs are typically dispersed in a solvent for these measurements for the purpose of quasi-homogeneity, heat dissipation, and limitation of sample degradation by using a sizable sample reservoir.

Bulk powders and suspensions are not the only potential sample types for measuring MOFs. In certain scenarios, a bulk powder may be mixed with a dispersing medium to produce a homogeneous pressed pellet, for instance in THz measurements. For time-resolved measurements involving a pump pulse that must homogeneously excite the sample, such a geometry is not typically preferable due to reflection losses and low excitation efficiency. More

typically, a thin film sample may be used as a relatively homogeneous, supported sample form. Some MOFs may be grown directly onto a transparent substrate, such as glass or quartz in the visible range, or other suitable substrates depending upon the experiment. If homogeneous films can be prepared, this is often the optimum sample type because it can be measured in air or a chosen gas environment, in solvents, or even under potentiostatic control if deposited on a conductive substrate. Often, homogeneous films are unattainable, and researchers must explore alternative measures. Polymeric dispersions have been used to prepare homogenous films by dispersing the particulate MOF in a Nafion or polystyrene solution, depositing the dispersion, and allowing a film to dry. As with various solvents and/or guest molecules, matrix effects must be considered.

Spectroscopy is, of course, possible and common with non-ideal samples, but the reader is encouraged to remember that values reported from such experiments are sample parameters and not material parameters. Once a wealth of knowledge is obtained on the "sample parameters", the material parameters may be approximated or at least understood under various conditions. The influence of guest molecules, and in particular solvent molecules, on the light-initiated dynamics of MOFs need to be considered when MOFs are measured as-prepared or in specific solvents. Furthermore, because MOFs are particulate and do not homogenously dissolve in solutions, great care needs to be taken to achieve a pseudo-homogenous dispersion during the measurement. Similar challenges are present when powder samples are used for experiments that can measure a bulk powder. These samples constitute a mixture of air and material and absolute numbers on injection yield or material conductivity are challenging to determine from such samples. We encourage experimentalist to reproduce any results

rigorously, measuring on different locations of a solid or film sample (preferably continuously translated if homogeneous), or multiple solutions of a solvent sample. Controlled variations of the sample preparation conditions can then be used to separate solvent and MOF effects properly and present the most reliable data.

Finally, as described in more detail above, experimental considerations also command the sample preparation. The core question is whether the sample will be measured in transmission or reflection, as this defined the needed/prohibited thickness of the sample. Similarly, great care needs to be applied to ensure that solvents used in the experiment do not contribute to the measured signals, or that their effects can be understood or separated.

In the following examples we highlight the sample preparations used by the cited authors and emphasize what influence this has on the presented result. This is in particular crucial when quenching molecules or intentional guest molecules are used which alter the measured dynamics. For many MOFs in this nascent field, only limited sample preparations have been measured, and there is therefore opportunity for rigorous studies to gain critical knowledge.

4. Exciton Transport via Energy Transfer

Excitonic energy transfer is at the core of several photo-driven catalytic systems, such as natural photosynthesis. An effective transfer of excitation energy to the catalytic center at which this energy is transformed into useful processes, such as a redox reaction, is crucial for high product yields. In synthetic systems, an understanding of these mechanisms on the ultrafast and nanoscopic scale is needed to optimize and effectively utilize them for functional applications. For instance, the optimization of such energy transfer processes can be leveraged to improve the

performance of photocatalysis. Metal-organic frameworks (MOFs) provide a unique opportunity to optimize energy transfer processes due to their inherent nature of crystallographically-orienting chromophores in a fixed and tunable position. Based on this characteristic, many efforts have been made to design and understand MOFs having such excitonic energy transfer. In particular, ultrafast techniques have been applied to shed light on photocatalytically relevant MOFs. Apart from this practical goal, understanding the underlying physics of these mechanism provides insight into new phenomena and can guide the field towards novel and even better materials.

4.1 Overview and Time-Resolved Techniques Applied

Energy transfer between the building units of MOFs has been observed in both the weakly-coupled Förster resonance energy transfer (FRET) regime and the strongly-coupled Dexter regime. Dexter electron exchange mechanisms rely on wavefunction overlap between the donor and acceptor and, therefore, occur at distances of less than 10 Å.[52] FRET is a dipole-mediated energy transfer mechanism not relying on wavefunction overlap and can occur at distances greater than 10Å, so long as the dipole-dipole orientation is correct between the donor and acceptor species.[53] MOFs can serve to crystallographically orient chromophores at appropriate separation distances and orientations to yield such energy transfer events. As a result, the exciton is able to migrate between linker sites thereby leading to a “mobile” exciton in the structure. Such a mechanism is similar to antennae complexes in photosynthetic chromophores that transfer energy over long distances to reach reaction centers in Photosystem (PS) II.[54]

The main technique that has been used is time-resolved photoluminescence spectroscopy, which probes the radiative decay of light emitting species. Two main chemical design strategies have been utilized in MOFs to reveal time-resolved information supporting the conclusions of energy transfer via exciton migration: variation of the concentration of chromophores in the host framework and use of quenchers that reveal, through their concentration dependence, mechanistic information related to energy transfer in the framework with fixed chromophore concentration. Two exemplary types of systems, namely ruthenium dye-based systems studied by the Morris and Lin groups and porphyrin-based systems studied by the Hupp group, are highlighted below that rely on these design strategies, respectively. The examples herein are representative of the field as it relates to the application of time-resolved techniques and do not aim to fully review the field of energy transfer processes in MOFs, which has been covered in a recent review.[53] For example, even though excellent examples exist for lanthanide-based MOFs having f-manifold energy transfer mechanisms and structures comprising organic chromophores, they will not be discussed in detail here.[55]

4.2 Energy transfer in $Ru(bpy)_3$ based UIO-67 MOFs

The Morris and Lin groups have extensively studied energy transfer in Ru-chromophore doped zirconium(IV)-based metal–organic framework (Zr-MOF), UIO-67.[53,54,56] Zr-MOFs are recognized for their exceptional chemical and thermal stability compared to other MOFs. UIO-67 is composed of Zr_6O_8 clusters, and 12 points of connection bind the Zr and the linkers to form the framework. UIO-67 has additional benefits including large pore size and surface area, and can be functionalized by replacement of biphenyl ligands with bypiridine dicarboxylate (dcbpy) ligands.[57] This modification allows the incorporation of diverse libraries of bipyridine (bpy) based

photosensitizers and catalysts, such as $[Ru(dcbpy)(bpy)_2]^{2+}$ (Ru-dcbpy), an analogue of $Ru(bpy)_3^{2+}$.[54] $Ru(bpy)_3^{2+}$ based dyes are commonly used as photosensitizers due to their rather long-lived excited states and redox activity due to the excited state being simultaneously more reducing and more oxidizing than the ground state.[53,58] They are also stable and have well-understood photophysical phenomena. Therefore, the dcbpy-modified analogues are an excellent choice for substituting diphenyl or bipyridyl building units of MOFs to incorporate a photo-active redox center. These incorporated species form a structural component of the framework, interconnecting the Z_6O_8 nodes. To this end, there is great importance in understanding the manner in which the incorporated chromophores interact with the host framework and with one another.

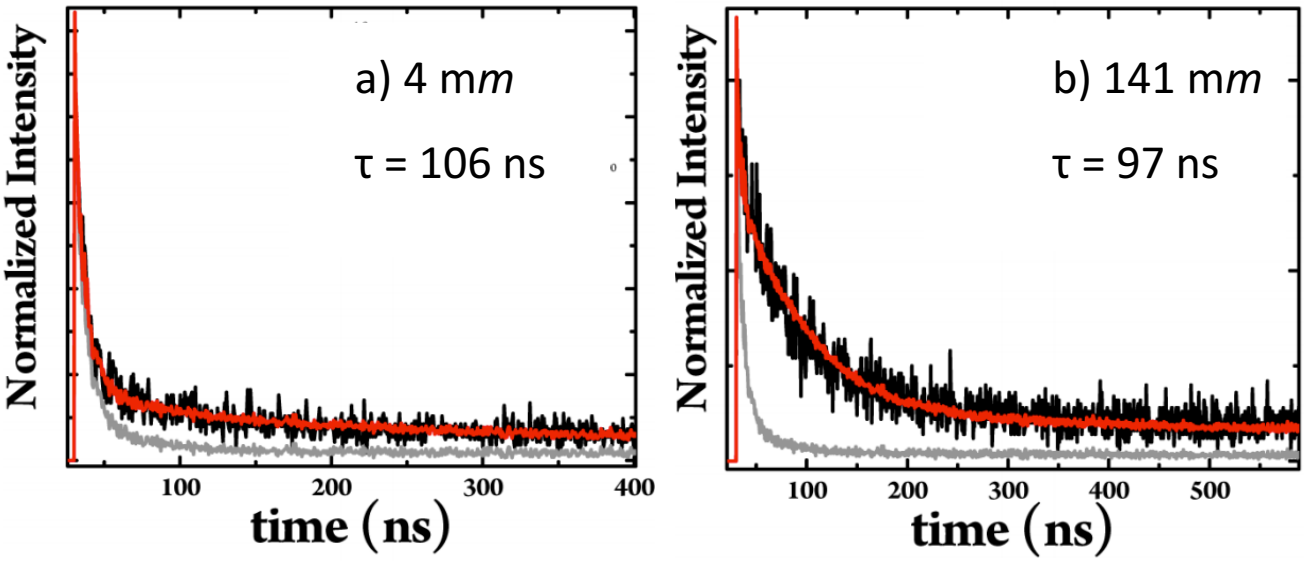

Figure 4. Emission lifetime decays (black) of Ru-dcbpy-UIO-67 samples at (a) 4 m*m* (millimole of Ru-dcbpy per kilogram of MOF) and (b) 141 m*m* and photoexcited with a pulsed LED at 510 nm and measured by time correlated single photon counting. Corresponding exponential

fits (red) done by a deconvolution/convolution of the instrument response function (gray). The deviation from monoexponential at higher Ru-dcbpy concentration is indicative of two populations of Ru-dcbpy forming. The long-lifetime component of Ru-dcbpy-UIO-67 at both chromophore loadings above was attributed to the Ru-dcbpy incorporated into the backbone of the material, while the short-lifetime component at high loading was attributed to encapsulated Ru-dcbpychromophores. Adapted from Maza et al.[59], Copyright 2015 ACS.

The incorporation of Ru-dcbpy as a linker in UIO-67 results in an energy transfer pathway that dominates over charge transfer.[59] More specifically, the Morris group found that upon photoexcitation, the Ru-dcbpy structural units of UIO-67 interact with one another and undergo self-quenching via a resonance energy transfer mechanism.[59] The MOFs were solvothermally synthesized and doped post-synthesis in a Ru-dcbpy-containing ethanol solution. Fluorescence quenching was measured using a time correlated single photon counting technique wherein Ru-dcbpy doped UIO-67 was suspended and stirred in DMF and selectively excited with 510 nm. As the chromophore dopant concentration increased, a deviation from monoexponential behavior was observed. The authors proposed a model in which at least two populations of Ru-dcbpy could be found within UIO-67 at higher doping concentrations: one in which Ru-dcbpy incorporates into the backbone of the larger octahedral cavity, dominant for low doping concentrations, and a second population involving encapsulation of Ru-dcbpy within the octahedral cavity (i.e. non-structural Ru-dcbpy units were incorporated), which was observed for higher concentrations. Using this strategy, it was possible to better understand the photophysics of the chromophores in the MOF structure.

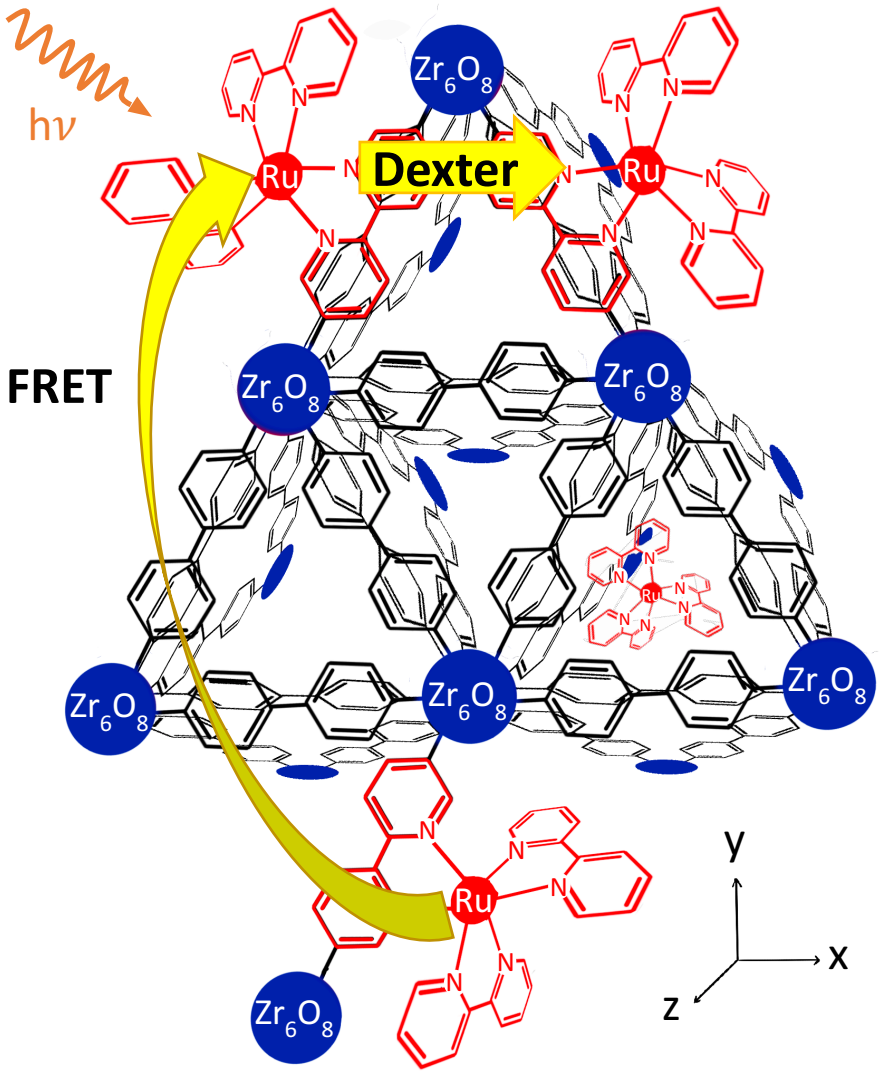

Figure 5. Tris(bipyridine)ruthenium(II) ($Ru(bpy)_3$) incorporated into 3D MOF, UIO-67. Energy transfer upon photoexcitation is illustrated between $Ru(bpy)_3$ chromophores at short ranges (Dexter exchange mechanism) relying on wavefunction overlap and long ranges >10 Å (Förster resonance energy transfer (FRET) mechanism) utilizing weak dipole coupling.

The placement of chromophores within the MOF will affect energy transfer. The Morris group further observed the rate of energy transfer between Ru-dcbpy centers of Ru-dcbpy-UiO-67 and found an $1/R^6$ separation distance dependence; characteristic of FRET.[59,60] The emission lifetime and emission maxima magnitude decrease with increasing chromophore dopant concentration. Additionally, exciton mobility depends on the chromophore concentration. Different populations of chromophore develop with increasing dopant concentration, with the Ru-dcbpy primarily acting as a linker in the framework of the UIO-67 structure. Increased concentrations lead to encapsulation of the Ru-dcbpy within the pores of the MOF. Laser photolysis data was measured for Ru-dcbpy-UIO-67 MOF in DMF photoexcited at 355 nm. At low loadings, the data was fit to a single exponential, while higher loading were fit to either biexponential or stretched exponentials. The emission lifetime data was found to differ between low loading (20-30 μs) and high loading (100 μs) due to energy transfer between the neighboring Ru-dcbpy chromophores in the octahedral cavity of the MOF. Figure 5 shows Ru-dcbpy incorporated into the backbone of UIO-67 and different energy transfer pathways.

Energy transfer has also been observed in another class of non-porous 3D microcrystalline MOFs with caged $Ru(bpy)_3^{2+}$ chromophores.[56] Zn-oxalate and Na/Al-oxalate MOFs were synthesized to entrap $Ru(bpy)_3^{2+}$ as chromophores and $Os(bpy)_3^{2+}$ as energy transfer traps. This is possible because the emission of $Ru(bpy)_3^{2+}$ overlaps with the absorption of $Os(bpy)_3^{2+}$ while the emission of $Os(bpy)_3^{2+}$ is too low in energy for overlap with the absorption of $Ru(bpy)_3^{2+}$. While FRET does not involve emission and concurrent absorption, the energy conservation can be understood by these criteria. The MOFs were suspended in ethanol and stirred for the measurements. Emission lifetimes are sensitive to triplet-triplet annihilation with oxygen,

especially for these heavy-metal containing chromophores that exhibit fast and efficient intersystem crossing, so all experiments were carried out on samples prepared in an oxygen-free environment. The rigid framework led to high emission yield from Ru-centers and chromophores that were shielded from the solvent. Excited state lifetimes in these samples were found to be on the order of 1300 ns when photoexcited at 580 and 680 nm using time resolved emission spectroscopy. These measurements were found to be indicative of intra-MOF energy transfer, benefitting from both the longer range Förster $1/R^6$ energy transfer and the exponential Dexter mechanism. At high Ru loadings, the Dexter mechanism dominated given the short-range between donor and acceptor chromophores. Additionally, a time-dependent growth in the Os emission transient of the Os-doped sample was consistent with Ru(II)* to Os(II) energy transfer after selective excitation of $Ru(bpy)_3^{2+}$. Os-doped samples therefore led to efficient energy transfer quenching.

A theoretical work investigated two Zn-MOF systems with incorporated Ru-based chromophores using ab initio electronic structure theory with kinetic network analysis.[61] The first MOF embeds Ru and Os-trisbipyridal chromophores in a network formed by Zn-oxalate bonds and the second links Ru and Os-trisbipyridal chromophores to Zn-carboxylates. The energy transfer between donor and acceptor chromophores is understood by two-electron Coulomb interactions. Ab initio computations determined the lowest energy metal to ligand charge transfer (MLCT) excited triplet and singlet electronic states and were used to estimate the magnitudes of the Dexter and Förster couplings. Following the initial excitation of the Ru chromophore at 850 nm, the Ru* lifetime decreased in both structures with increasing Os concentration, consistent with energy transfer from Ru* to Os. A Dexter mechanism dominated

the energy transfer dynamics, leading to a strong dependence of energy transfer to metal-metal distance in the MOF and localized electrons. Utilizing the Dexter mechanism could potentially direct energy transfer in specific directions toward a more efficient photocatalyst for solar materials.

Crystal size plays an important role in light harvesting efficiency in photocatalytic systems. To enable catalytic reactions on the surface for functional applications, the MOF crystal composing a polycrystalline film must be able to absorb a high fraction of the incident light but be small enough so that the majority of excited states reach the surface before excited state decay. Microscale Zn MOFs were synthesized from photoactive Ru(II)-bpy building blocks for strong visible light absorption and long-lived triplet metal-to-ligand charge transfer (^{3}MLCT) excited states.[54] 2D MOF crystals were grown using a solvothermal method.[62] Interfacial electron transfer quenching experiments were conducted by both nanosecond emission intensity and lifetime measurements on stirred suspensions of the MOFs in degassed acetonitrile around room temperature with added benzoquinone oxidative quencher. The chromophore in this MOF exhibited behavior similar to an “antenna”, acting as a light-harvesting system by combining intraframework energy migration and interfacial electron transfer quenching. Electron transfer quenching took place at the MOF-solution interface following rapid energy migration by ^{3}MLCT excited states. Electron transfer efficiencies were high (>98%) toward both oxidative and reductive quenching. These energy transfer phenomena can be further utilized in the design of MOFs, such as shortening metal-metal distances to improve energy transfer for efficient photocatalytic applications.

4.3 Energy Transfer in Porphyrin-containing MOFs

Porphyrins are a class of well-studied dyes for light harvesting applications. The favorable excited state energy with respect to the conduction band of several semiconductors (like TiO_2) and the large extinction coefficient (≈ 100,000 $M^{-1}cm^{-1}$) make porphyrins an excellent material for photo-driven processes. Likewise, porphyrin-based MOFs are highly absorbing and have great potential for use in light harvesting and photocatalysis.

The Hupp group found that efficient energy transfer occurs in boron dipyrro-methene (bodipy) and porphyrin-based Zn MOFs.[63] While this study relied only upon steady-state spectroscopic techniques, it provided strong evidence for energy transfer in porphyrin-based MOFs. A porphyrin was chosen as the primary chromophore because it has structural and chromophoric similarities to various chlorophylls, mimicking natural PSI and PSII. These complexes were designed to have a well-organized donor-acceptor assembly from the porphyrin linker to the metal oxide polyhedral node within the MOF. The bodipy serves as "antenna" chromophores for the excitation of porphyrin linkers, absorbing more of the visible spectrum than the porphyrin alone. Energy transfer within the framework was evidenced by measuring the solid-state fluorescence spectra of the two MOFs and fluorescence excitation spectrum of the bodipy-por MOF. Excitation of the bodipy MOF at 520 nm resulted in a typical bodipy emission maximum at 596 nm. Excitation of the bodipy-por MOF results in no emission at 596 nm, and instead has a maximum absorption typical of the Zn node and features attributable to both chromophores in the MOF. These observations confirmed energy transfer between the bodipy and the porphyrin of the MOF.

To follow up on the previous results, a MOF with more structural similarity to PSI/PSII was designed by the Hupp group. This MOF was based on highly ordered porphyrins.[64] Two MOFs, namely DA-MOF and F-MOF, were prepared entirely composed of two different Zn(II) porphyrin struts. The DA-MOF has enhanced π-conjugation compared to the F-MOF due to two acetylene moieties in the porphyrin molecules. The MOFs were suspended in ethanol, photoexcited at 446 nm, and the time resolved photoemission at 446 nm was measured. The π-conjugation in DA-MOF led to greater Q-band absorption intensity and faster exciton-hopping (energy transfer between adjacent porphyrin struts). Rapid exciton migration within the DA-MOF resulted in dramatic fluorescence quenching after the addition of only small amounts of quencher, pyridyl-ferrocene. By varying the concentration of quencher, it was found that the exciton traversed ~90 porphyrin linkers in DA-MOF compared to ~6 in F-MOF within the nanosecond exciton lifetime. This exciton hopping mechanism between adjacent chromophores was described by a FRET mechanism which was then used to calculate exciton lifetimes within the crystal structure. The authors suggested an effective strategy to further develop these porphyrin containing MOFs, that was to increase the electronic asymmetry of the porphyrin linker in DA-MOF in order to increase oscillator strengths in the Q-band region and boost both spectral overlap and coupling constants.

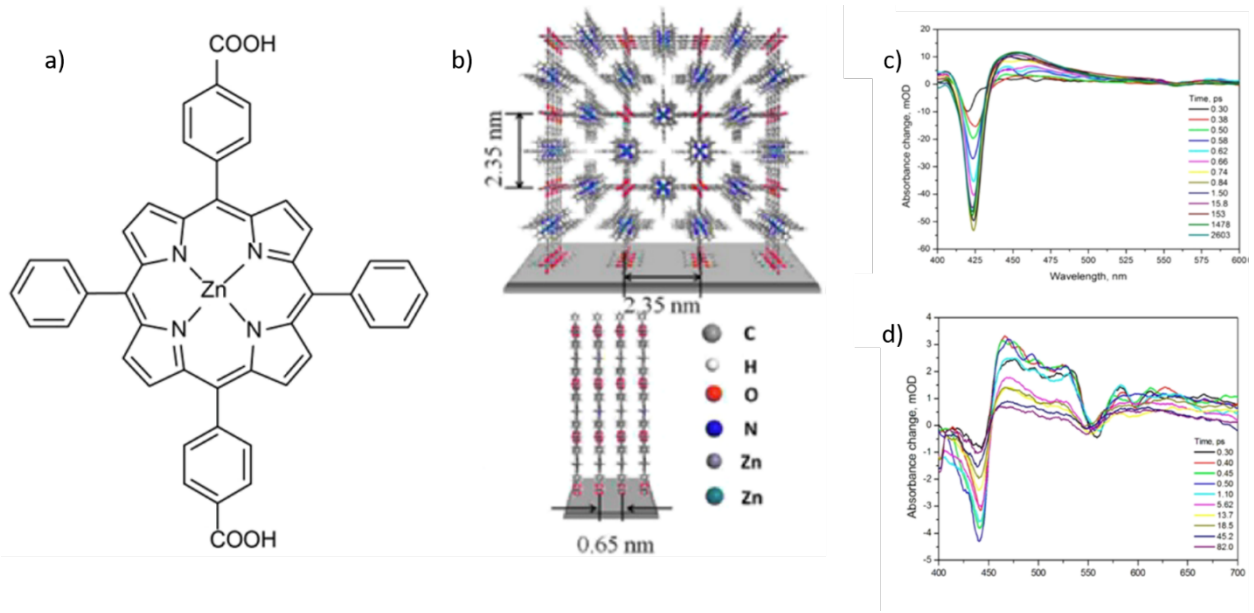

Figure 6: a) Molecule structure of ZnTPP, acting as linker in the ZnTPP SURMOF structure shown in b). Ultrafast transient absorption of the ZnTPP linker (c) compared to SURMOF (d). Reproduced from Li et al[66], Copyright ACS 2018.

In contrast to 3D exciton transport, lateral 1D transport was observed in thin films of palladium-porphyrin-based surface-anchored MOF (SURMOF).[65] Nanosecond transient absorption measurements confirmed one-dimensional transport of triplet excitons with a transfer rate on the order of tens of nanoseconds, highly mobile within single crystalline domains. Excitons diffused and were annihilated faster than mononuclear decay, enabling triplet exciton annihilation. Time-dependent DFT calculations, utilizing hybrid B3LYP, suggest strong π–π intermolecular interactions and substantial electronic coupling between porphyrin linkers in one dimension enhancing the energy transfer. This improves the Dexter exchange coupling during exciton transfer. Exciton diffusion lengths are predicted to be on the order of several

micrometers in perfectly ordered, single-crystalline SURMOFs. The design and development of highly conjugated MOFs could greatly affect the efficiency of energy transfer as studied here with nanosecond transient absorption spectroscopy.

The used linkers influence the properties of the resulting MOF, but the interaction within the framework tailors and alters the resulting MOF properties. An excellent study illustrating this was performed by Li et al. In this study the excited state dynamics of a free-base tetraphenyl porphyrin (TPP) linker and the TPP-MOF formed by those linkers were compared.[66] The TPP has carboxylate linkers on two opposing phenyl groups resulting in the formation of a planar surface-mounted MOF (SURMOF). This MOF was grown on quartz via a layer-by-layer deposition process with zinc acetate and TPP, each in ethanol. Steady-state fluorescence measurements showed enhanced fluorescence from the porphyrin S_2 state in the MOF, which was not observed in H_2TPP. Time-resolved fluorescence (10 ps time resolution) and TA measurements (50 fs time resolution) were performed on SURMOF samples in air and H_2TPP ligands dissolved in EtOH. An ultrafast rise time was observed in the TA data for the SURMOF not observed in the TPP ligand, which was assigned to the $S_2 \rightarrow S_1$ internal conversion process. The rise-times observed for the S_1 absorption in TA (on the order of 50 to 190 fs) agree well with the short S_2 decay observed in fluorescence experiments, which were limited to 10 ps resolution by the detection scheme. Computational modeling predicted the fluorescence decay dynamics in good agreement with the measured data and explained the slow $S_2 \rightarrow S_1$ decay in SURMOF as, mainly, a coupling factor of vibrational modes to the dissipative environment.

A similar study on SURMOF with ZnTPP linkers (Shown in figure 6a and 6b; TPP dicarboxylate with Zn^{2+} bound in the porphyrin macrocycle) was performed by Li et al.[67]

Interestingly, ZnTPP in EtOH, unlike TPP in EtOH, displayed both S_2 and S_1 fluorescence whereas ZnTPP SURMOF displayed mainly S_2 emission and relatively weak S_1 emission. Each were quenched compared to the emission of ZnTPP linker in EtOH. Time-resolved emission on ZnTPP linker in EtOH showed a distinct S2 → S1 process whereas ZnTPP SURMOF had contribution from each of the S_1 and S_2 states at each fluorescence wavelength analyzed via a biexponential decay model. Even at emission wavelengths at the red side of the Q-band absorption, the dominant process in the decay is on the timescale of $S_2 \rightarrow S_1$ conversion, including vibrational cooling in the S_1 state on a 25 ps timescale, as supported further by fs-TA measurements shown in figure 6c and 6d. In the ZnTPP SURMOF, efficient energy transfer between adjacent ZnTPP moieties was supported by the time-resolved data and modeling, and further due to large overlap between the absorption and fluorescence spectra as a result of the MOF structure.

Both nanosecond and femtosecond TA spectra were collected for PCN-223 (freebase) MOF constructed from meso- tetrakis(4-carboxyphenyl)porphyrin (TCPP) in a study by Shaikh et al.[68] These MOFs were suspended in air-free water at pH 8. Due to poor orbital spatial overlap, the Dexter mechanism did not dominate energy transfer, and FRET was invoked to describe the through space energy migration in this MOF. The lifetime of the MOF was shorter compared to TCPP, 260 ± 7 μs compared to 201 ± 27 μs, suggesting energy transfer within the donor-acceptor framework. The energy transfer efficiency of this PCN-223 (freebase) MOF was evaluated by relating the concentration of a quencher to photoluminescence quenching. The rate of exciton hopping and exciton hopping time in this MOF were estimated using the FRET model. Rate and efficiency are dependent on spectral overlap, orientation, and distance of the donor and

acceptor. The rate of exciton hopping and exciton hopping time were approximately 1.9 ps^{-1} and 0.53 ps^{-1} respectively.

Energy and charge transfer have been explored in a variety of MOFs, including those with ruthenium-based structural units and porphyrin-based structural units. In some cases, the density of chromophores in MOFs plays a role in the excited state energy migration mechanism. Designing MOFs to effectively direct energy transfer in the short and long range could improve future photocatalysts. As shown in the examples above, numerous time-resolved emission and absorption spectroscopies gain insight into energy transfer processes, enabling for further insight into MOF tunability.

5. Photoinduced Dynamics, Charge Transfer, and Localization

This section is certainly the broadest section of this review, owing to its focus on excited state electronic dynamics in MOFs that are not specifically related to, or limited to, energy transfer events. Keeping in the spirit of the description of light harvesting mechanisms in MOFs set for in Section 2, several examples are presented that we attempt to view through the appropriate lens with respect to the photoinduced processes. In some examples, ligand-centered or metal-centered excited state features are dominant, whereas other examples involve excimeric or excitonic behavior. Photoexcitations are either described in a semiconductor band picture or invoke a more localized description. Regardless of the language used, this section aims to present a comprehensive overview of photoinduced dynamics and charge localization, transport, and transfer in MOFs as determined by several time-resolved techniques.

The first subsection 5.1 will briefly reiterate the used spectroscopic techniques and emphasize the challenges in the sample preparation. Section 5.2 highlights work performed using a combination of multiple spectroscopic techniques focusing on the well-studied MIL-125(Ti)-NH_2. The subsection 5.2 concludes with various functional examples of MOF photocatalysts and devices where time-resolved spectroscopy gave insight into the photocatalytic mechanism or device function, respectively. Section 5.3 then brings in X-ray transient absorption (XTA), which has been used to gain further insight into charge localization.

5.1 Sample Preparation and Time-Resolved Techniques Applied

While time-resolved emission spectroscopy remains an important technique in this section, it is often complemented by other time resolved techniques such as femtosecond or nanosecond TA spectroscopy. These measurements are mainly performed in transmission geometry which imposes a sample limitation – transmission of light. Diffuse reflection-mode measurements are possible, but they are not a standard practice in most groups and transmission-mode measurements are most common. Many MOFs can be measured as a solvent suspension, limited by particle size/agglomeration and scattering. High-quality films, in terms of their homogeneity and light transmission, are used in some cases on transparent substrates. Solid polymer film suspensions, such as Nafion or polystyrene, have been applied taking advantage of both homogeneous dispersion of MOF particles and better refractive index-matching compared to air, thereby yielding enhanced transmission. As we caution in the concluding remarks, matrix effects may not always be accounted for in studies thus far due to difficulties in measuring

samples prepared in any other way. For each example cited, the sample preparation technique will be explicitly stated.

Insight has also been gained by applying element-specific time-resolved X-ray absorption spectroscopy (XAS). High-flux synchrotron sources can generate sufficient photon flux for transmission mode measurements of MOF samples, however, fluorescence mode detection is generally more sensitive and is therefore typically applied, removing any limitations on sample thickness.[43] XAS is capable of probing individual metal atoms in MOF systems, yielding local structure and oxidation state information. These techniques have been combined with other transient absorption techniques to paint a full picture of the localized and delocalized aspects of light-initiated dynamics in MOFs.

5.2 Studies in the Visible-NIR frequency regime

5.2.1. Correlating Structure with Light-Initiated Dynamics

The structure of a MOF ultimately dictates its light-initiated dynamics. From a band perspective, the physical structure is inherently linked to the electronic structure. From a more localized perspective, the proximity and orientation of structural units dictate the photophysical events that can occur. In addition to structure, the identity of inorganic nodes and organic linkers also clearly influence the light-initiated dynamics. With the diversity of structure and composition that exists, there has been great progress in correlating these factors with light-initiated dynamics. For instance, in some MOFs an energy transfer process might dominate whereas in other MOFs, a charge transfer process is dominant. A charge transfer may involve a formal transfer of charge from one MOF structural unit to another or could alternatively be an excimeric-

type interaction where charge delocalizes over adjacent units. An energy transfer event might precede a charge transfer event, or vice-versa. In this subsection, we highlight several works aim to gain insight on how the structure and/or composition affect the light-initiated dynamics.

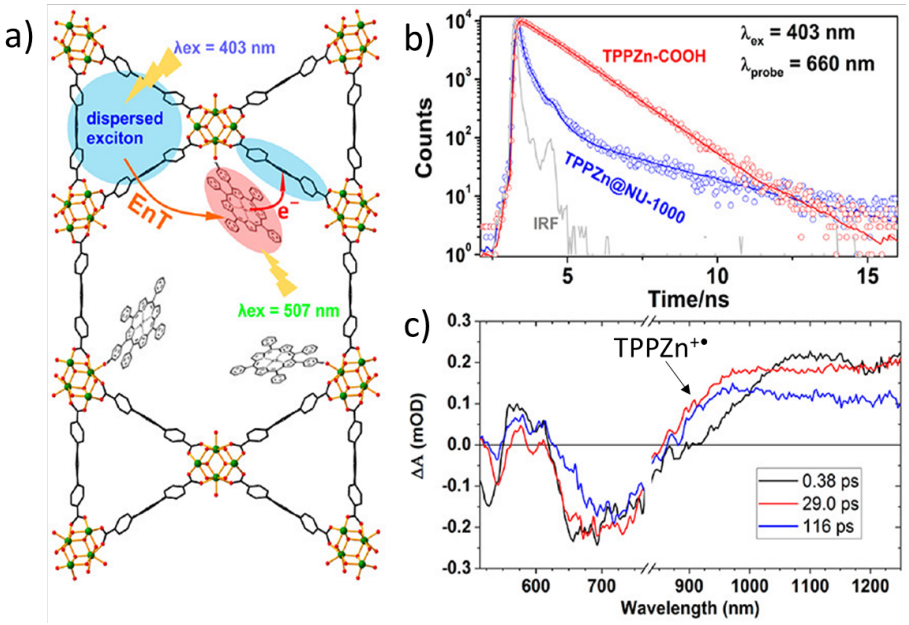

Figure 7. (a) Depiction of the photophysical processes in NU-1000 with Zn tetraphenylporphyrin (TPPZn) modifications. (b) Time-resolved fluorescence spectroscopy comparing the free Zn tetraphenylporphyrin (TPPZn-COOH) to the MOF sample. (c) Femtosecond TA of the MOF with a porphyrin-centered cation radical feature labeled. Adapted from Li et al.[69], Copyright 2019 ACS.

A system comprising sequential energy transfer and charge transfer steps was studied by Li X. et al. using the combination of time-resolved photoluminescence and visible-NIR TA spectroscopy.[69] The study investigated NU-1000, a Zr-based MOF constructed from a tetratopic linker with a pyrene core. As shown in Figure 7, NU-1000 was functionalized at its Zr nodes with

a TPPZn (Zinc tetraphenyl) porphyrin controllably via a carboxylate linker to investigate the interaction between the chromophore and the host framework. Samples were suspended in degassed CF_3-toluene and MeTHF, and time-resolved fluorescence and TA was measured.

Insight into the photoinduced dynamics of TPPZn@NU-1000 were gained by performing solvent-dependent photoluminescence experiments in MeTHF and CF_3-toluene. NU-1000, the framework without TPPZn functionalization, and the molecular porphyrin TPPZn were studied alongside and presented significantly different decay dynamics compared to NU-1000 at their characteristic emission wavelengths. In both MeTHF and CF_3-toluene, the emission of the NU-1000 host framework in TPPZn@NU-1000 was selectively probed and revealed highly similar decays (Figure 7b). Building on assignments made in steady-state excitation-emission maps in this study, the independence on solvent polarity supported that NU-1000 was quenched via a polarity-independent FRET mechanism that transferred energy to TPPZn. Emission features of TPPZn, however, were found to have solvent polarity dependence, implying charge transfer character in the TPPZn decay. TA experiments preferably excited TPPZn and gave support of the formation of a charge transfer state, based on assignments of the TPPZn cation radical and NU-1000 anion radical features (Figure 7c).

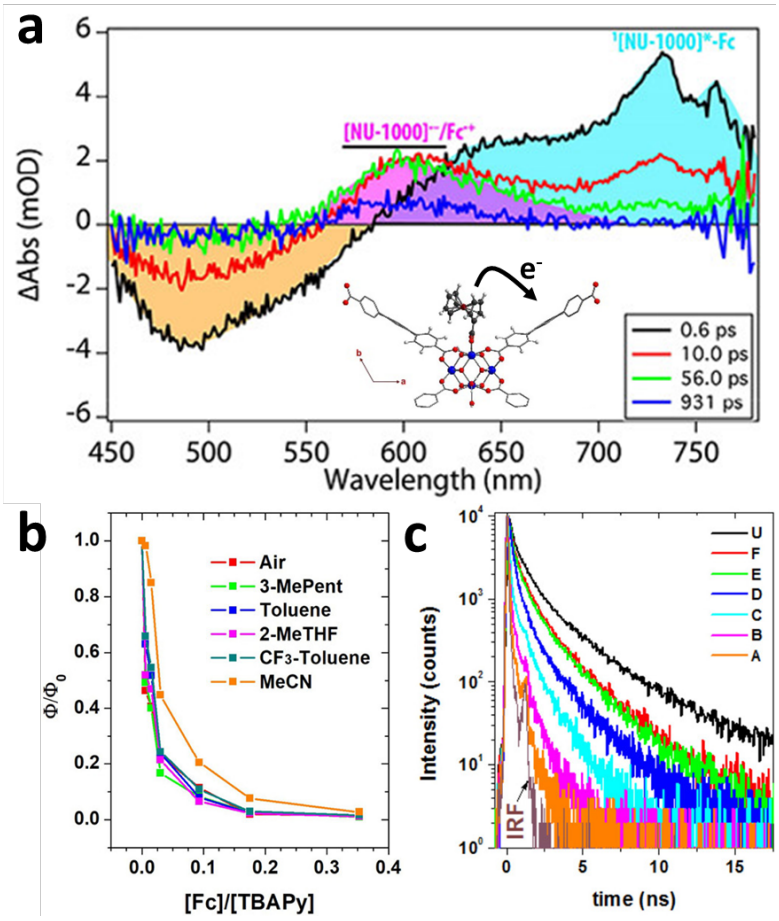

Figure 8. (a) Representative femtosecond TA spectra of Fc@NU-1000 in N_2 purged toluene. (b) Steady-state quenching efficiency and (c) time-resolved emission quenching in 2-MeTHF at varying ferrocene:TBAPy rations ((0.000 (U), 0.006 (F), 0.015 (E), 0.030 (D), 0.093 (C), 0.175 (B), and 0.353 (A)). Inset of (a) shows a scheme for the photoinduced hole transfer from the ligand to ferrocene. Adapted from van Wyk et al.[70], Copyright 2018 ACS.

A NU-1000 structure was also investigated by Van Wyk et al. with ferrocene carboxylate (Fc) anchored to the Zr nodes of the structure (Fc@NU-1000).[70] The ligands in the structure are pyrenetetrabenzoate (TBAPy). Electrochemical data suggested a favorable photoinduced charge transfer from the ferrocene moiety to the pyrene-containing TBAPy linkers of the MOF leading

to the formation of a charge separated state in the MOF structure. Femtosecond TA spectroscopy was performed with the ferrocene-modified MOF suspended in N_2 purged toluene using 400 nm to excite the pyrene linkers. The formation of the predicted charge separated state was observed in the TA spectra, where $[NU\text{-}1000]^{\bullet-}$ was observed as a well-resolved feature formed 10 ps after photoexcitation at a Ferrocene/TBAPy ratio of 0.175 (Figure 8a). Steady state (Figure 8b) and time-resolved (Figure 8c) emission experiments were performed at varying ferrocene/TBAPy ratios revealing more pronounced and faster quenching with increasing amounts of ferrocene. The authors estimated the quenching rate time constant to be 13 ps from fluorescence experiments which agreed well with the 9 ps time constant from femtosecond TA. The authors then sought to understand the effect of solvent dielectrics on the charge transfer using the Marcus formalism, and reported a large reorganization energy for the charge transfer due to the polar nodes of the MOF to which the ferrocene redox partner was bound, leading to a water-like dielectric environment. This finding suggested that polar nodes in MOFs, such as those containing polar hydroxyl or aqua ligands, may have a deleterious effect on charge transfer interactions and the energy penalty for reorganization needs to be taken into consideration.

Further delving into the NU family of MOFs, Yu et al. report a comparative time-resolved and computational study of NU-901 (scu) and NU-1000 (csq).[71] Each of the MOFs are chemically identical but topologically (structurally) different as emphasized by the three-letter topologies *scu* and *csq*. Each MOF has Zr(IV) nodes and 1,3,6,8-tetrakis(p-benzoicacid)pyrene linkers but exhibits very different structure wherein NU-901 has a shortest inter-ligand distance of 9.52 Å while NU-1000 has a shortest inter-ligand distance of 10.92 Å. The relative orientation of linkers also differs as a function of structure. Significant variation in the UV-visible absorption spectrum

was observed between the MOFs, with NU-901 having lower energy absorption as supported by the computational spectra. Computational results also suggested spectroscopically-relevant charge separated states in each of the MOFs, with NU-901 potentially harboring a greater overall charge separation. The visible-NIR fs-TA spectra were performed on MOFs deposited in a polystyrene matrix using parallel pump/probe polarization under 400 nm excitation. In each MOF, the ground-state bleach position was consistent with the steady-state UV-visible absorption and each showed broad excited state absorption in the 750 – 1200 nm range consistent with a charge separated state. Unlike NU-1000, NU-901 had an additional feature at approximately 650 nm that rose with a time constant of 2 ps and was assigned to an excimeric state. The observation of the state could be rationalized by the closer chromophores in NU-901 that are more cofacially-oriented than the chromophores in NU-1000. Therefore, the MOF structure played an important role in its photophysics. Time-resolved fluorescence experiments with the MOFs suspended in different solvents suggested that the excited state decay in NU-1000 had a strong solvent dependence while that of NU-901 was less affected by the solvent enviroment. This result indicated that low-lying polar excitonic states may more strongly influence the excited state decay of NU-1000 compared to NU-901.

Two works from Gutierrez et al. find an interplay between energy transfer and charge localization events within Zr-based MOFs.[72,73] The first work investigates a Zr-based MOF from the UIO family with mixtures of 2,6-napthalenedicarboxylate (NDC) linkers with their 4-amino substituted analogues (NADC). Measurements were performed in dichloromethane suspension. Steady-state emission showed energy transfer from the unsubstituted linker to the 4-amino substituted linker and also showed an excimer between unsubstituted linkers in the structure.

Both femtosecond and picosecond time-resolved emission measurements were performed to gain dynamic insight into these two states. It was determined that energy transfer events occurred on a picosecond timescale whereas excimer formation occurred on a timescale closer to a nanosecond. In samples containing a large relative number of 4-amino substituted linkers, the energy transfer process was found to outcompete the excimer formation, resulting in the excitation localizing on 4-amino linkers instead of between unsubstituted linkers as an excimer.

The second work by Gutierrez et al. builds further on the Zr-NDC system by investigating Zr-NDC and Zr-NADC, where Zr-NDC is the single ligand analogue and Zr-NADC is mixed-ligand and contains 35% NADC, in both DCM and DMF solvent suspensions.[73] Using femtosecond TA spectroscopy, a charge transfer was observed between NDC and Zr nodes, denoted ligand-to-cluster charge transfer (LCCT) in Zr-NDC which could not be observed in the prior work that utilized only fluorescence techniques.[72] The sub-100 fs charge transfer was observed in both DCM and DMF via femtosecond TA. The recombination lifetime of the LCCT state was highly solvent dependent, measured via nanosecond TA spectroscopy. Analogous studies on the Zr-NADC mixed ligand system showed that selective excitation of NDC resulted in competing LCCT and energy transfer processes whereas selective excitation of NADC resulted in radiative NADC emission in addition to an LCCT process. Nanosecond TA in the presence of molecular quenching species demonstrated that the separated charges could be extracted, making the system of potential interest for photocatalysis. Other work from the group has revealed time-resolved fluorescence properties of dye molecules loaded in a host 2D MOF structure, and the material is of potential utility in photonics.[74]

As the previous studies illustrated, charge transfer events in MOFs not only depend on the chemical constituencies but also the structure and geometry of the formed MOF. Deria et al extended these structural studies of the NU family by comparing two NU MOFs with a similar chromophoric MOF (ROD-7) to gain an even more detailed understanding of structural effects on the charge transfer events between chromophores and MOF nodes.[75] Each of these three MOFs utilized either In^{III} or Zr^{IV}-based inorganic nodes and tetraphenyl-pyrene (1,2,6,8-tetrakis(*p*-benzoic acid)pyrene; shortened as H_4TBAPy) linkers. The MOFs studied were ROD-7 ($In_2(OH)_2$TBAPy; *frz* topology), NU-901 (*scu* topology), and NU-1000 (*csq topology*), each orienting the same linker in different configurations that the authors hypothesized would lead to different interchromophoric interactions. Steady-state emission experiments showed a significant bathochromic shift (0.4 eV) in ROD-7 and NU-901 compared to the free linker, suggesting a ground state interaction between the pyrene-containing linkers. In contrast, NU-1000 exhibited a much smaller shift (0.05 eV). To investigate the excited state interactions, time-resolved emission spectroscopy was performed in both single wavelength and spectrally resolved experiments with the MOF samples sealed in capillary tubes under low dielectric media such as argon or anhydrous 3-methylpentane. A long-lived fluorescence decay component was observed in the MOFs that was not observed in the ligand, suggesting that the excited state is characteristically different from the free linker. Time-resolved emission spectra showed a time-dependent broadening and shift in the *fwhm* of the emission peak in the MOF samples. Spectral decomposition suggested the contributions of two peaks – namely a higher energy peak with more localized character and a lower energy peak assigned to an excimeric state. The excimeric

state was shown to be topology-dependent, reinforcing that the relative orientation of crystographically-oriented chromophores in MOFs determine their photophysical properties.

5.2.2. Specific Insights into MIL-125(Ti)

MIL-125(Ti) has Ti(IV) nodes and benzenedicarboxylate linkers in a quasi-cubic tetragonal structure, and the light harvesting properties can be modified by constructing the MOF from substituted linkers.[23,76] MIL-125(Ti) was extensively studied and selected as a model system to investigate different experimental conditions and, as a whole, demonstrate the importance of approaching the scientific challenge of understanding light-initiated dynamics in MOFs from as many angles as possible to build a comprehensive understanding. In addition to the more fundamental studies presented first, some more applied studies related to photocatalyisis with MIL-125(Ti) are presented.

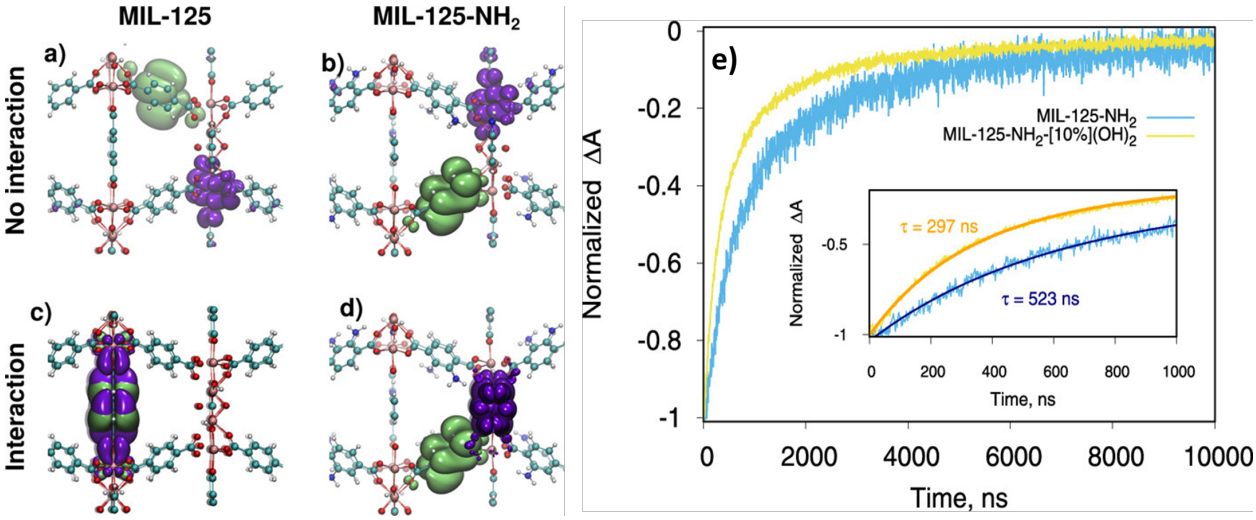

Figure 9. (a-d) Interacting and non-interacting isodensity representations of the photo-excited electron (violet) and hole (green) in MIL-125(Ti) and MIL-125(Ti)-NH_2. (e) Nanosecond TA of MIL-125(Ti)-NH2 and a -OH modified analogue. Adapted from Capano et al.[76], Copyright 2020 ACS.

The combination of theory and experiment is employed by Capano et al. to investigated the optical properties of MIL-125(Ti) and MIL-125(Ti)-NH_2.[76] DFT calculations employing a PBE0 hybrid functional were used to calculate the bandgaps of MIL-125(Ti) and MIL-125(Ti)-NH_2, revealing an approximately 1 eV smaller bandgap for MIL-125(Ti)-NH_2 in agreement with the experimental results. However, the absolute values of the bandgaps needed to be re-calculated using LR-TDDFT and quantitatively adjusted for thermal effects to reach close agreement to the experimental values. The discrepancy of DFT and LR-TDDFT results was explained as being due to an excitonic effect, implying necessity to understand the interaction between charges and lattice structure changes. In Figure 9, it is shown that the non-interacting singlet state has electron (violet isosurface) localization on the Ti nodes in both structures. This result is in agreement with the computational work by Butler et al. discussed earlier in Section 2.[13] The lower energy triplet state was found to be interacting in MIL-125(Ti), exhibiting a negative interaction energy, whereas the triplet state in MIL-125(Ti)-NH_2 was found to be non-interacting with a positive interaction energy. The authors then *a priori* predicted and calculated that replacing 10% of the -NH_2 modified linkers with -OH modified linkers would result in a less positive (i.e. more interacting) state that should correlate with faster charge recombination. Nanosecond TA results on acetonitrile suspensions of the synthesized MOFs showed excellent agreement with the theoretical prediction and observed longer lifetime of the bandgap bleach in MIL-125(Ti)-NH_2 compared to the partially -OH modified analogue. The work demonstrates that computational techniques can be powerful tools to interpret and understand time-resolved phenomena in MOFs.

A study on MIL-125(Ti)-NH_2 by de Miguel utilized diffuse reflectance nanosecond TA on the dry MOF sample and also performed measurements with the MOF suspended in water.[77] Each measurement was performed separately under O_2 and under N_2. In both cases, a broad TA feature was observed in the visible region of the spectrum that lived beyond the 400 μs limit of the instrument. While the decay dynamics of the broad positive feature appear to be slightly different in H_2O compared to dry sample, the main difference observed was the shape of the spectrum under the different gas environments. These spectral features were correlated to photochemical results that investigated the ability of MIL-125(Ti)-NH_2 to photochemically oxidize or reduce donor/acceptor species. One takeaway is that the nanosecond TA data obtained is highly dependent on a number of factors, including both sample and measurement preparation conditions, as the long-lived TA features of the de Miguel et al. study contrast with the Capano et al. study (Figure 9), where more significant decay was observed by the 100 μs time point. It is worth noting that the Capano et al. study, in addition to being performed in a different solvent, probes the bleach signal of the bandgap while the de Miguel et al. study probes an excited state absorption. While the typical ca. 10 ns time resolution of nanosecond TA eliminates, for instance, the possibility of observing ultrafast cooling processes, other various recombination events likely play a role. It is not clear exactly what processes are being probed in either case to explain why the signals are so different, highlighting the importance of experiment conditions, sample preparation, and environment on measured dynamics.

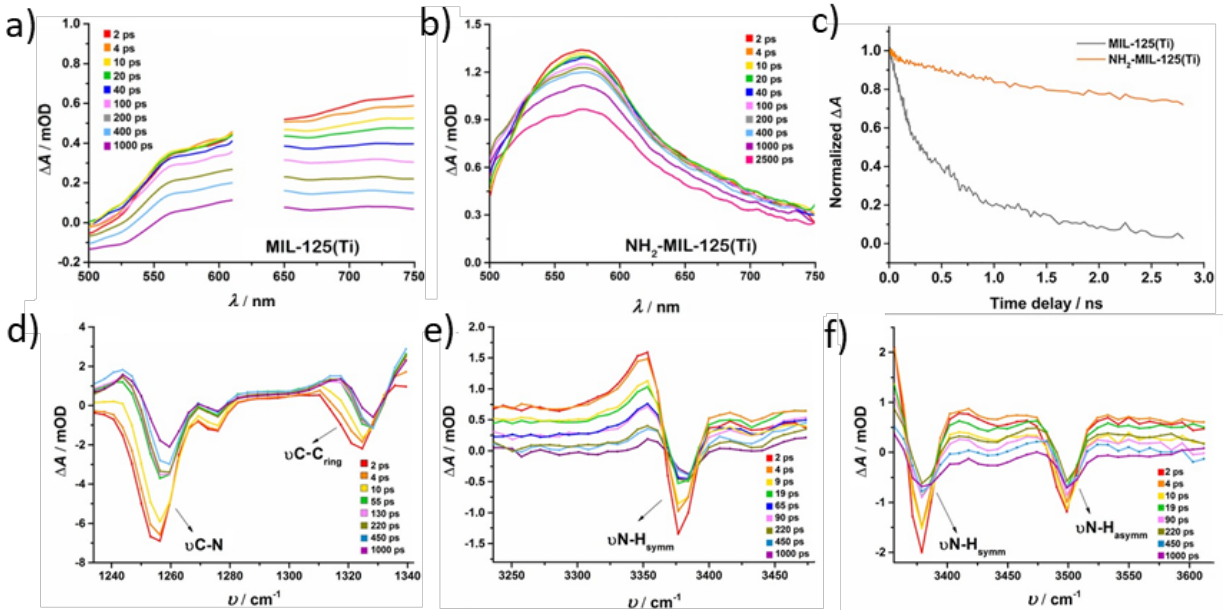

Figure 10. (a) Visible transient absorption spectrum of MIL-125(Ti) and (b) NH_2-MIL-125(Ti) in aqueous suspension with 400 nm pump. (c) Kinetic traces averaged over the wavelength range of 560-610 nm. (d) Infrared transient absorption spectra for NH_2-MIL-125(Ti) in the C-N stretching region, (e) in the N-H symmetric stretch region, and (f) in the N-H symmetric and asymmetric stretch regions. Adapted from Santaclara et al.[78].

The influence of NH_2 modification on this model MOF was further investigated using femtosecond TA spectroscopy comparing MIL-125(Ti)-NH_2 and the unmodified MIL-125(Ti) analogue.[78] In the work, Santaclara et al. found that, in agreement with the later-published theoretical predictions of Capano et al (Figure 9), MIL-125(Ti)-NH_2 had significantly longer excited state lifetime than MIL-125(Ti) in aqueous suspension (Figures 10 a-c) The TA in the visible region of the spectrum for both samples showed only positive features with differing shape, potentially implying a role of the -NH_2 ligand in the transient feature. The established LCCT mechanism in

MIL-125(Ti) guided interpretation which was further supplemented with spectroelectrochemical data on model systems for both the ligand and metal node. The aminoterepthalate dimethyl ester, a model of the linker, displayed a cation feature in excellent agreement with the transient spectrum of MIL-125(Ti)-NH_2. The metal node anion yielded a broad absorbance feature in the same region of the spectrum. Therefore, the visible femtosecond TA decays were unambiguously attributed to the decay of ligand cation and metal node anion species following the LCCT event. The authors also applied femtosecond transient mid-infrared spectroscopy to MIL-125(Ti)-NH_2 in $C_2H_2Cl_4$ solvent (Figures 10d-f) and observed C-N relaxation dynamics comparable to those observed in the visible region of the spectrum, suggesting that those features are related to the LCCT state. The transient mid-IR studies also yielded information on the timescale of vibrational cooling, as an ultrafast decay component was observed in N-H, N-C, and C-C features.

Given the interest in MIL-125 as a photocatalyst material, further studies have employed time-resolved techniques to understand photo physics in MIL-125 and related analogues in the context of photocatalytic results. Nasalevich et al. report on a comparative study of MIL-125(Ti) to MOFs containing IVth group metals (Zr and Hf).[79] Enhanced photocatalytic hydrogen evolution reaction was observed in MIL-125(Ti) compared to the Zr and Hf MOFs. This activity was correlated with EPR signals showing reduction of Ti in MIL-125(Ti) under steady-state illumination. Femtosecond TA, in good agreement with the Santaclara et al. study,[78] showed a long-lived LCCT state for MIL-125(Ti) whereas the Zr and Hf MOFs decayed nearly to baseline within < 1 ns. Another Santaclara et al. study employed nanosecond time-resolved fluorescence and visible femtosecond TA spectroscopy to demonstrate that the ligand-localized hole could be

extracted by molecular donor species having appropriate reduction potentials – a strong support of photocatalytic applications.[80]

Further understanding on the importance of the metal node in MIL was gained by Wang et al. using nanosecond TA to compare two Fe-based MIL MOFs as oxidative condensation photocatalysts.[81] Catalysis experiments showed superior activity for 1,3,5 benzenetricarboxylate-based MIL-100(Fe) compared to 1,4 benzenedicarboxylate-based MIL-68(Fe). Argon-purged acetonitrile suspensions were measured in transmission mode using nanosecond TA revealing a longer-lived excited state in MIL-100(Fe) correlating with enhanced photocatalytic activity. Another example by Guo et al. investigated MIL-101(Cr)-Ag composites for CO_2 reduction and time-resolved photoluminescence was applied to correlate an excited state quenching process with photocatalytic results.[82]

Chen et al. developed MOF photocatalysts for the hydrogen evolution reaction by modifying MIL-125(Ti)-NH_2 with Cu atoms to yield MIL-125(Ti/Cu)-NH_2.[83] The MIL-125(Ti/Cu)-NH_2 MOF was prepared by stirring MIL-125(Ti)-NH_2 and copper acetate. XPS and EXAFS characterizations suggested that Cu^+/Cu^{2+} sites were formed in the MOF, and the Cu atoms were determined to be coordinated to N atoms of the linkers with a bond length of approximately 1.98 Å. The EXAFS analysis suggested a coordination number of 3.5, which could suggest either a 3-coordinate or 4-coordinate environment potentially involving coordinated solvent atoms. MIL-125(Ti/Cu)-NH_2 was shown to be much more catalytically active than the non-Cu modified MOF and a Pt-loaded MOF under photocatalytic conditions in water using triethylamine as a sacrificial electron source and 420 nm irradiation. Each of the non-Cu modified and MIL-125(Ti/Cu)-NH_2 MOFs were measured via fs-TA in a 2 mm flow cell to investigate their light-initiated dynamics

under 400 nm excitation. While the kinetics each show a long-lived component, they cannot be sufficiently compared because of the extremely different spectra features observed. The non-Cu modified MOF exhibits only a ground-state bleach feature in the 430 – 500 nm range in agreement with the steady-state UV-Vis. Though the Cu modification did not significantly change the UV-Vis absorption, the fs-TA shows a new intense positive TA feature from 475 nm to beyond 700 nm. The authors suggest that the feature could be a Cu-localized trap state based upon the photocatalytic activity.

5.2.3. Photocatalysis

In photocatalysis, photons provide the energy, or voltage, to drive a chemical reaction. A core challenge for photocatalysis is efficient charge separation because a charge-separated state is typically required for sufficient electron-hole lifetimes to drive a redox reaction before electron-hole recombination "wastes" energy as heat or light. The following examples represent a broad collection of MOFs for which the photocatalytic mechanism was better understood using time-resolved spectroscopy.

In addition to the well-studied MIL-MOFs highlighted above, several other MOFs were explored for their catalytical activity and understood using time-resolved techniques. Deng et al. reported on MOF-253 based system for photocatalytic CO_2 reduction.[84] MOF-253 is constructed from Al-O clusters and 2,2'-bipyridine-5,5'-dicarboxylic acid (dcbpy) linkers. A light harvesting moiety $[Ru(bpy)2(dcbpy)]^{2+}$ was installed in place of some of the dcbpy linkers. A Rhenium complex ($[Re(CO)_3(dcbpy)Cl]^{1+}$) was also incorporated to facilitate catalytical CO_2 reduction. Characterizations including PXRD, FTIR, SEM, and TGA analysis showed the successful

incorporation of each moiety into the structure and photocatalytic activity under visible light was observed in the presence of sacrificial electron donors. The MOF containing only Re (i.e. MOF-253-Re) was shown to be catalytically active and the further addition of the Ru-based light harvesting moiety (i.e. Ru-MOF-253-Re) was provided even better photocatalytic activity. Such photocatalytic activity supported the presence of a charge transfer mechanism between the light harvesting moiety and the catalytic moiety. The samples were then further interrogated using time-resolved spectroscopy. Nanosecond TA experiments were performed on MOF-253, MOF-253-Re, and Ru-MOF-253-Re suspensions in acetonitrile to demonstrate that the long-lived transient species likely involved in the photocatalytic cycle were different between the samples. Quenching experiments were performed either under O_2 or Ar, and additionally in the presence of isopropanol, wherein a loss of signals was assigned to be due to charge localization on the Re complex. Therefore, as a whole, the nanosecond TA studies supported the photocatalytic studies, despite the time resolution being insufficient to capture the charge transfer events in the MOF structure directly.

Goswami et al. developed two Zr-based MOFs for the selective oxidation of the mustard gas simulant 2-chloroethyl ethyl sulfide (CEES).[85] The MOFs developed are based upon the PCN-57 structure which is composed of a triphenyl linker and Zr-based nodes. A benzothiadiazole or benzoselenadiazole group was installed at the central phenyl group of the linker to prepare PCT-57-S or PCN-57-Se, respectively. Catalytic studies revealed that PCN-57-Se performed the catalytic transformation much faster than PCN-57-S, and also showed that both light and oxygen were required. This evidence necessitated time-resolved fluorescence and TA measurements to gain further insight into the catalytic mechanism and to explain the better activity of the Se-

bearing MOF. The ester-protected linkers in dichloromethane were measured via TA as a proxy for the MOFs, which could not have been measured directly due to strong light scattering by the sample. Femtosecond TA under air-free conditions showed spectral evolution commensurate on the same timescale as intersystem crossing. DFT calculations reproduced the triplet absorption spectrum of the Se-containing ligand. The S-containing ligand showed similar singlet features that did not decay to an observable triplet state within the instrument time window of approximately 7.5 ns. Nanosecond TA of the Se-containing ligand with and without oxygen at the triplet absorption wavelength revealed fast quenching of the triplet in the presence of oxygen, suggesting an energy transfer mechanism forming catalytically-active singlet oxygen ($^1O_2$). Time-resolved fluorescence measurements on each MOF showed faster singlet decay in PCN-57-Se compared to PCN-57-S, consistent with TA measurements on the ligands and with the hypothesis that enhanced spin-orbit coupling in the Se-bearing MOF resulted in more efficient $^1O_2$ formation and increased catalytic activity.

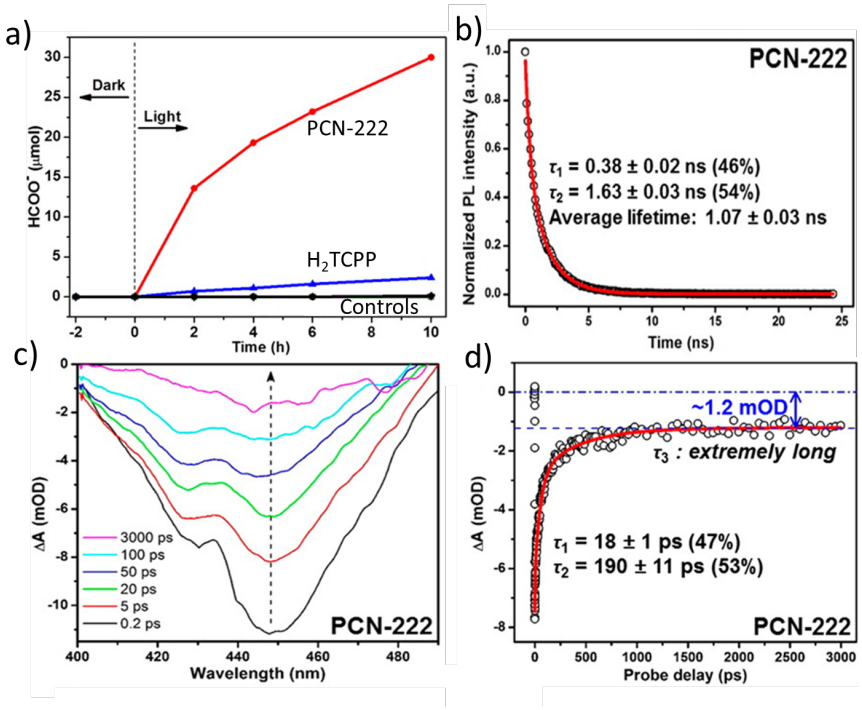

Figure 11. (a) Photocatalytic experiments with PCN-222 MOF or H_2TCPP ligand in ACN/TEOA. Controls excluded either PCN-222, TEOA, or CO_2. (b) Time-resolved photoluminescence of PCN-222 in DMF at 712 nm under 515 nm photoexcitation with biexponential fit. (c) fs-TA spectra of PCN-222 under 500 nm excitation. (d) fs-TA kinetics of the ground-state bleach feature in (c) and triexponential fit. Adapted from Xu et al.[86], Copyright 2015 ACS.

Xu et al. performed a study on PCN-222, a free-base porphyrin-based MOF with Zr nodes, which was shown to be active for photocatalytic CO_2 reduction in acetonitrile with triethanolamine as a sacrificial electron donor (Figure 11a).[86] The reaction was selective for formate as a CO_2 reduction product, which is of interest because it bypasses the simpler carbon monoxide pathway to selectively form a more complex product. The efficacy of PCN-222 toward

the photocatalytic transformation was investigated using time-resolved spectroscopy with the MOF suspended in DMF. The subnanosecond time-resolved photoluminescence dynamics (Figure 11b) show biexponential behavior with an average lifetime of about 1 ns. The trace decays fully to baseline indicating that the emissive state decaying radiatively is depleted on a 1 ns timescale. Conversely, the fs-TA spectrum (Figure 11c) shows a broad ground-state bleach that does not decay within 3 ns. The kinetics of the ground-state bleach feature (Figure 11d) agree with that observation and show a long-lived component with a lifetime >> 1 ns. The combination of time-resolved photoluminescence and fs-TA illustrate that while time-resolved photoluminescence is capable of selectively observing only certain excited states that have a radiative relaxation or recombination component, it is blind to certain non-radiative processes. The fs-TA shows a long-lived excited state, which the authors assign as a non-emissive electron trap state. As indicated by the photocatalysis results, the trap state is likely localized at least partly on the Zr nodes of the structure that are implicated in the photocatalytic reduction of CO_2.

Yan et al performed a study on another MOF active for CO_2 reduction photocatalysis.[87] The Eu-Ru(phen)$_3$-MOF has Ru(phen)$_3$ linkers where phen = 4-(1H-imidazo[4,5-f][1,10]phenanthrolin-2-yl) benzoic acid, and [$Eu_2(\mu_2\text{-}H_2O)(H_2O)_3(\text{-}COO^-)_6$] node building units. The Ru(phen)$_3$ linkers are generally similar to Ru tris-bypiridine complexes that have an important role in many photocatalytic systems due to their stability, reasonably large extinction coefficient, and excellent excited state reduction potential. Keeping these properties in mind, it is important to understand where electrons and hole localize in the MOF structure in order to gain insight into the photocatalytic mechanism. It is well known that Ru tris-bipyridine complexes undergo a metal-to-ligand charge transfer (MLCT) mechanism after photoexcitation involving a Ru^{II} to Ru^{III}

oxidation state change, opening the possibility of either electron or hole transfer to the surrounding Eu nodes. Steady-state quenching experiments were performed using the protonated $Ru(phen)_3$ linker in solution with either TEOA or a model Eu cluster $[Eu_2(MMA)_6(H_2O)_4]$ (MAA=methacrylic acid) to test for reductive or oxidative quenching of $Ru(phen)_3$, respectively. The emission of $Ru(phen)_3$ was quenched efficiently by the Eu clusters but not by TEOA, implying an oxidative quenching mechanism where $Ru(phen)_3$ transfers an electron to the Eu cluster. The Eu-$Ru(phen)_3$-MOF or $Ru(phen)_3$ ligand were dissolved or suspended in DMF for the time-resolved experiments. Time-resolved fluorescence spectroscopy showed faster quenching of the MOF excited state compared to the free $Ru(phen)_3$ ligand suggesting an excited state relaxation mechanism in the MOF such as energy or electron transfer. While the absence of Eu f-manifold emission in the MOF suggested that energy transfer was insignificant, fs-TA was used to further investigate whether energy transfer or electron transfer occurred in the MOF. The fs-TA spectra for the MOF compared to the free ligand are quite different, with the former featuring a strong ground-state bleach and a weaker excited state absorption. Contrarily to the free ligand, near-complete quenching of the $Ru(phen)_3$-centered excited state was observed in conjunction with a long-lived ground-state bleach persisting well beyond 7 ns. The fs-TA results therefore strongly supported an electron transfer process. Steady-state EPR under light irradiation further confirmed the formation of a charge-separated state in the MOF. Together, the steady-state and time-resolved techniques in this work gave strong support to the proposed light harvesting mechanism underlying the photocatalytic performance for CO_2 reduction.

A study by Yang et al. involved a $Ru(bpy)_3$-modified MOF with catalytic $CoCl_2$ species anchored to the ligands therein active for photocatalytic proton reduction.[88] Ru-UIO-67 was constructed from Zr nodes and dcbpy linkers, including $Ru(bpy)_2(dcbpy)$, resulting in $Ru(bpy)_3$ being incorporated as linkers in the MOF. If $CoCl_2$ was included in the synthesis, the $Co(dcbpy)Cl_2$ species were formed as a second type of functionalized linker in the MOF. Photocatalytic experiments revealed that the Ru moiety was necessary for sufficient visible light harvesting and the Co species was required for efficient photocatalysis, suggesting their roles as light harvesters and catalytic centers, respectively. Steady-state EXAFS confirmed the structure of the catalytic Co metal center and *in situ* EXAFS observed a reduced Co intermediate. The photocatalytic experiments were performed under 447 nm LED illumination (where the $Ru(bpy)_2(dcbpy)$ moiety absorbs primarily) in acetonitrile with triethanolamine as a sacrificial electron donor. Therefore, an electron transfer from the photoexcited Ru moiety to the Co moiety for reductive photocatalysis was implicated. Femtosecond TA was utilized to investigate each of the samples under 447 nm excitation, which were suspended in a Nafion matrix by sonicating the MOF in an aqueous/isopropyl alcohol solution of Nafion. The Nafion-MOF suspension was drop-cast on glass substrates and allowed to dry in air to produce films. An analogue containing only Co species (no Ru photosensitizer) did not yield transient signal under the experimental conditions. Compared to the Ru-only analogue (Ru-UIO-67), the analogue containing both Co and Ru (Co-Ru-UIO-67) had a redshifted ground state bleach that decayed on the same timescale as that of Ru-UIO-67, however had significantly faster decay in its excited state feature owing to a mechanism where the excited state of the Ru chromophore decays but does not return to ground state. The

fs-TA data strongly supports and quantifies an electron transfer from Ru photosensitizer to Co catalyst, as observed in the *in situ* EXAFS and photocatalytic data.

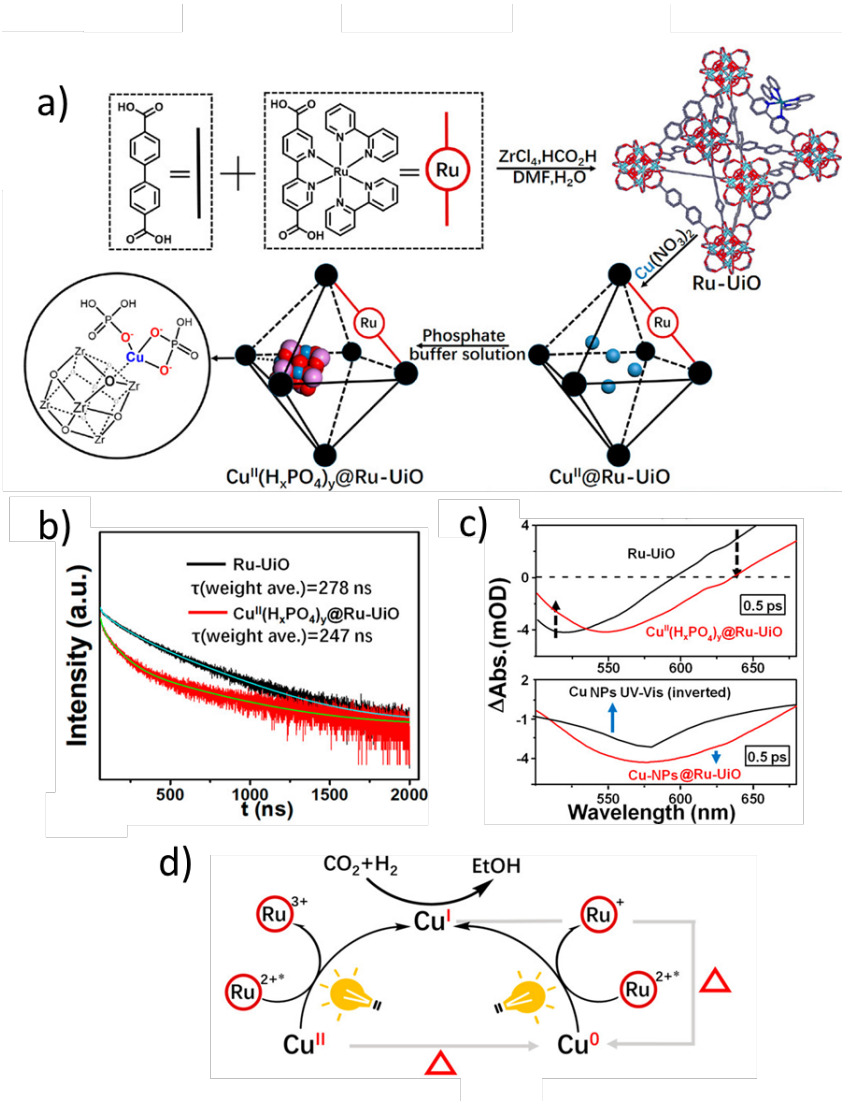

Figure 12. (a) Synthetic scheme for production of the photocatalytic UI MOF harboring a copper phosphate CO_2 hydrogenation catalyst. (b) Time-resolved photoluminescence results with 377 nm excitation and 640 nm emission for Ru-UiO and the copper containing MOF. (c) Transient absorption spectra comparing the two MOFs. (d) Proposed mechanism for generation of Cu^I via light-induced single electron transfer. Adapted from Zeng et al.[89], Copyright 2020 ACS.

Zeng et al. utilized a UIO-67 based structure incorporating $Ru(bpy)_2(dcbpy)$ as some of the linkers, with equivalent single building units (SBU), bipyridyl dicarboxylate linkers as the remainder as a CO_2 hydrogenation catalyst to selectively generate ethanol.[89] Copper(II) phosphate clusters were anchored onto the Zr-based nodes within the Ru-UIO MOF cavities to generate the catalytically active species (Figure 12a). The catalytic hydrogenation was carried out in 3:1 H_2:CO_2 at 150 ˚C with or without light activation. Characterizations found that in the absence of light, Cu nanoparticles were formed, which were active for CO_2 hydrogenation to MeOH whereas, under light activation, Cu nanoparticles were not formed and the MOF catalyst remained active for CO_2 hydrogenation to EtOH. This finding was rather peculiar in that adding light irradiation somehow bypassed a degradative mechanism for the Cu species under catalytic CO_2 hydrogenation conditions. Time-resolved fluorescence and fs-TA provided the necessary insight to understand this finding by studying the MOF samples suspended in EtOH. Time-resolved fluorescence (Figure 12b) showed Ru-UIO samples had enhanced fluorescence decay when modified with the Cu^{2+} phosphate catalyst, suggesting a deactivation mechanism such as electron transfer from Ru-moiety to Cu^{2+}, forming Ru^{3+} and Cu^{1+}. This was further supported by steady-state Stern-Volmer analysis. The fs-TA experiments (Figure 12c) on Cu^{2+}-modified Ru-UIO supported the formation of Ru^{3+} and Cu^{1+} after photoexcitation, which is predicted to be energetically feasible. This result, however, does not explain why Cu^0 species are avoided under light irradiation. Further fs-TA experiments on a Cu^0 nanoparticle modified sample, Cu-NPs@Ru-UIO, suggested that photoexcitation of the Ru moiety reduced the number of Cu^0 species present. Therefore, a model was proposed (Figure 12d) wherein Cu^I can be regenerated by photooxidation of Cu^0 via photoexcited Ru^{2+}. This finding generally relies on the fact that photoexcitation of

$Ru(bpy)_3$ and related molecules form an excited state that is both more reducing and more oxidizing than the ground-state molecule, leading to its dual-role in Ru-UIO as reported by Zeng et al. Further global analysis of the fs-TA data suggested that both the Cu^{II} – Cu^{I} reduction and Cu^{0} – Cu^{I} oxidation occur on the order of 100 – 200 fs, further supporting that the dominating mechanism is largely dependent on the concentration of Cu species present (a factor highly dependent upon the catalytic conditions) and is not over-compensated by a faster charge transfer in reduction or oxidation.

A study by Liu et al investigated the effect of Cu-doping UIO-66-NH_2 on its excited state properties and photocatalytic activity for hydrogen evolution in water.[90] The MOF is constructed from 2-amino-1,4- benzenedicarboxylic acid linkers (NH_2-BDC) with Zr-based nodes and both Cu-UIO-66-NH_2 and Cu@UIO-66-NH_2 were prepared. The former Cu-doped MOF has Cu^{2+} atoms doped into the nodes whereas the latter is intercalated with Cu^{2+} ions that are not a structural component of the nodes as confirmed by pXRD and FT-IR. Femtosecond TA was performed on each sample (including the undoped UIO-66-NH_2) dispersed in stirred ethylene glycol using 400 nm excitation. Each of the samples displayed a broad positive TA feature between approximately 500 – 750 nm ascribed to a ligand-to-cluster charge transfer state that was observed to decay on two timescales via biexponential modeling. UIO-66-NH_2 and Cu@UIO-66-NH_2 decay on a similar timescale while Cu-UIO-66-NH_2, which has Cu^{2+} atoms incorporated into the node/metal cluster, decays much faster. Biexponential fitting of Cu-UIO-66-NH_2 had an amplitude-weighted average lifetime almost 3 times faster than the undoped version. This finding implicates that Cu^{2+} atoms in the nodes of MOF likely participate in a photoinduced ligand-to-cluster charge transfer in Cu-

UIO-66-NH_2. Lastly, it was found that photocatalytic hydrogen generation was significantly improved with Cu^{2+} ions incorporated into the nodes compared to the intercalated analogue. However, the photocatalysis was performed with an auxiliary photosensitizer, limiting the insights into the role of the ligand-to-cluster charge transfer process on the photocatalytic efficiency.

Gutiérrez et al. performed a postfunctionalization of MOF-520 with perylene-3-carboxylic acid (MOF-520-PC1) or perylene-3-butyric acid (MOF-520-PC2) to yield active organophotoredox catalysts.[91] MOF-520 is constructed from Al-based nodes and BTB ligands (BTB = 4,4',4''-benzene-1,3,5-triyl-tris(benzoate)) and modification with the perylene units did not alter the bulk crystal structure observed via pXRD. Fluorescence microscopy data of single crystals showed that the perylene units anchored to the nodes of the MOF and significantly enhanced their visible light absorption. Photocatalytic tests showed that the modified MOFs were photocatalytically active for various reductive coupling reactions using N,N-diisopropylethylamine (DIPEA) as an electron source. MOF-520-PC2 could perform photocatalytic reduction reactions under aerobic conditions, which is surprising because oxygen reduction typically proceeds instead of the desired reaction under such conditions. Various reductive coupling reactions were investigated in parallel reactors and flow reactors, suggesting a broad scope of applicability of the MOF photocatalysts. Time-resolved photophysical studies were performed to gain further insight particularly into the DIPEA photocatalytic reduction. The solid-state time-correlated single photon counting results under 470 nm excitation and 560 nm emission showed biexponential decay dynamics for each MOF with approximately 30 ns lifetime for the dominant longer-lived components. DIPEA concentration-dependent time-resolved fluorescence decays of ball-milled

suspensions in CH_3CN/CH_3OH (3:2) showed DIPEA concentration-dependent quenching which showed a linear Stern Volmer relationship. Nanosecond TA of MOF-520-PC2 with 355 nm excitation (suspension in CH_3CN) showed the formation of a MOF radical in the presence of DIPEA, suggesting a fast photooxidation of DIPEA to yield a long-lived radical anion MOF species. When a catalytic substrate was added into the solution, the anion feature was significantly quenched, suggesting that electron transfer to the catalytic substrate occurred in agreement with the photocatalyic results.

Contrary to the previous work in which the catalytical site was located at the node within the UIO-68 MOF, Yang et al. employed a strategy to incorporate a catalytic unit onto the linker instead of using a post synthetic modification.[92] UIO-68 is based upon 2'-Amino-[1,1':4',1''-terphenyl]-4,4''-dicarboxylic acid linkers and Zr-based nodes. Initially, the UIO-68-NH_2 MOF was synthesized and then modified at the NH_2 position of the ligand via amine-aldehyde condensation with 4’-methyl-[2,2’-bipyridine]-4-carbaldehyde. In a following step, $FeCl_3$ was added resulting in an Fe bpy complex - $Fe(bpy)Cl_3$ – being anchored to the ligands. A molecular complex control – TPDC-Fe-bpy was used to investigate the role of the MOF in photocatlytic CO_2 reduction under visible light conditions where both the MOF and the Fe-bpy complex absorb. While both the control and the MOF performed similarly for CO_2 reduction to CO, it was found that the control complex lost efficiency over time compared to the UIO-68-Fe-bpy MOF catalyst remained stable and was recyclable for multiple catalysis runs. Femtosecond TA found a slightly longer excited state lifetime for the MOF compared to the control compound. The experiments were performed with 440 nm excitation and the MOF sample was in a solid Nafion film suspension. Additionally,

an enhanced excited state absorption was observed which, while not assigned, may imply some interaction with the host framework or may be a signal from the non-interacting host framework.

5.2.4. Solar and Optical Devices

The potential energy created by light absorption can also be harnessed in more device-oriented applications, such as in a sensor or solar cell. While, as discussed below, some MOFs have actually been applied to functioning solar cells, there is also an importance in understanding the light-initiated dynamics in thin film geometries that are amendable to device applications. Such applications often involve interface with an electrode, which could potentially facilitate time-resolved studies under controlled potential as an *in situ* experiment, although no such reports are known so far. As a further application, MOFs have even been investigated for data storage applications relying upon structural changes.

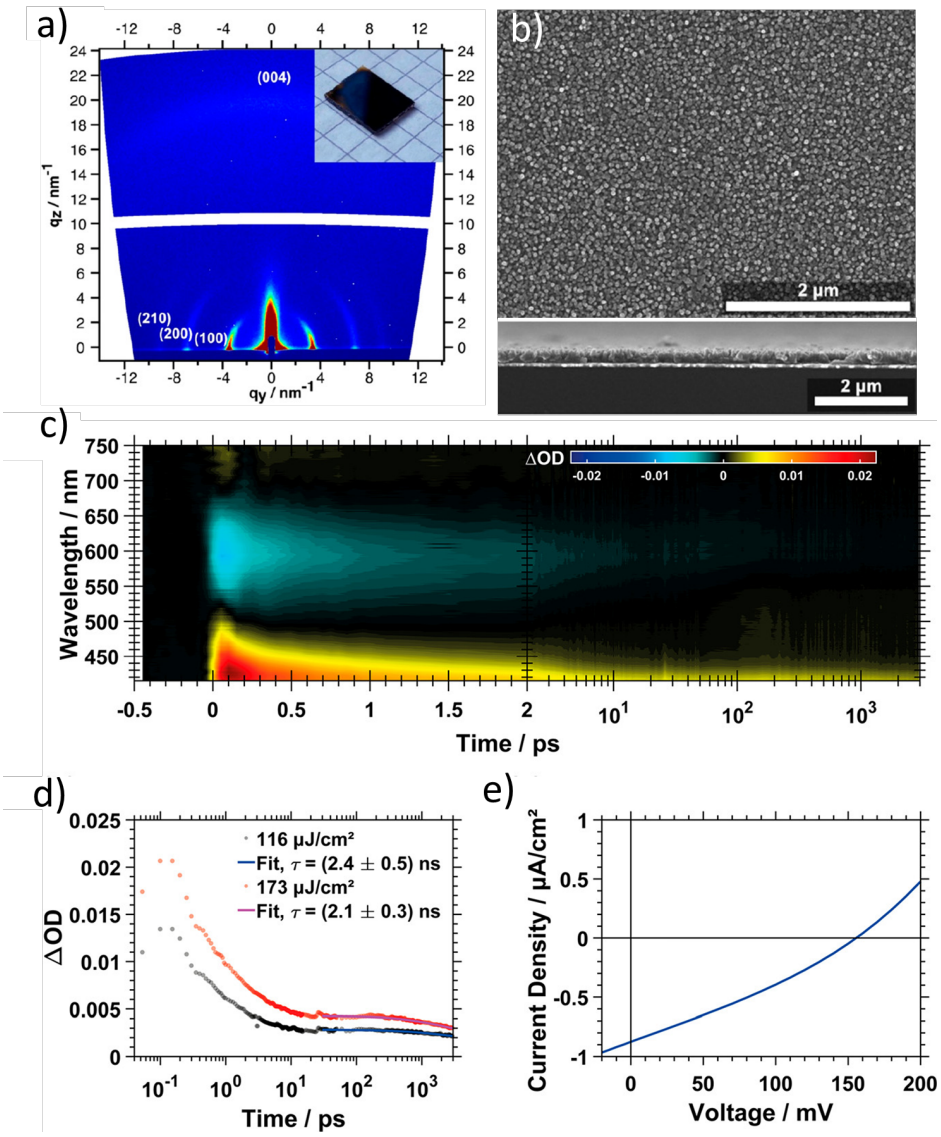

Figure 13. (a) 2D Grazing Incidence Wide Angle X-ray Scattering, GIWAXS, pattern of Ni-CAT-1 MOF film on gold showing in-plane diffractions oriented orthogonally to the substrate and (b) SEM images of film. (c) fs-TA spectrum of Ni-CAT-1 film on quartz with 400 nm excitation and (d) fluence-dependent kinetic traces of the positive absorption feature between 415 – 450 nm. (e) Current-voltage measurement of an ITO/Ni-CAT-1/Al solar cell device under 100 mW/cm^2 AM 1.5 G illumination. Adapted from Mähringer et al.[93], Copyright 2019 ACS.

Additional to the fundamental research presented in the previous examples, functional applications of engineered MOF films have been reported, including work by Mähringer et al. on oriented films of triphenylene-based 2D MOFs.[93] A vapor-assisted deposition method was developed to prepare oriented MOF films with Ni^{2+} (Ni-CAT-1), Co^{2+} (Co-CAT1), or Cu^{2+} (Cu-CAT1) on gold substrates. Further addition of an acid modulator allowed for oriented films to be grown on quartz or conductive transparent indium tin oxide (ITO). Triphenylene-based 2D MOFs tend to be electrically conductive and are thus intriguing for functional applications that rely upon efficient charge transport. From the selected characterization data shown in Figure 13a-b, it can be seen that the MOF forms a homogeneous film with sub-micron thickness and is oriented orthogonally (i.e., the 2D MOF sheets are perpendicular to the substrate) as evidenced by the out-of-plane (100), (200), and (210) 2D GIWAXS peaks. The representative example Ni-CAT-1 has a bandgap of approximately 3 eV, corresponding to 413 nm photons, and has an additional absorbance feature centered at approximately 600 nm assigned to oxidized triphenylene ligands. Ni-CAT-1 was excited close to the band edge at 400 nm for fs-TA (Figure 13c). A ground state bleach is observed at the triphenylene cation absorption wavelength indicating an electron density change at the ligands due to photoexcitation and a positive absorption feature was observed at wavelengths shorter than 500 nm. The observation of a charge-separated state is supported further by the absence of time-resolved fluorescence dynamics within the 80 ps instrument response. The analysis of the long-timescale portion of the kinetics of the positive feature (Figure 13d) suggested a long-lived component. Finally, the MOF was used as both a light absorber and charge transport layer in a simple ITO/Ni-CAT-1/Al photovoltaic cell device,

demonstrating that the oriented MOF film is capable of useful photoinduced charge separation, as suggested by the time-resolved spectroscopic insights.

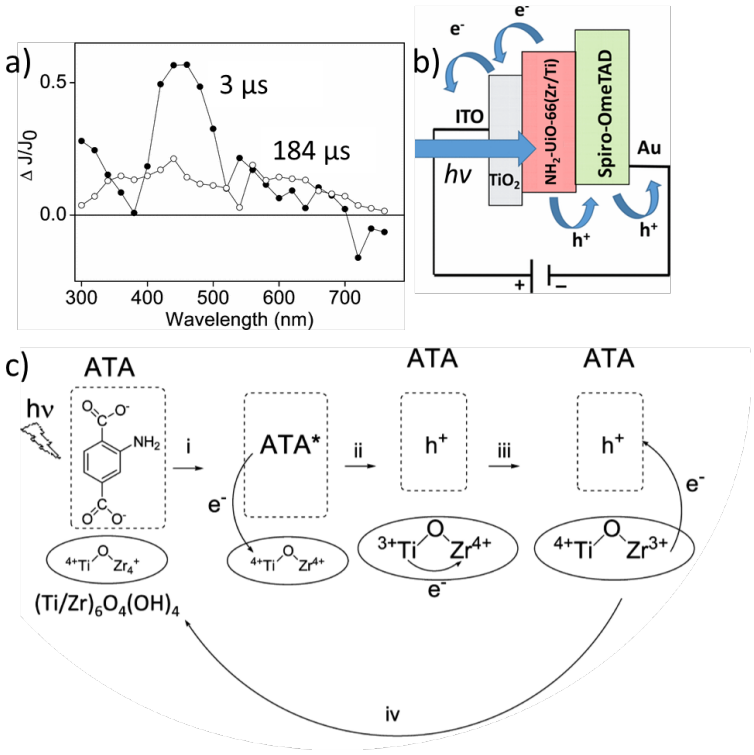

Figure 14. (a) Diffuse reflectance ns-TA spectrum of NH_2-UIO-66(Zr/Ti) at 3 µs and 184 µs under 355 nm ligand-centered excitation. (b) Schematic of a solid-state solar cell device based upon NH_2-UIO-66(Zr/Ti) as the light harvesting and charge separation layer, a semiconductor photoanode as the electron transport layer and an organic hole transport layer (Spiro-OmeTAD). (c) Proposed scheme for light harvesting (steps i. – iii.) and recombination (step iv.) in NH_2-UIO-66(Zr/Ti). Adapted from Portillo et al.[94], Copyright 2017 ACS.

Functional catalytical devices demand an understanding of charge separation steps in assembled cells. These mechanism were studied by Portillo et al. using TA measurements.[94] The MOF investigated in this work is NH_2-UIO-66(Zr/Ti), wherein the ligand is 2-aminoterepthalate

and the inorganic Zr nodes are substituted with varying amounts of Ti. Additionally, the single metal NH_2-UIO-66(Zr) MOF was measured as comparison. Diffuse reflectance ns-TA using a 355 nm pump was performed on NH_2-UIO-66(Zr) powder which identified a TA feature at 420 nm with partial character of both trapped electrons and triplet absorption (Figure 14a). This assignment was made by performing quenching experiments in the presence of oxygen, dichloromethane, or methanol. Further quenching experiments, namely aqueous transmission-mode ns-TA experiments of the ligand (2-aminoterepthalic acid) with aqueous Zr^{4+}, suggested that electron transfer from the ligand to Zr^{4+} is energetically feasible. Similar experiments with aqueous Ti^{4+} again suggested feasibility of Ti^{4+} reduction by the photoexcited ligand. Diffuse reflectance ns-TA experiments on the mixed Zr/Ti analogues showed spectral profile different from the single metal Zr MOF, with an additional feature at 540 nm that grows on the same timescale as decay at 450 nm in the spectrum. The feature at 540 nm was assigned to Ti^{3+} absorption.

The overall light harvesting mechanism was, based upon the ns-TA data, proposed to be a two-step mechanism in NH_2-UIO-66(Zr) and a three-step mechanism in NH_2-UIO-66(Zr/Ti) to form a long-lived electron hole pair (Figure 14c) and is described as follows. Photoexcitation of the 2-aminoterepthalate ligand in NH_2-UIO-66(Zr) (step i) results in an electron transfer from the ligand to Zr^{4+} (step ii) to form a long-lived charge separated state with a ligand-localized hole and Zr-localized electron. The charge-separated state then persists for hundreds of microseconds before recombining. For the Ti-containing analogue NH_2-UIO-66(Zr/Ti), the ligand photoexcitation (step i) is followed by electron transfer to Ti^{4+} (step ii), forming an intermediate charge-separated state. This intermediate state with a ligand-localized hole and Ti^{3+} then decays

to a state with a Zr-localized electron (step iii), forming a long-lived charge separated state with a ligand localized hole and Zr-localized electron, akin to the long-lived state in NH_2-UIO-66(Zr). Enhanced solar cell device efficiency was demonstrated for NH_2-UIO-66(Zr/Ti) on the basis of the enhanced metal-metal electron exchange which yielded an order of magnitude increase in efficiency. The authors in this work performed a transient diffuse reflectance ns-TA spectroscopic study on dry MOF powder with conditions as similar as possible to the demonstrated solar cell device (Figure 14b), thereby providing an understanding of how the changes in MOF composition underlie the fundamental and applied characteristics of the material.

Functional properties have also been investigated in single crystal MOFs, such as $[(Zn_2(TBAPy)(H_2O)_2)\cdot 3.5DEF]_n$ (1) (TBAPy: 1,3,6,8-tetrakis(*p*-benzoate)pyrene; DEF:diethylformamide), which we abbreviate Zn_2TBAPy, as reported by Milichko et al.[95] Spatial anisotropy of layered 2D MOF crystals, as well as their composition, can lead to photogenerated excitons with high binding energy, long recombination lifetime, and narrow line width. Using polarized two-photon absorption, a steady-state technique, the authors identified two excitons contributing to the UV-Visible absorption spectrum – one being intralayer and the other being interlayer. The MOF ligand emission occurs at 2.46 eV, which is well resolved from the excitonic emission at 2.77 eV. This allowed for time-resolved photoluminescence measurements of each type of emission in the MOF crystal independently, showing that the excitonic emission lifetime was 0.8 ns compared to the 4 ns emission lifetime of the ligand. Unpolarized *cw* white-light exposure experiments demonstrated that the two excitons are dipole-coupled resulting in a non-linear pump-power dependence of the excitonic absorption. Furthermore, the authors used UV radiation to selectively damage the MOF structure suppressing the interlayer excitons. The

change persisted for days, but could be reversed almost fully by injection of coordinating DEF molecules. Therefore, this excitonic MOF material was suggested as a potential new type of MOF-based optical data storage.

Cd_2TTFTB features a columnar stack of π-stacked TTFTB ligands which are known to stabilize cation radicals formed in air due photooxidation. This MOF was investigated by Wang et al. using time-resolved emission and fs-TA spectroscopy. It should be noted this MOF is also conductive and will be discussed further in Section 6. The Cd_2TTFTB MOFs in this work were studied as single crystals of approximately 200 μm size. The authors performed fs-TA on these crystals in a N_2 atmosphere through a 100 μm pinhole to avoid pump/probe scattering at the crystal edges. A broad ground state bleach feature was observed with a short-lived component which was fit with two exponentials, and a long-lived component of multiple nanoseconds, which was fit with a third exponential. The free ligand in THF solvent (H_4TTFTB) displayed a single exponential lifetime of 54 ps in fs-TA experiments, indicating very different excited state dynamics in the MOF. A broad-band steady state emission was observed in the range of approximately 1 – 1.8 eV and was assigned as doublet emission from TTF-centered cation radicals. Temperature-dependent time-resolved photoluminescence experiments with sub-nanosecond resolution were performed on single crystals and showed the same spectral profile throughout the time window indicating that the doublet state was solely responsible for the emission within the available time resolution. Temperature-resolved kinetic data was fit with a biexponential function and temperature dependence on the decay rate was observed in the first time constant (120 ps at 296K) but not in the second time constant (1 ns at 296K). Suggesting that the first component is phonon-mediated. A flattening of the decay rate vs 1/T curve at

approximately 80 K was concurrent with a phase transition observed in Raman spectroscopy at approximately 70-80 K, which may also play a role.

In a further practical application of TTFTB-based MOFs, Pattengale et al. developed conductive MOF photoanodes using Zn_2TTFTB as a photosensitizer and mesoporous TiO_2 nanoparticles as the semiconductor anode.[96] In the photophysical and computational studies therein, TiO_2 sensitized with the Zn_2TTFTB MOF (Zn_2TTFTB-TiO_2) was compared to TiO_2 sensitized with the TTFTB ligand chromophore (TTFTB-TiO_2). Time-resolved THz spectroscopy relied upon TiO_2-centered conductivity signals to confirm that photoinduced electron injection from the MOF and ligand were feasible. Computational investigations on the interfacial electron transfer supported that both the MOF and ligand could rapidly (sub-100 fs) inject electrons into TiO_2 to yield a ligand-centered or MOF-centered cation species. The UV-Vis absorption of the cation species was observed experimentally using spectroelectrochemistry and was confirmed with computations. The cation radical absorption of the MOF and the TTFTB ligand was well-separated from any other features in the spectra and was therefore an excellent probe for the charge separated state via ns-TA. By probing the cation radical feature in ns-TA, it was observed that the photogenerated cation radical in the MOF-sensitized system had at least two orders of magnitude longer lifetime than the cation radical in the ligand-sensitized system. These findings indicated that the extended conductive MOF architecture allowed for enhanced electron-hole separation due to the spatially overlapped ligands in the structure. This result finds a potentially important role for conductive MOF architectures in photoelectrocatalytic devices.

5.3 Studies Involving X-ray Transient Absorption

Optical techniques employed in section 5.2 tend to probe properties of the MOF ligand or charge transfer states involving both the ligand and inorganic node. While those insights gained are highly valuable, they most often cannot provide direct insight into the charge localization and structure of the inorganic nodes of the MOF and assignments of UV-Visible-NIR features may be subject to interpretation. Element-specific hard X-ray absorption spectroscopy, specifically the time-resolved variant, has been effectively applied to understand photoinduced charge localization in MOFs. This XTA technique most typically utilizes a visible excitation pulse synchronized with a bunch (i.e. the circling electron bunch responsible for providing an X-ray pulse) at a synchrotron facility, yielding sub-100 ps time resolution. X-ray free electron laser sources are capable of pushing this time resolution into the sub-100 fs time regime, however there are no reports yet of their application to investigate MOFs. The soft X-ray core hole clock technique has also been applied to a S-containing MOF to gain attosecond hole relaxation information related to charge delocalization in the structure.[97] As a whole, atom-specific X-ray techniques complement other time-resolved spectroscopic techniques and can provide particularly strong evidence to assign time-resolved structural or electronic effects inferred from non-atom-specific techniques.

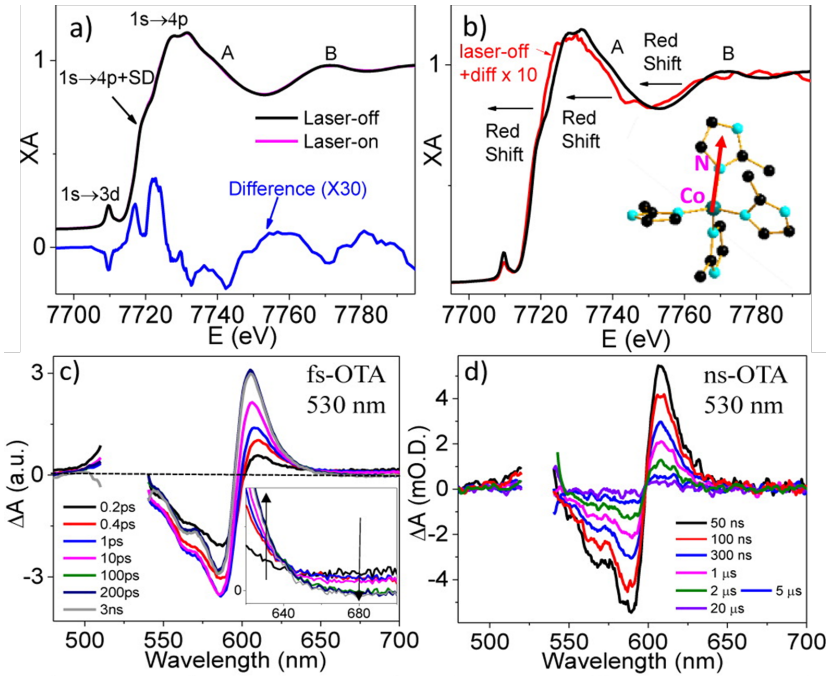

Figure 15. (a) XTA spectra in the XANES region for ZIF-67 photoexcited at 527 nm at a 500 ps delay time. The difference spectrum is obtained by subtracting the laser-off spectrum from the laser-on spectrum and is scaled by a factor of 30 for presentation. (b) Regeneration of a hypothetical laser-on XANES spectrum (red) using a difference spectrum scaled by a factor of 10 to show the spectral changes observed. (c) fs-TA and (d) ns-TA spectra of ZIF-67 thin films under 530 nm excitation. Adapted from Pattengale et al.[21], Copyright 2016 ACS.

Pattengale et al. combined XTA with fs-TA and ns-TA to understand photophysical effects in ZIF-67, a zeolitic imidazolate framework composed of 2-methylimidazolate and Co^{2+} nodes.[21] In the structure of ZIF-67, the Co^{2+} ion is tetrahedrally coordinated by imidazolate. This structural geometry was verified by steady state X-ray absorption near edge structure (XANES, Figure 15a), which showed a relatively strong dipole forbidden 1s-3d transition due to the lack of a center of inversion in the tetrahedrally coordinated Co^{2+} ion. The Co d-manifold transitions in ZIF-67 are also prominent in the visible and NIR regions of the UV-Vis spectrum, which were selectively

excited in this study at 530 nm and 1000 nm. Co K-edge X-ray transient absorption (XTA) experiments were performed on a continuous jet of ZIF-67 suspended in methanol, which serves to homogeneously suspend the material and prevent photoinduced heating damage. The XTA difference signal in X-ray transient absorption (Figure 15a and 15b) were collected with a 527 nm excitation pulse at a 500 ps delay time and revealed both an oxidation state and structural change at the Co metal ion due to selective photoexcitation of the Co d-d transitions. Photoinduced reduction of Co^{2+} was consistent with a shift in the XANES edge to lower energy and a reduction of the intensity of the dipole forbidden 1s-3d transition. The above-edge redshift observed suggested an expansion of the coordination environment of Co.

Both femtosecond (Figure 15c) and nanosecond (Figure 15d) transient absorption spectroscopies were applied to investigate the excited state dynamics after Co d-d excitation using a 530 nm pump on ZIF-67 film samples directly grown on etched glass substrate. A clear spectral evolution on an approximately 1 ps timescale suggested the formation of an intermediate state after the initial formation of the Co-centered d-d excited state. This state then persisted into the microsecond time scale. The derivative shape of the spectrum was attributed to the Stark effect as a result of local fields due to the charge separation process observed in the XTA experiment. The long-lived charge separated state evidenced the potential applicability of ZIF-67 as a photocatalyst material.

A follow-up study by Pattengale et al. utilizing femtosecond transient absorption spectroscopy observed that the charge-separated electron could be extracted by an electron acceptor species, methylene blue, further implying catalytic utility.[98] Yang et al. applied ZIF-67 as a photocatalyst for the proton reduction reaction, utilizing femtosecond transient absorption

spectroscopy to understand the interaction between a chromophore and ZIF-67.[99] It was found that the chromophore transferred energy to the Co d-d states, thereby providing the required charge separation for the photocatalytic process.

Mixed-metal ZIF systems were utilized in a study by Pattengale et al. to investigate whether communication between the metal nodes was relevant in the photoinduced charge separation and charge transport in ZIFs.[100] ZIF-67 was synthesized with varying amounts of Zn^{2+}, a closed shell d^{10} ion, or open shell Cu^{2+}. Femtosecond transient absorption experiments showed that closed-shell Zn^{2+} ions perturbed the formation of the charge separated state whereas open-shell Cu^{2+} ions did not. This result implied that node-to-node communication is important in the formation of the photoinduced charge separation. SQUID magnetometry measurements also supported the presence of exchange/superexchange interactions in ZIF-67 and the Cu^{2+}-containing analogues whereas Zn^{2+} shut down the magnetic ordering. Element-specific X-ray transient absorption (XTA) observed reduction of Cu nodes after selective excitation of Co nodes in a mixed Cu/Co ZIF. The complementary techniques employed supported the existence of charge transport pathways in ZIF-67 and their potential applications to light harvesting and photocatalysis.

The ZIF studies demonstrate that the combination of more traditional pump-probe transient absorption techniques with XTA can provide a fuller picture of the excited state dynamics and charge localization in MOFs. This strategy was also utilized by Hanna et al. to study MIL-100(Fe), which is composed of Fe_3-μ_3-oxo clusters and benzenetricarboxylic acid.[101] A model system for the inorganic node was employed, i.e. Fe_3O-BzPy, where BzPy denotes benzoic acid and is used as the proxy for the carboxylate-bearing ligand, and pyridine capped the Fe atoms in

the cluster. In this work, the authors were unable to obtain sufficient data for MOF using transmission mode femtosecond transient absorption due to scattering, an all-too-common plight in the field. However, the reference node could be measured and displayed a subnanosecond lifetime. XTA spectroscopy, which is not limited by transmission restrictions due to the utilization of fluorescence mode detection, was applied to both MIL-100(Fe) and the model node system. The samples were dissolved in 100% ethanol and measured in a 2 mm path length fused silica cuvette. XTA experiments demonstrated that, while both the model system and MOF experienced photoinduced reduction, the MOF had a more pronounced and long-lived signal owing to its more effective charge separation. Specifically, the model cluster had a lifetime of about 100 ps whereas the MOF showed a charge separated state lifetime on the order of 100 ns or more.

Further exploring photo physics in the MIL-125 family, Hanna et al. performed a study on NH_2-MIL-125(Ti) with heterometal incorporation, namely Fe^{3+}, into the nodes of the MOF.[102] The Fe^{3+} incorporation had only a minor effect on the UV-visible absorption spectrum of the MOF and the bulk structure was maintained as confirmed via pXRD. Steady-state x-ray absorption spectroscopy suggested that the Fe^{3+} species was incorporated into the Ti nodes of the MOF. Femtosecond TA was used to investigate the effect of Fe^{3+} incorporation on the photoinduced dynamics of the MOF. The MOFs were suspended in DMF and then centrifuged at 2500 rpm for 20 minutes to remove large MOF particles. The supernatant containing only the smallest particles to prevent probe scattering was then measured in a 2 mm cuvette under 400 nm excitation. Each of the NH_2-BDC linker, NH_2-MIL-125(Ti,Fe), and NH_2-MIL-125(Ti) samples showed a broad positive absorption feature from approximately 500 nm – 770 nm. The NH_2-BDC linker showed almost no

excited state decay during the 1 ns time window while NH_2-MIL-125(Ti) near-fully decayed within the 1 ns window. In contrast, NH_2-MIL-125(Ti,Fe), showed a much longer lifetime, potentially suggesting the stabilization of a charge separated state. The Fe^{3+} center was then selectively probed in XTA experiments under 400 nm excitation. The samples were prepared as a suspension in acetonitrile and measured in a flowing jet. The XTA results indicated the formation of a Fe-centered reduced state after photoexcitation that persisted for tens of microseconds. This finding demonstrates that the charge-separated state suggested by fs-TA could be directly observed in XTA to provide further understanding of NH2-MIL-125(Ti,Fe) as a potential photocatalytic material.

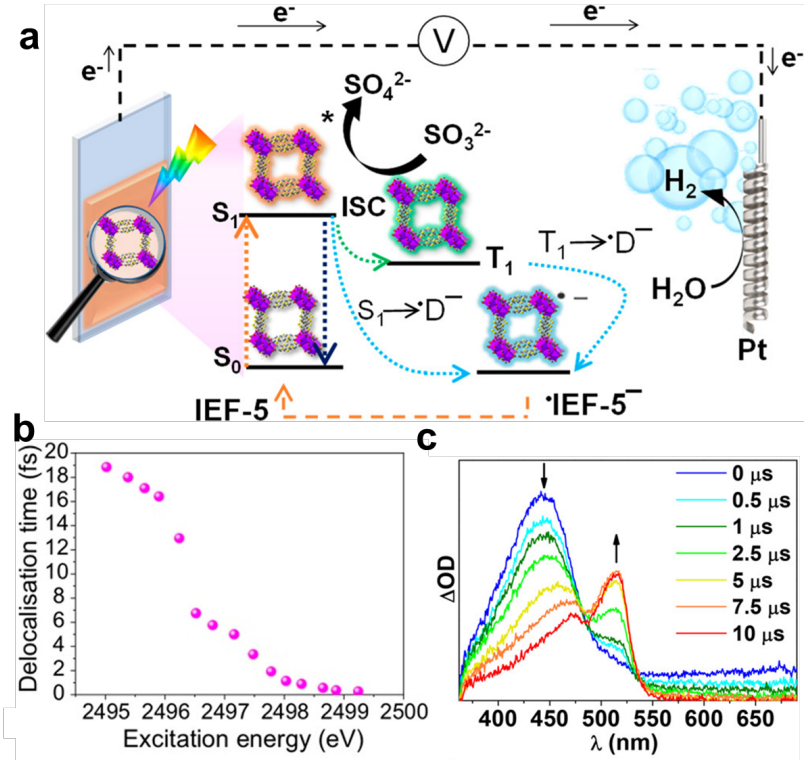

Figure 16. (a) Cartoon for the bismuth-based MOF IEF-5 proton reduction photoanode with inset scheme showing the light-initiated dynamics in the presence of an electron donor SO_3^{2-}. ISC denotes inter system crossing between singlet (S) and triplet (T) states. (b) Sulfur K edge core

hole clock measurement of IEF-5 and (c) nanosecond transient absorption spectrum in the presence of SO_3^{2-}. Adapted from Garcia-Sánchez et al.[103], Copyright 2020 ACS.

Garcia-Sánchez et al. recently reported a novel MOF photoanode, IEF-5, composed of bismuth and dithieno[3,2-b:2',3'-d]thiophene-2,6-dicarboxylic acid (DTTDC).[103] The MOF acted as a light harvester and photoanode in the presence of electron donor SO_3^{2-} to assist the electrochemical reduction of protons at a platinum counter electrode. Core hole clock x-ray spectroscopy experiments were utilized to gain insight into the charge delocalization on an attosecond timescale at the Sulfur K edge using drop-cast films. The technique is not time-resolved in the traditional sense and rather relies upon the known lifetime of the core excitation, i.e. the lifetime of the 1S hole of sulfur, 1.27 fs. The authors assigned the energy-dependent delocalization time (Figure 16b) to a charge delocalization process in the MOF. Nanosecond transient absorption experiments (Figure 16c) were performed on aqueous suspensions and demonstrated a long-lived signal that decayed faster in the presence of oxygen (i.e. a triplet signal). The spectrum in Figure 16c was collected in the presence of SO_3^{2-} hole acceptor wherein the decay of the MOF triplet state correlated to the formation of a MOF anion state detected via an isosbestic point in the spectrum on a timescale commensurate with a diffusion-limited process. Further kinetic nanosecond transient absorption experiments gained insight into the concentration dependence of the reductive quenching process. The spectroscopic observation of anion formation thus explains the photocatalytic applications demonstrated in the work.

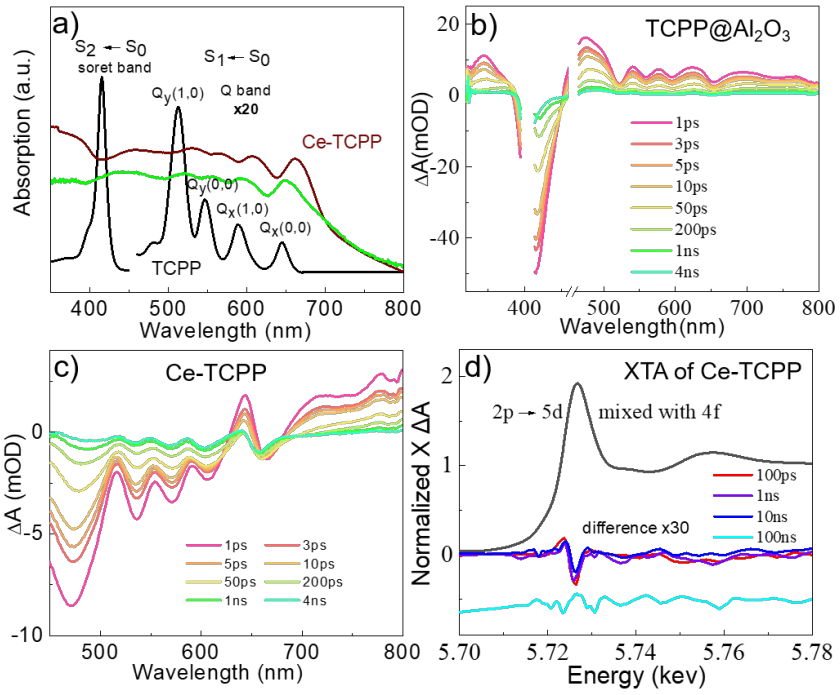

Figure 17. (a) UV-visible absorption spectra of TCCP ligand in methanol (black), TCCP solid DR-UV-Vis (blue) and Ce-TCCP MOF DR-UV-Vis (red). (b) Femtosecond transient absorption of TCCP ligand-sensitized Al_2O_3 under 400 nm excitation and (c) Ce-TCCP drop-cast film. (d) XTA at the Ce L3 edge using 490 nm excitation at various delay times. The difference spectra are the laser-on minus laser-off spectra enlarged by a factor of 30. Provided by the authors of .[104]

Yang et al. reported a photophysical study on a cerium-based MOF with a tetrakis(4-carboxyphenyl)porphyrin ligand (TCCP).[104] Owing to the porphyrin linkers, the MOF has a high extinction coefficient at wavelength range 400 – 700 nm and therefore potential applications in photocatalysis, especially given the ligand-to-cluster charge transfer (LCCT) identified in this work. Steady-state XANES measurements suggested a Ce^{3+} oxidation state in the as-prepared material compared to the Ce^{4+} oxidation state of the precursor. Femtosecond transient absorption experiments showed an elongated excited state lifetime in the MOF drop-cast onto

glass from ethanol in comparison to the porphyrin linker control (TCCP-sensitized Al_2O_3). (Figure 17b-c) XTA experiments using 490 nm excitation were performed at the Ce L_3 edge corresponding to the $2p_{3/2}$-5d transition (Figure 17d) with the sample dispersed in an acetonitrile jet. A clear difference signal corresponding to a shift of the Ce L_3 edge to lower energy was consistent with reduction of Ce^{3+} to Ce^{2+} via an LCCT mechanism and persisted for at least tens of nanoseconds, revealing a long-lived LCCT state. The observation of the quasi-instantaneous difference spectrum (100 ps spectrum, as the technique has approximately 100 ps instrument response) is consistent with the spectral evolution observed in femtosecond-TA experiments suggesting that the initial ligand-centered excitation in Ce-TCCP relaxes to the LCCT state on a sub-100 ps timescale. The evolution of the XTA difference spectrum lineshape from 100 ps to longer delays is consistent with electronic or structural relaxation after LCCT. The observed photophysical phenomena for Ce-TCCP suggest applicability to multi-electron photocatalytic processes.

Another report from Yang et al. investigated a modified UIO-67 based photocatalyst for photocatalytic hydrogen generation via the proton reduction reaction.[105] UIO-67 is a zirconium-based MOF known to be stable under catalytic conditions. The biphenyl linkers of UIO-67 were replaced with bipyridine linkers bearing light-absorbing chromophores $[Ru(dcbpy)(bpy)_2]^{2+}$, where dcbpy is the dicarboxylate bipyridine used as the linker and bpy are the ligands on the inorganic chromophore. Additionally, $Pt(dcbpy)Cl_2$ moieties were incorporated as catalysts in catalytically active samples. Femtosecond transient absorption spectroscopy revealed spectral differences and a faster excited state quenching process in samples that incorporated the catalytic $Pt(dcbpy)Cl_2$ moiety compared to those with only the chromophore, suggesting the

possibility that charge transfer from the chromophore to the catalyst occurred. For the transient absorption experiments, the samples were suspended in Nafion polymer and drop-cast to form homogenous films and to improve the light transmission. The inferred charge transfer process was confirmed by performing XTA at the Pt L_3 edge, which showed reduction after photoexcitation at 480 nm in an acetonitrile jet. The photophysical finding provided direct evidence that charge transfer from the chromophore to the catalyst occurred in the MOF, which served the role as a stable structure to orient the moieties for the favorable charge transfer process and resulting photocatalytic activity.

6. Photoconductivity

MOFs are formed by metal nodes separated by organic linkers, making conductivity rather unintuitive. However, the previous sections demonstrated that excited charges can be transferred within a MOF, hence ground state charge transfer – aka conductivity – could also occur. In a typical structure, metal nodes separate spatially-distant and non-isoenergetic linkers thereby prohibiting band-like charge transport that is the hallmark of conductors and semiconductors. In recent years, this inherent characteristic has been overcome by engineering MOFs with charge transport bands. Generally, such bands can be designed by utilizing spatially overlapped ligand species in a through-space approach or by designing isoenergetic bands through ligands and metals in a through-bond approach. Several important review articles have covered the current breadth and challenges in the field of conductive MOFs.[106-108]

In particular, semiconducting materials can be photoconductive because bandgap excitation populates bands where charges are mobile. Thus, photoconductive MOFs are of

interest for development in the many areas where semiconductor light harvesters or active layers are used. Time-resolved techniques are generally useful for probing the photoconductivity of materials by using a probe that is sensitive to mobile charges. It should be clarified that these techniques cannot differentiate between an electron and a hole. While the effective mass of electrons is smaller than that of a hole in most materials (i.e. electron mobility is larger), this characteristic is not universal to all materials.

6.1. Overview and Time-Resolved Techniques Applied

The two techniques applied to study photoconductive MOFs are time-resolved microwave conductivity (TRMC) and time-resolved THz spectroscopy (TRTS). Unlike TA techniques, the long wavelength probe is more easily transmitted through MOF samples and is not scattered, removing some limitations on sample thickness. Each technique samples the broad-band AC conductivity in their respective energy regions by means of absorption with and without a pump pulse, as photogenerated mobile charges attenuate the radiation in both the microwave and THz energy ranges. Over time, the mobile charges may relax to lower-lying non-mobile states, recombine, or trap, each of which can result in decay of the signal and yields a transient kinetic trace similar to those observed in TA experiments. TRTS can further be performed in a frequency-dependent manner to obtain frequency and phase information for the complex photoconductivity, allowing for modelling, typically with classical models such as the Drude or Drude-Smith models, to extract further information. A final pull for spectroscopic photoconductivity techniques is that they are contact-free and not susceptible to anisotropy (in

a non-oriented sample), thereby overcoming many difficulties related to DC conductivity methods, and even further they provide time resolution to the measurement. While the field of conductive MOFs is growing, such spectroscopic conductivity techniques will be important in order to understand and engineer the next generation of photoconductive MOFs.

6.2. Photoconductivity via TRMC

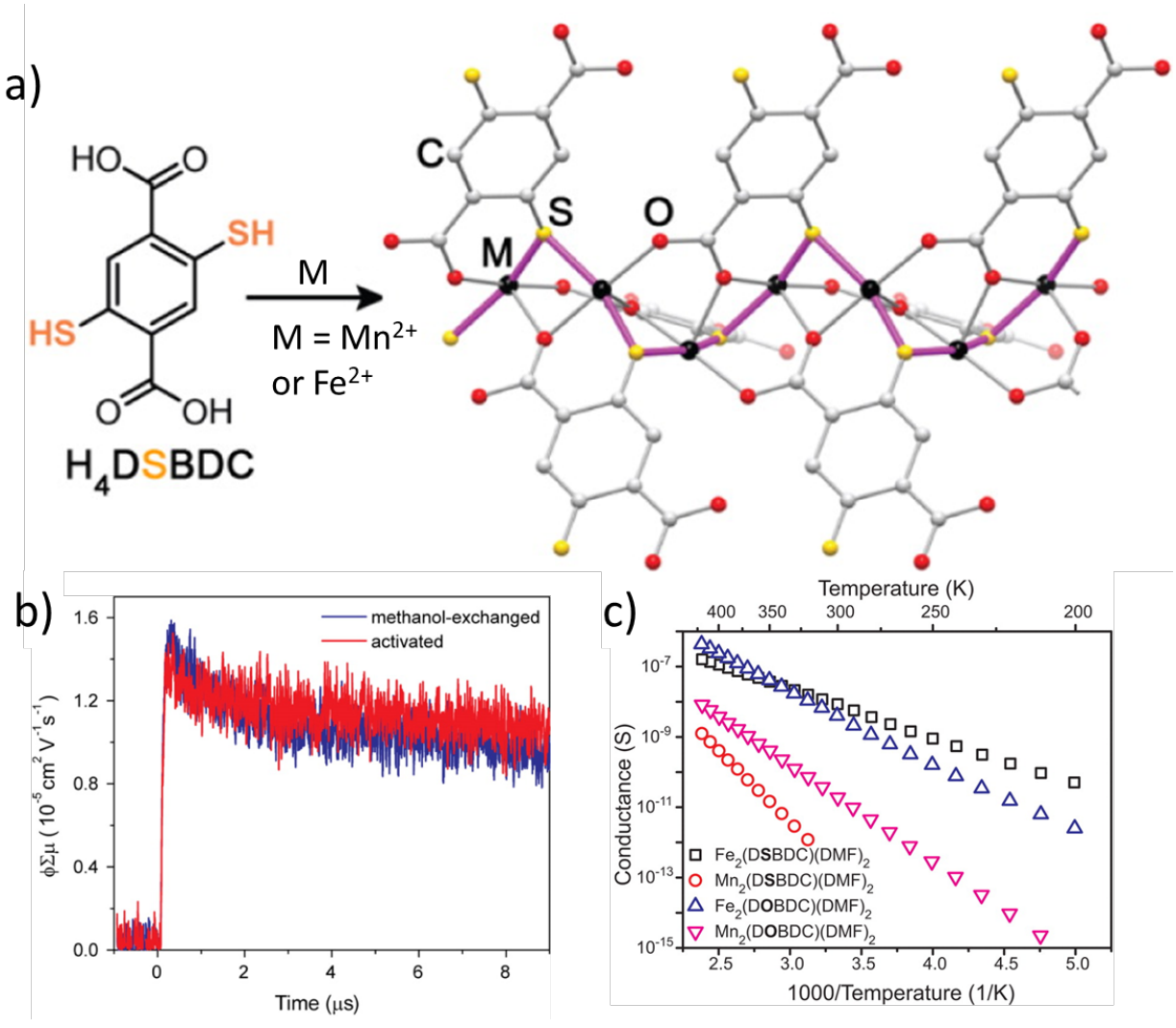

Figure 18. Synthetic scheme for preparation of M_2DSBDC conductive MOF with proposed infinite -M-S-M-S- charge transport pathway illustrated in violet. (b) Time-resolved microwave conductivity of Mn_2DSBDC. (c) DC temperature-conductance chart for M_2DSBDC and MOFs with similar structure but modified linkers and metal nodes. Adapted from Sun et al.[109,110], Copyright 2013 and 2014 ACS.

The first photoconductive MOFs were published in two studies from Sun et al. in which the authors investigated a MOF structure developed using 2,5-dithiolbenzene-1,4-dicarboxylic acid linkers and either Mn^{2+} or Fe^{2+} metal nodes.[109,110] As shown in Figure 18a, the MOF forms a continuous -M-S-M-S- chain that has been suggested to be the charge transport pathway. In the Mn^{2+}-based MOF Mn_2DSBDC, the photoconductivity was investigated via flash photolysis time-resolved microwave conductivity (TRMC). It should be noted that the samples were prepared by suspending the MOF in poly(methylmethacrylate) (PMMA), which was then drop-cast onto quartz substrates forming a 6-10 µm thick film The measured MOFs were either methanol-exchanged (i.e. containing methanol guest molecules) or activated (containing no guest solvent atoms). The TRMC traces for both cases (Figure 18b) are essentially identical within the time window. The instrument response is on the order of hundreds of nanoseconds. A follow-up study did not involve TRMC however explored the conductivity of structural variants where “S” was replaced with “O”, and/or Mn^{2+} was replaced with Fe^{2+}.[110] From the DC conductivity data (Figure 18c), it can be seen that each replacement has an effect on the conductivity. In disagreement with the TRMC results in the earlier study, the DC conductivity showed that Mn_2(DOBDC) has superior conductivity to Mn_2(DSBDC). This highlights several differences in the measurements

because spectroscopic TRMC measures a more localized AC photoconductivity while DC conductivity measures long-range conductivity in the ground state.

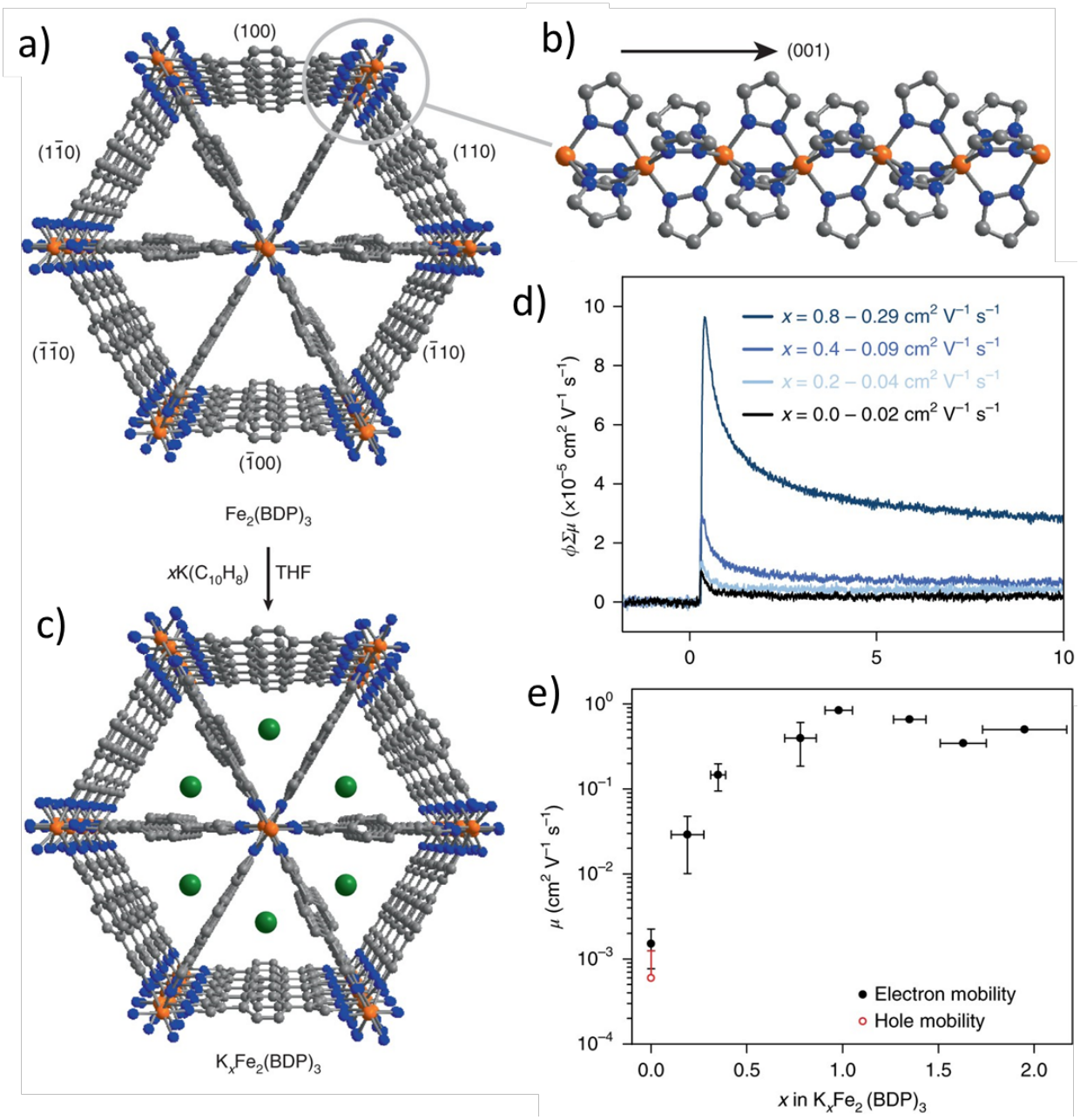

Figure 19. (a) Structure of pristine $Fe_2(BDP)_3$ MOF and (b) depiction of charge transport pathway. (c) depiction of $K_xFe_2(BDP)_3$ having reductively inserted potassium ions. (d) Conductivity transients measured by TRMC with 355 nm excitation at 6.5x10^{15} photons cm^{-2} for $K_xFe_2(BDP)_3$ (*x*

= 0, 0.2, 0.4, and 0.8). (e) Measured electron and hole mobilities in FET devices for different potassium concentration. Figure supplied by the authors of Aubrey et al.[111].

The influence of mixed valency was explored by Aubrey et al. study on $Fe_2(BDP)_3$, where BDP^{2-} = 1,4-benzenedipyrazolate, making the native Fe oxidation state Fe^{3+} (Figure 19a).[111] The authors hypothesized that mixed Fe^{2+}/Fe^{3+} valency would contribute significantly to conductivity within the proposed transport chain (Figure 19b). To this end, a series of mixed-valency MOFs were prepared by controlled reductive insertion of potassium ions, where a higher amount of potassium indicates a higher electron doping in order to maintain overall charge neutrality. The MOFs are denoted $K_xFe_2(BDP)_3$ with x = 0, 0.2, 0.4, or 0.8 and a depiction is shown in Figure 19c. The TRMC data is highly supportive of mixed valency leading to an increased photoconductivity as shown in Figure 19d, with the charge mobilities reported in the legend therein. For the measurement, each of the MOFs was suspended in a poly(methylmethacrylate) (PMMA) films cast onto quartz substates. The authors demonstrated that controlled reduction increases the photoconductivity by an order of magnitude, measured using TRMC. By using single microcrystal field effect transistor (FET) devices on interdigitated electrodes, the electron mobilities for each of several MOFs with varying potassium concentration were determined (Figure 19e). The result is in agreement with the TRMC photoconductivity results and confirm that the TRMC spectroscopic measurement is indeed probing the conductivity of the MOF.

A SURMOF, similar to those discussed previously in Section 4 (MOF grown on a substrate in a layer-by-layer deposition process), was made by Liu et al. from Zn nodes and either free-base or Pd tetraphenyl porphyrins with two opposed carboxylate linkers on meso-linked phenyl groups.[112] Each were incorporated into photovoltaic devices where better performance was

observed for the Pd-SURMOF compared to the free porphyrin version. Several techniques provided photophysical insights and helped to understand the excited state dynamics and the photoconductivity of the free-base- or Pd-SURMOFs grown. Time-resolved photoluminescence of the dry films showed that the Pd-SURMOF had an IRF-limited singlet emission lifetime that was shorter than that of the free-base-SURMOF, likely due to enhanced intersystem crossing to a non-emissive triplet state due to enhanced spin-orbit coupling with Pd. Femtosecond transient absorption measurements on the dry films with 400 nm excitation showed a spectral evolution on an ultrafast timescale for the Pd-SURMOF followed by the formation of a long-lived state. The free-base-SURMOF had a slightly slower decay but also formed a long-lived state. Each of these support that a long-lived triplet state is likely responsible for the photovoltaic behavior. The photovoltaic results also suggest that mobile charges are generated in the SURMOF, which was investigated with TRMC. Each of the free-base- and Pd-SURMOFs measured as dry films yielded a TRMC decay after 355 nm photoexcitation confirming that they exhibit photoconductivity. Nanosecond transient absorption measurements with 355 nm excitation probed the triplet state of each MOF and the kinetic traces directly overlaid with those of the TRMC measurements, suggesting that the triplet state formed is conductive throughout its lifetime, explaining the photovoltaic performance of the SURMOF-based devices. This work is a particularly strong example of combining several complementary techniques to thoroughly investigate light-initiated dynamics in a conductive MOF, and the authors were able to measure the same type of sample with each technique (i.e. a dry film) because of the high-quality SURMOF film preparation procedure, which is quite different from studies that rely on a bulk powder sample.

Tetrathiafulvalene is a well-known conductive organic molecule that forms π-stacked assemblies of mixed-valence character in air due to photooxidation. Harvesting these properties Narayan et al. synthesized a tetrathiafulvalene-based conductive MOF (Zn_2TTFTB; where TTFTB – tetrathiafulvalene tetrabenzoate).[113]. The prepared MOF (see Figure 20a in Section 6.3 below) has helically-arranged tetrathiafulvalene columns running through the structure that provide conductivity pathways through overlapping S atom orbitals. The photoconductivity of Zn_2TTFTB was investigated using TRMC. Zn_2TTFTB MOF and the protonated ligand H_4TTFTB were prepared as poly(methylmethacrylate) (PMMA) films on quartz and measured under 355 nm excitation. Each exhibited photoconductivity with the MOF showing an overall larger signal with similar dynamics to the ligand. The H_4TTFTB ligand in PMMA was further measured using transient absorption with 355 nm excitation, which showed a long-lived feature on the timescale of the photoconductivity. The MOF could not be measured due to probe scattering in the visible probe range, which is not an issue in the low-energy microwave TRMC measurements. This study highlights the importance of integrating structural design with time-resolve spectroscopic techniques in order to understand important photoinduced properties for the design of conductive MOFs.

6.3 Photoconductivity via TRTS

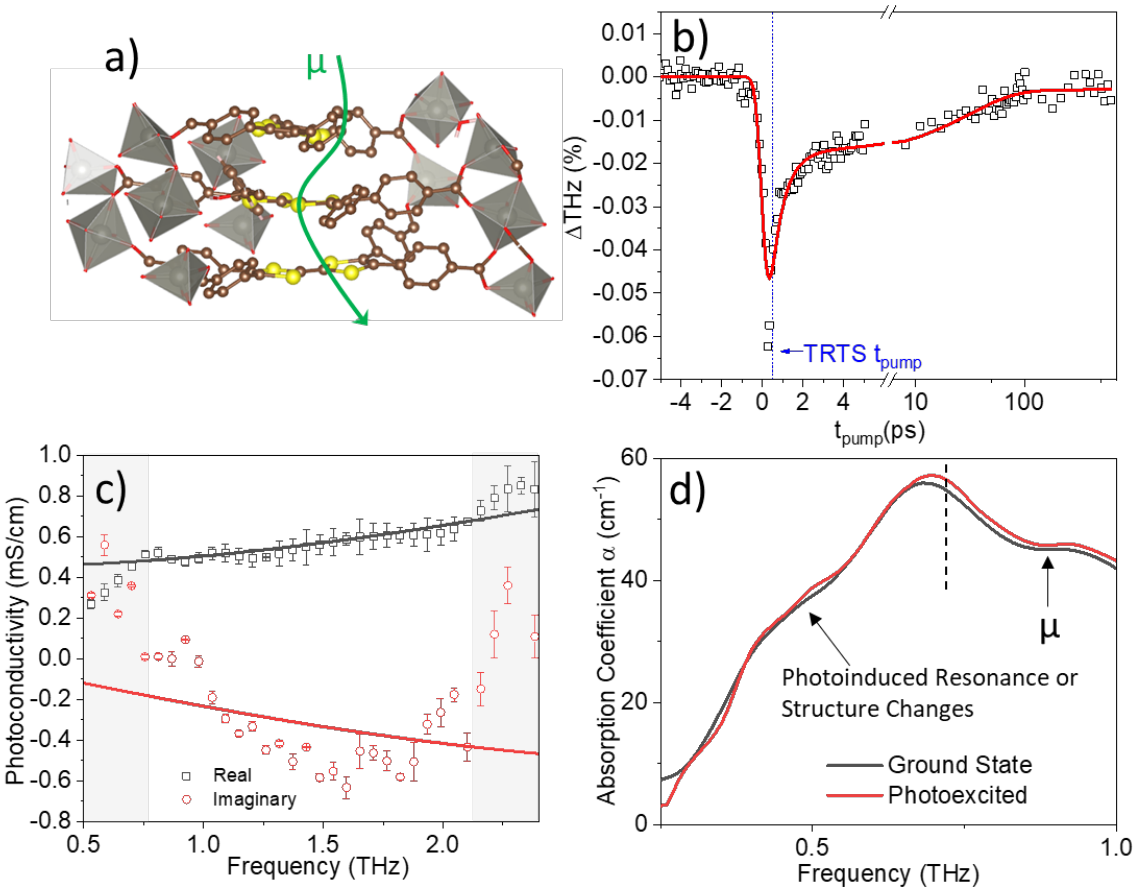

Figure 20. (a) Depiction of Zn_2TTFTB and the proposed photogenerated charge transport pathway. (b) Representative optical pump THz probe trace and triexponential best fit. (c) TRTS Photoconductivity data collected at a pump delay of 500 fs with Drude-Smith best fit results. The grayed-out region is not included in the fit due to resonance changes (at low energy) and instrument bandwidth (at high energy). (d) The resonant changes observed below approximately 0.75 THz are shown with the ground state compared to photoexcited absorption coefficient. At energies above the dashed line, the offset is ascribed to photoconductivity. Adapted from Pattengale and Neu et al.[114], Copyright 2019 ACS.

Building on the previously reported TRMC results on Zn_2TTFTB, Pattengale and Neu et al. used TRTS to gain insight on the ps dynamics in this MOF, inaccessible to TRMC experiments.[114] In this study the authors also developed a method to measure the as-prepared bulk powder without a potentially interfering (PMMA) matrix. Optical pump terahertz probe was performed with 400 nm excitation (Figure 20b), revealing rich photoconductivity dynamics on a subpicosecond, approximately 30 ps, and a longer timescale as modeled by a triexponential function convoluted with a gaussian instrument response function of 0.6 ps. At a delay time of 500 fs, corresponding to a reasonably large signal and long enough after time zero to exclude non-linear pump-probe interaction, frequency dependent TRTS was measured under unchanged pump conditions. The frequency-dependent photoconductivity (Figure 20c) was well-modeled with the Drude-Smith equation, validating that the observed traces are indeed due to conductivity. One insight gained from the Drude-Smith fit is that charge transport in the structure is likely strongly influenced by grain boundaries which could be inherent to the structure, or are potentially indicative of defects. The low-energy region of the absorption spectrum (Figure 20d; 0.3 – 0.75 THz), which is well within the spectrometer bandwidth, exhibited changes in the prominent resonant feature indicating that the MOF potentially has photoexcited structural changes. This aspect has piqued our interest and may have relevance in future applications of TRTS as outlined in Section 8.3.

Alberding et al. reported the first TRTS study on MOFs, namely Cu_3(1,3,5-benzenetricarboxylate)$_2$ (HKUST-1) and Cu[Ni(pyrazine-2,3-dithiolate)$_2$].[115] Neither of these MOFs are conductive unless intercalated with a redox-active species, which the authors proceeded to prepare with 7,7,8,8-tetracyanoquinodimethane (TCNQ) or iodine. The MOF

samples in this study were pressed on top of THz-transparent polyethylene pellets and measured with 400 nm excitation. Three MOFs, denoted as Intercalant@MOF, yielded photoconductivity: $TCNQ^-$@HKUST-1, $TCNQ^-$@Cu[Ni(pdt)$_2$], and I_3^-@Cu[Ni(pdt)$_2$]. For each, the photoconductivity was relatively short-lived and decayed almost fully within 2 ps.

Dong et al. performed TRTS studies on the 2-dimensional MOF $Fe_3(THT)_2(NH_4)_3$ (THT = 2,3,6,7,10,11-triphenylenehexathiol).[116] The MOF was prepared as a free-standing film material with no substrate support, making the interpretation potentially more straightforward. The photoexcitation used was 800 nm and the photoconductivity exhibited a biphasic decay largely on a picosecond timescale. The TRTS results were compared closely with DC conductivity results to gain insights into the photoconductivity mechanism. Temperature dependence in neither the carrier mobility nor the carrier density was observed in TRTS experiments. The lack of change in the carrier mobility suggested that there is a dominant mechanism limiting the mobility at all temperatures, such as grain boundaries or defect scattering. The DC conductivity showed an expected decrease in carrier density with temperature because thermal population is required for ground state conductivity.

In addition to conductivity in the excited state (i.e. photoconductivity), THz spectroscopy has been applied to obtain ground-state photoconductivity information. While not technically time-resolved, an ultrafast pulsed laser is required to obtain sufficient temporal resolution to measure the time-domain terahertz transmission data. Pattengale and Neu et al. measured the ground state conductivity of Mn_2DSBDC and cation-exchanged analogues with Cu^{2+}, Co^{2+}, or Ni^{2+} atoms replacing Mn^{2+} at approximately 10 at%.[43] The samples were prepared as pressed pellets with a known mass mixed in a THz transparent host material (PTFE). It was determined that cation

had a negligible effect on the conductivity, suggesting that the exchanged materials may offer functionalization while retaining the conductivity property important for applications. For each, the complex permittivity was fit using the Drude-Smith equation to describe the photoconductivity mechanism. These results showed that the conductivity in Mn_2DSBDC and its cation-exchanged analogues is mainly limited by defect or grain boundary scattering. This work showed that THz spectroscopy can be applied to investigate ground state conductivity and that, in combination TRTS, THz spectroscopy can measure both ground-state and excited-state conductivity in MOFs.

While only a few examples of applying TRTS to investigate conductive MOFs exist so far, we expect it to be an important technique that will be applied in the future because it is the only spectroscopic conductivity technique that can obtain subpicosecond time resolution. We have excluded one report from this section to cover it in the separate Section 7 to follow.

7. Interplay Between Carrier Localization and Delocalization

We include this section to highlight a single report involving our group which brings together the concepts introduced up to this point and assembles the most complete grouping of techniques reported thus far to give a comprehensive overview of the light-initiated dynamics in a 2D conductive MOF. The motivation is not to disproportionately highlight our own research, but rather to provide discussion about the relationship between carrier localization and delocalization as a function of probe wavelength, which has vast implications on understanding many functional aspects of such MOFs in photoactive devices. We will highlight both the

strengths and weaknesses of the methods and sample preparations used, which often place a functional limit on such investigations.

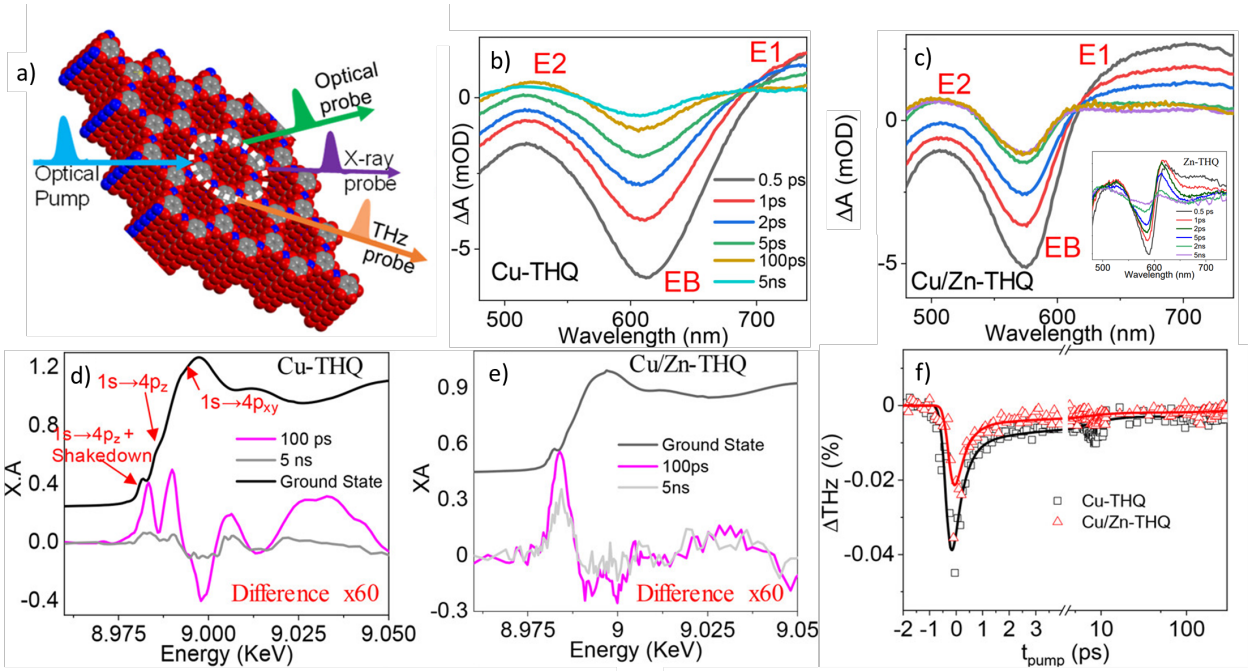

Figure 21. (a) Cartoon depicting the employed time-resolved techniques to Cu-THQ, Cu/Zn-THQ, and Zn-THQ MOFs. (b) Cu-THQ and (c) Cu/Zn-THQ fs-TA spectra excited at 450 nm. Exciton bleach (EB), positive feature (E1), and positive feature (E2) are highlighted. E1 is attributed to electron absorption from lower to higher levels in the CB. E2 negligibly contributed to photoconductivity and could originate from interlay excitons from π-π conjugation. Inset of (c) is Zn-THQ data. (d) Cu-THQ and (e) Cu/Zn-THQ difference XANES spectra at Cu K-edge using 400 nm excitation. (f) Optical-pump THz probe traces using 400 nm excitation. Adapted from Nyakuchena et al.[117], Copyright 2020 ACS.

The highlighted study by Nyakuchena et al., including the authors of this review, investigated 2D MOFs based on tetrahydroxy-1,4-benzoquinone (THQ) ligands and either Cu, Zn, or a mixture of Cu and Zn (Cu-THQ, Zn-THQ, and Cu/Zn-THQ, respectively).[117] Cu-THQ was known

to be a conductive MOF, and based upon its structure it has two potential conductivity pathways – either an in-plane mechanism (through-bond conductivity) or an out-of-plane mechanism involving carrier transport between MOF layers (through-space conductivity).[118] The MOF was investigated using a combination of three techniques that (discontinuously) span the entire breadth of probe frequencies discussed throughout this review, excluding microwave which cannot be pushed to sufficient time resolution. The report also includes computational support, which provided important understanding but will not be discussed here in view of the focus of this review.

The three techniques utilized in this study were fs-TA in the visible range, XTA, and TRTS (Figure 21a). XTA provides the most localized perspective by probing the constituent metal atoms individually. On quite literally the other end of the spectrum, the THz probe measures only delocalized (mobile) charges. Between these frequency ranges, fs-TA in the visible frequency regime provides an interesting intermediate perspective because both localized and delocalized signals are often observed in this region of the spectrum. Often, localized signals yield more energetically-localized features (peaks) while delocalized signals that may probe tightly-spaced intraband transitions have less-localized, broad features. This is not a hard and fast rule in materials partly due to heterogeneity, among other factors. Therefore, care must be taken to provide the most relevant comparisons between samples in order to make conclusions.

Beginning with the fs-TA results, a 450 nm pump was used to excite each of the MOFs which have broad UV-Visible absorption into the NIR with stronger NIR absorption in Cu-containing MOFs. The transient absorption spectra are shown in Figures 21b-c, at various time delays out to the spectrometer limit of 5 ns (legend in Figure 21b). The overall spectral shape in

each tends to be defined within the first picosecond followed by decay. Interestingly, the spectra shape is highly dependent on the metal node. Zn-THQ (inset of Figure 21c) gives a narrow exciton bleach feature akin to those observed in quantum dots which feature spatially-constrained electron-hole pairs.[119-121] In Cu-THQ (Figure 21b), a much broader exciton bleach is observed consistent with carrier delocalization. Cu/Zn-THQ (Figure 21c) yields an intermediate breadth implying that Zn plays a role in limiting delocalization. It should be noted that Zn^{2+} is a d^{10} ion that is quite redox-inert due to its closed shell and therefore may inhibit through-bond transport. The fs-TA studies were performed on dry drop-cast MOF films on SiO_2.

XTA provides a more localized perspective on the photoinduced charge density. The Cu K-edge in Cu-THQ and Cu/Zn-THQ was probed (Figures 21d-e). In the steady state, each MOF features a 1s-$4p_z$ transition and a 1s-$4p_{x,y}$ transition separated in energy owing to the planar structure. With photoexcitation, Cu-THQ shows electron localization (reduction) in both the 1s-$4p_z$ and 1s-$4p_{x,y}$ orbitals while Cu/Zn-THQ shows a difference only in the 1s-$4p_z$ indicating that the presence of Zn reduces the in-plane delocalization of photogenerated carriers in the MOF leading to localization on the 1s-$4p_z$ orbital. It should be noted that the time resolution of synchrotron-based XTA is approximately 100 ps, however fs-TA did not observe significant spectral evolution from time zero to 100 ps and therefore XTA probes this species throughout its decay. It should be noted that the sample preparation for XTA is quite different, as the sample is suspended in acetonitrile to prepare a continuous jet. The dry sample is not measured because significant pump heating has a pronounced effect on local structure and cannot be easily separated from electronic effects. The solvent homogenously disperses the MOF and acts as a dissipation

medium. However, this necessary preparation does potentially influence comparability to the other techniques that were performed on dry samples.

Finally, TRTS was performed on dry powder samples using 400 nm excitation (Figure 21f). Cu-THQ and Cu/Zn-THQ give a measurable photoconductivity signal while Zn-THQ (not shown) does not yield a measurable signal. In agreement with fs-TA and XTA, higher photoconductivity (roughly 2x larger) is seen in Cu-THQ compared to Cu/Zn-THQ, while their dynamics are similar. A major portion of the photoconductivity decays within a few ps to form an overall less-conductive or non-mobile state with slight baseline offset. From the fs-TA and XTA, this state still has variable delocalization depending on the node composition.

As we point out, it was not possible to maintain the exact same sample preparation for each measurement due to measurement limitations, however a best effort was made to use similar conditions where possible. Furthermore, it would be excellent to use a higher time-resolution XTA measurement at a free-electron laser (FEL) source in order to probe both the high-conductivity and low-conductivity states revealed in TRTS with picosecond resolution. However, as we point out elsewhere, there have not yet been any reported FEL studies on MOFs thus far. As a whole, the results demonstrate that each technique provides a unique perspective on more delocalized and localized aspects of the MOF after photoexcitation, which coexist and contribute to the light-initiated dynamics.

8. Structural Dynamics

As another consequence of their structure, MOFs are soft materials meaning that they are deformable and may be altered by thermal fluctuations and external pressure.[122] To a

spectroscopist, this begs the question of whether or not dynamic structural information can be obtained in MOFs using time-resolved techniques. The probe in such experiments needs to report on a specific or inferred structure change in a MOF or structural components thereof.

8.1. Overview and Time-Resolved Techniques Applied

One potential technique to probe structural dynamics which has not been, to the best of our knowledge, published on for MOFs is time-resolved powder X-ray diffraction. Synchrotron facilities provide ca. 100 ps X-ray pulses that can be synchronized with a laser excitation to provide time-resolved diffraction data. Such data would be sensitive to bulk structure changes, such as unit cell contraction or expansion, or potentially to photoinduced phase changes. In lieu of such results to discuss, X-ray transient absorption (XTA) can provide local structure changes at varying time delays (i.e. dynamics), however it is currently extremely difficult to collect such data efficiently enough to be conclusive. For instance, inferred structure changes were observed in the XANES region of ZIF-67,[21] however collecting extensive EXAFS data to quantify the changes at various delay times would be insurmountably challenging due to signal to noise partly due to needing to measure the sample as a powder suspended in a solvent jet. In molecular systems, such time-resolved EXAFS investigations are possible.[44]

Interestingly, there is a report of using electron paramagnetic resonance (EPR) with a guest molecule reporter to investigate temperature-induced structural changes in MOFs.[123] This opens the possibility of time-resolved EPR as a potential strategy in certain cases, such as with a guest molecule reporter in a MOF that does not give background signal in order to infer photoinduced structural changes. In MOFs that are not EPR-silent, it could be difficult to infer

structural changes if oxidation state changes at nodes or ligands interfere due to a charge transfer mechanism which was observed in many of the MOFs discussed herein.

In certain MOF structures having a strong oscillator or incorporating a molecular reporter, it has been possible to apply time-resolved IR spectroscopy to investigate structural dynamics in MOFs. The few existing examples will be described and may suggest an important role of time-resolved IR spectroscopy to MOF photoinduced structural dynamics. We then further suggest that the far-infrared region of the spectrum (i.e. THz) that probes low-energy collective motions may be particularly suited to such time-resolved structural dynamics investigations, based upon the steady-state examples existing in the field. A recent review highlighted static spectroscopic techniques exploring structural properties, motivating the potential for future and ongoing research on a variety of pump-probe structural techniques.[123]

8.2. Studies Utilizing Time-resolved IR spectroscopy

The work by Santaclara et al. on NH_2-MIL-125(Ti) included time-resolved IR spectroscopy and was described in detail in Section 5.2.b.[78] However, it is worth reiterating here briefly that the authors were able to probe the N-H stretches of non-coordinated NH_2 moieties on the ligands of the MOF as well as C-N and C-C_{ring} stretches. The MOFs were measured in IR-transparent $CHCl_3$ solvent. Each of these modes was found to be highly correlated with the electronic excitation and, interestingly, different relaxation kinetics/dynamics were observed in C-N vibrations compared to C-C_{ring}, suggesting a different electronic environment and likely photoinduced structural distortions associated therewith.

With particular relevance to photocatalytic moieties incorporated into MOF linkers, Blake et al reported a time-resolved IR study on MOFs incorporating Re(2,2'-bipyridine)$(CO)_3$X where X

is Cl or Br as a linker and Mn as the node.[124] The relatively intense C-O stretches in CO were probed via picosecond time-resolved IR spectroscopy on MOFs pressed in KBr discs. After photoexcitation, an MLCT band was observed in addition to an instantaneously formed π- π* feature, the former of which decays fully to the latter with a 20 ps time constant. The ^{3}π- π* state is typically not accessible in solution due to its energetic position higher than the ^{3}MLCT state, the ordering of which is shown to be switched within the MOF environment. As a result, interesting chemistry at the ligand site was accessed, leading to a *fac*- to *mer*- isomerism, which was confirmed with steady-state experiments including single-crystal X-ray structures. This isomerism is a structural change observed dynamically via time-resolved IR spectroscopy and represents, to the best of our knowledge, the first dynamic structural information captured in MOFs.

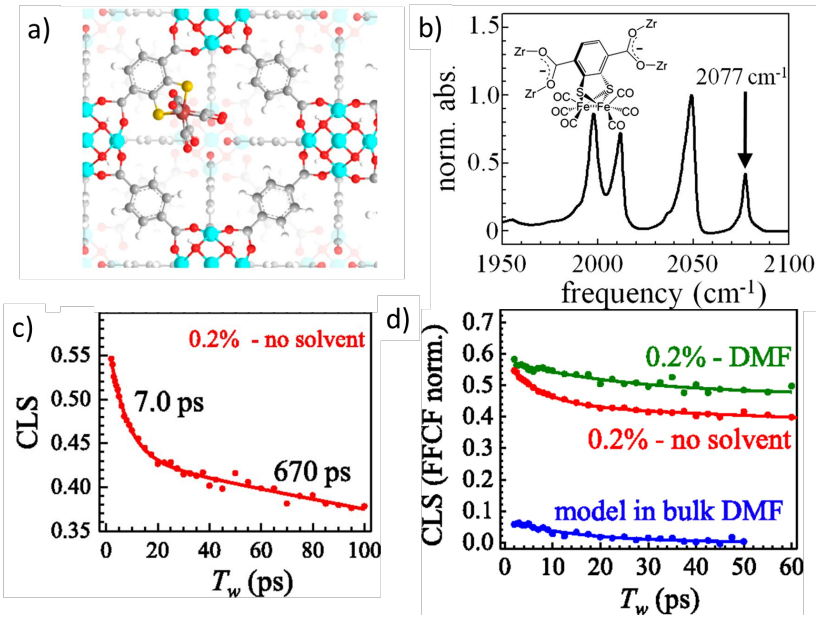

Figure 22. (a) Structure depiction of the functionalized UiO-66 MOF. (b) Linear IR absorption spectra for four IR-active C-O stretching modes of the functionalized UiO-66 MOF without solvent. The arrow at 2077 cm^{-1} points to the peak selectively excited using a shaped pulse. (c) The center line scope (CLS) decay method is used for the 0.2 % sample, which is free of excitation transfer due to isolated vibrational probes and the decay therefore arises from MOF structural fluctuations. (d) CLS data in DMF solvent compared to no solvent. Adapted from Nishida et al.[125], Copyright 2014 National Academy of Sciences.

Nishida et al. performed the first time-resolved 2D-IR experiments to observe structural dynamics in the Zr-based UiO-66 MOF (Figure 22a).[125] One interesting aspect that will be further discussed is the observed effect of solvent guest atoms that must be considered in many aspects of MOF characterization, including dynamic structural studies. In order to perform these studies, a percentage, namely 14%, 2.5%, or 0.2 %, of the benzenedicarboxylate linkers were replaced with [FeFe](dcbdt)$(CO)_6$(dcbdt =1,4-dicarboxylbenzene-2,3-dithiolate) vibrational probes. This complex was used because the CO modes are relatively strong and have long vibrational relaxation lifetimes. 2D IR vibrational echo spectroscopy was performed using a shaped pulse tuned to 2070 cm^{-1} to selectively excite the 2077 cm^{-1} mode (Figure 22b). Dynamic information was extracted using the center line slope method (CLS) and are presented with the CLS as the Y-axis as a function of delay time T_w which is the arrival time of a read-out pulse that generates the vibrational echo signal. A dependence in the CLS decay time was observed based upon the concentration of vibrational probes which was ascribed to Förster vibrational excitation transfer at high vibrational probe concentration. At 0.2% (Figure 22c), the vibrational probes are sufficiently isolated to avoid such excitation transfer and the CLS decay is attributable to

structural dynamics. Furthermore, it was observed that introduction of solvent (DMF) led to a change in the structural dynamics (Figure 22d). This study shows that, with an appropriately designed system, 2D IR is well suited to obtain dynamic structural information in MOFs on ultrafast timescales.

In another work, Nishida et all applied both a more general IR pump-probe technique and time resolved 2D-IR to investigate guest molecule hydrogen bond dynamics in MIL-53(Al), which is constructed from benzene-1,4-dicarboxylate and Al^{3+} nodes.[126] The structure contains μ_2-OH bridging hydroxyls on ligand oxygen atoms interconnecting Al^{3+} ions that were deuterated to provide spectrally separated μ_2-OD stretches in the 2635-2735 cm^{-1} energy range that are within the tunable range of the infrared pump and probe pulses. Steady-state IR showed that the peak position of the μ_2-OD shifted based upon hydrogen bonding with the guest molecule, which was wither benzonitrile (BzCN), phenyl selenocyanate (PhSeCN), benzene, or cyclohexane. Each was shifted to an energy lower than that of the non-guest infiltrated MOF. Pump-probe IR experiments showed an excellent correlation between the peak positions and the relaxation rate, with a faster decay being associated with a stronger hydrogen bonding interaction due to enhanced coupling to the guest molecule thereby providing further modes for energy dissipation. In the case of the empty MOF, which gave the slowest decay, the energy must be dissipated through μ_2-OD bend and O-Al vibrational modes because no coupled hydrogen bonding partner is present. If such modes are energetically disparate from the μ_2-OD stretch, then lattice phonons would be required for relaxation. 2D-IR experiments probed the homogeneity in spectral diffusion using the CLS method, which showed a biphasic decay with a < 2 ps component dependent upon hydrogen bond strength and an additional >100 ps component in some

instances. A weak trend based upon the hydrogen bonding strength could not be made for the long time-scale component, especially with benzene exhibiting an exceptionally slow decay. This may have been due to adopting a range of different configurations, leading to further inhomogeneity.

8.3. Potential Applications of TRTS

One intriguing aspect of structural dynamics studies is the degree of localization that is probed in a given energy range. Time-resolved IR, for instance, can observe specific modes associated typically with two or slightly more atoms, depending on their structure in the system. Clearly, 2D-IR has been demonstrated to be powerful in observing the homogeneity of structural dynamics, which indirectly probes a larger collection of atoms. Time-domain terahertz spectroscopy, conversely, applies lower energy and therefore probes resonant and energetically-defined collective motions of many atoms. This technique has been applied to various crystalline systems,[127,128] and has been further applied to metal-organic frameworks.[129-132] In such studies, periodic boundary condition DFT is typically used to assign resonant absorption features to understand what motions are involved. MOF photoinduced structural dynamics have not yet been investigated using time-resolved terahertz spectroscopy (TRTS), but we see this as a technique ripe for development in this least-traversed area of light-initiated dynamics in MOFs. Visible-pump THz-probe experiments may be able to access distinctly different electronic landscapes in the material and probe electronic and structural contributions to THz-active modes. Temperature-controlled THz-pump THz-probe experiments may be further configurable to access dynamic structural information in the electronic ground state.

As a practical example, our group did observe clear photoinduced changes in a resonant feature in Zn_2TTFTB after visible light photoexcitation (Figure 20d in Section 6.3).[114] These changes were observed at room temperature and would be expected to be more pronounced with temperature control. However, Zn_2TTFTB is a conductive MOF and the photoconductivity overlaid with the resonant contributions, and this system is not likely the best starting point for developing the technique. As such, an ideal MOF to select for these endeavors would have only well-resolved resonant contributions to the THz spectrum. Without intending to pontificate further on the matter, the authors hypothesize that non-photoconductive Ni-porphyrin-based MOFs may be well-suited for such investigations, as Ni-porphyrins are well-known to rapidly convert to a d-manifold excited state that structurally deforms the porphyrin macrocycle – and a concerted deformation in a MOF structure may very well be observable since the energy transfer to the d-manifold excited state would likely simultaneously destroy conductivity and lead to pronounced structural changes.

It will furthermore be, as demonstrated in all aspects of the studies in this work, important to take guest atoms, such as solvent atoms, into account in materials preparation and analysis. While, ideally, multiple time-resolved techniques would be utilized to take advantage of their unique insights into the material, we believe TRTS will prove to be an important addition to the existing toolbox.

9. Conclusions and Future Outlook

Just as they draw compositional and structural characteristics from both molecular and solid-state materials, metal-organic frameworks (MOFs) harbor diverse and intriguing time-

dependent photoinduced dynamics that vary from localized (molecular-like) to delocalized (band-like). Exemplifying this, the MOF studies highlighted herein have investigated phenomena that have a highly localized contribution, such as energy transfer between discrete units or highly localized electronic signatures, and also phenomena that have a highly delocalized contribution, such as electrical conductivity or photoinduced structural dynamics. These characteristics set MOFs out as a truly unique class of materials requiring careful consideration in how to best approach their photoinduced dynamics.

While significant developments have been made in applying time-resolved techniques to MOFs, beyond the more abstract points above that remain equally important, we identify key experimental challenges to be overcome in order to best propel the field forward:

1. *Contribution of Guest Solvent Atoms* – Studies have been performed in conditions ranging from dry samples to solvated suspension samples. Coordinating solvent atoms typically used in MOF synthesis, such as DMF, have a tendency to remain in the structure after air or vacuum drying and have been shown to affect the photoinduced dynamics. Where possible, the degree of solvent incorporation should be determined and activated (solvent-free) samples should be additionally measured. Solvated suspension samples should be measured in solvents of varying polarity, taking into account hydrogen bonding, pH, and any other important characteristics that may alter the measurement.

2. *Matrix Effects* – Along the lines of point 1, several MOFs have been investigated in dried polymer suspensions such as Nafion or polystyrene. This is not often a first choice, but homogeneous dispersion of the sample and better refractive index

matching may improve transmission of UV-Visible-NIR for samples that are difficult to measure otherwise.

3. *Particle Size* – Reducing the particle size is another way to achieve better transmission in both dry and solvated suspensions. This may select for particle-size dependent phenomena, such as surface defect trapping, that would not be observed in larger particles. In the opposite direction, large homogenous single crystals of optical quality would also overcome scattering limitations. However, this approach is challenging and cannot be applied to arbitrary MOFs.

4. *Different Sample Preparation for Different Techniques* – Different sample preparations may be used for different techniques, making it more difficult to assemble a full picture of the light-initiated dynamics. While this fundamentally cannot be fully overcome in all aspects, researchers should identify which technique is the most restrictive in terms of sample preparation, and carry those conditions through the remainder of the measurements, where possible. Conclusions should be based upon the particular measurement conditions, or the certainty of conclusions should be tempered by highlighting any differences, unless control studies have shown the phenomena to be independent of the preparation conditions investigated.

The above challenges are exactly that, and set out the ideal conditions, which may or may not be reasonably achieved in a particular system. Researchers should take these points into account in order to approach these complex systems from a careful standpoint, thereby improving the quality and generality of any insights gained. Despite these challenges, the

application of time-resolved techniques to MOFs has provided extremely valuable insights thus far and will continue to be important as scientists further develop photoactive MOFs.

10. Abbreviations

B3LYP	Becke, 3-parameter, Lee-Yang-Parr, functional used for DFT
–bpy	2,2'-bipyridine
CCD	charge-coupled device, detector
CMOS	Complementary metal-oxide-semiconductor, detector
dcbdt	1,4-dicarboxylbenzene-2,3-dithiolate
dcbpy	2,2'-bypiridine 5,5'-dicarboxylate
DCM	dichoromethane
DEF	N,N-diethylformamide
DMF	N, N-dimethylformamide
FRET	Förster resonance energy transfer
GIWAXS	Grazing-Incidence Wide-Angle X-ray Scattering
GSB	ground state bleach
ITO	indium tin oxide

LCCT	ligand-to-cluster charge transfer
LCCT	ligand-to-cluster charge transfer
LMCT	ligand-to-metal charge transfer
LR-TDDFT	long range time dependent density functional theory
MIL	Materials of Institut Lavoisie
MLCT	metal-to-ligand charge transfer
NADC	4-amino 2,6-napthalenedicarboxylate
NDC	2,6-napthalenedicarboxylate
PBE	Perdew-Burke-Ernzerhof, functional used for DFT
PCN	porous coordination network
PCN	porous coordination network
phen	phenyl
PL	Photoluminescence
RuDCBPY	$[Ru(dcbpy)(bpy)_2]^{2+}$
SBU	single building units
Spiro-OmeTAD	2',7,7'-tetrakis(N,N-di-p-methoxyphenyl-amine)9,9'-spirobifluorene
SURMOF	Surface MOF (layer-by-layer deposited MOF film)
TA	Transient Absorption (spectroscopy)
TEOA	triethanolamine
TPDC	terphenyldicarboylate

TPP	tetraphenyl porphyrin
TR-PL	time-resolved photoluminescence
TTF	tetrathiafulvalene
TTFTB	tetrathiafulvalene tetrabenzoate
UIO	University of Oslo
XTA	X-ray transient absorption spectroscopy
ZIF	Zeolitic Imidazolate Framework

References

(1) Li, H.; Eddaoudi, M.; O'Keeffe, M.; Yaghi, O. M. Design and Synthesis of an Exceptionally Stable and Highly Porous Metal-Organic Framework. *Nature* **1999,** *402*, 276-279.

(2) Zhou, H.-C.; Long, J. R.; Yaghi, O. M. Introduction to Metal–Organic Frameworks. *Chem. Rev.* **2012,** *112*, 673-674.

(3) Yuan, S.; Feng, L.; Wang, K.; Pang, J.; Bosch, M.; Lollar, C.; Sun, Y.; Qin, J.; Yang, X.; Zhang, P.et al. Stable Metal–Organic Frameworks: Design, Synthesis, and Applications. *Adv. Mater* **2018,** *30*, 1704303-1704338.

(4) Yaghi, O. M.; O'Keeffe, M.; Ockwig, N. W.; Chae, H. K.; Eddaoudi, M.; Kim, J. Reticular Synthesis and the Design of New Materials. *Nature* **2003,** *423*, 705-714.

(5) Li, M.; Li, D.; O'Keeffe, M.; Yaghi, O. M. Topological Analysis of Metal–Organic Frameworks with Polytopic Linkers and/or Multiple Building Units and the Minimal Transitivity Principle. *Chem. Rev.* **2014,** *114*, 1343-1370.

(6) Qin, J.-S.; Yuan, S.; Wang, Q.; Alsalme, A.; Zhou, H.-C. Mixed-Linker Strategy for the Construction of Multifunctional Metal–Organic Frameworks. *J. Mater. Chem. A* **2017,** *5*, 4280-4291.

(7) Wang, Q.; Astruc, D. State of the Art and Prospects in Metal–Organic Framework (Mof)-Based and Mof-Derived Nanocatalysis. *Chem. Rev.* **2020,** *120*, 1438-1511.

(8) Baumann, A. E.; Burns, D. A.; Liu, B.; Thoi, V. S. Metal-Organic Framework Functionalization and Design Strategies for Advanced Electrochemical Energy Storage Devices. *Commun. Chem.* **2019,** *2*, 86-100.

(9) Stavila, V.; Talin, A. A.; Allendorf, M. D. Mof-Based Electronic and Opto-Electronic Devices. *Chem. Soc. Rev.* **2014,** *43*, 5994-6010.

(10) Zhang, T.; Jin, Y.; Shi, Y.; Li, M.; Li, J.; Duan, C. Modulating Photoelectronic Performance of Metal–Organic Frameworks for Premium Photocatalysis. *Coord. Chem. Rev.* **2019,** *380*, 201-229.

(11) Santaclara, J. G.; Kapteijn, F.; Gascon, J.; van der Veen, M. A. Understanding Metal–Organic Frameworks for Photocatalytic Solar Fuel Production. *CrystEngComm* **2017,** *19*, 4118-4125.

(12) So, M. C.; Wiederrecht, G. P.; Mondloch, J. E.; Hupp, J. T.; Farha, O. K. Metal–Organic Framework Materials for Light-Harvesting and Energy Transfer. *Chem. Commun.* **2015,** *51*, 3501-3510.

(13) Butler, K. T.; Hendon, C. H.; Walsh, A. Electronic Structure Modulation of Metal–Organic Frameworks for Hybrid Devices. *ACS Appl. Mater. Interfaces* **2014,** *6*, 22044-22050.
(14) Park, K. S.; Ni, Z.; Côté, A. P.; Choi, J. Y.; Huang, R.; Uribe-Romo, F. J.; Chae, H. K.; O'Keeffe, M.; Yaghi, O. M. Exceptional Chemical and Thermal Stability of Zeolitic Imidazolate Frameworks. *Proc. Natl. Acad. Sci.* **2006,** *103*, 10186-10191.
(15) Dan-Hardi, M.; Serre, C.; Frot, T.; Rozes, L.; Maurin, G.; Sanchez, C.; Férey, G. A New Photoactive Crystalline Highly Porous Titanium(Iv) Dicarboxylate. *J. Am. Chem. Soc.* **2009,** *131*, 10857-10859.
(16) Yang, L.-M.; Fang, G.-Y.; Ma, J.; Ganz, E.; Han, S. S. Band Gap Engineering of Paradigm Mof-5. *Cryst. Growth Des.* **2014,** *14*, 2532-2541.
(17) Yang, L.-M.; Fang, G.-Y.; Ma, J.; Pushpa, R.; Ganz, E. Halogenated Mof-5 Variants Show New Configuration, Tunable Band Gaps and Enhanced Optical Response in the Visible and near Infrared. *Phys. Chem. Chem. Phys.* **2016,** *18*, 32319-32330.
(18) Banerjee, R.; Phan, A.; Wang, B.; Knobler, C.; Furukawa, H.; O'Keeffe, M.; Yaghi, O. M. High-Throughput Synthesis of Zeolitic Imidazolate Frameworks and Application to Co2 Capture. *Science* **2008,** *319*, 939-943.
(19) Grau-Crespo, R.; Aziz, A.; Collins, A. W.; Crespo-Otero, R.; Hernández, N. C.; Rodriguez-Albelo, L. M.; Ruiz-Salvador, A. R.; Calero, S.; Hamad, S. Modelling a Linker Mix-and-Match Approach for Controlling the Optical Excitation Gaps and Band Alignment of Zeolitic Imidazolate Frameworks. *Angew. Chem., Int. Ed.* **2016,** *55*, 16012-16016.
(20) Butler, K. T.; Worrall, S. D.; Molloy, C. D.; Hendon, C. H.; Attfield, M. P.; Dryfe, R. A. W.; Walsh, A. Electronic Structure Design for Nanoporous, Electrically Conductive Zeolitic Imidazolate Frameworks. *J. Mater. Chem. C* **2017,** *5*, 7726-7731.
(21) Pattengale, B.; Yang, S. Z.; Ludwig, J.; Huang, Z. Q.; Zhang, X. Y.; Huang, J. Exceptionally Long-Lived Charge Separated State in Zeolitic Imidazolate Framework: Implication for Photocatalytic Applications. *J. Am. Chem. Soc.* **2016,** *138*, 8072-8075.
(22) Fu, Y.; Sun, D.; Chen, Y.; Huang, R.; Ding, Z.; Fu, X.; Li, Z. An Amine-Functionalized Titanium Metal–Organic Framework Photocatalyst with Visible-Light-Induced Activity for Co2 Reduction. *Angew. Chem., Int. Ed.* **2012,** *51*, 3364-3367.
(23) Hendon, C. H.; Tiana, D.; Fontecave, M.; Sanchez, C.; D'arras, L.; Sassoye, C.; Rozes, L.; Mellot-Draznieks, C.; Walsh, A. Engineering the Optical Response of the Titanium-Mil-125 Metal–Organic Framework through Ligand Functionalization. *J. Am. Chem. Soc.* **2013,** *135*, 10942-10945.
(24) Nasalevich, M. A.; Goesten, M. G.; Savenije, T. J.; Kapteijn, F.; Gascon, J. Enhancing Optical Absorption of Metal–Organic Frameworks for Improved Visible Light Photocatalysis. *Chem. Commun.* **2013,** *49*, 10575-10577.
(25) Song, T.; Yu, J.; Cui, Y.; Yang, Y.; Qian, G. Encapsulation of Dyes in Metal–Organic Frameworks and Their Tunable Nonlinear Optical Properties. *Dalton Trans.* **2016,** *45*, 4218-4223.
(26) Lu, G.; Li, S.; Guo, Z.; Farha, O. K.; Hauser, B. G.; Qi, X.; Wang, Y.; Wang, X.; Han, S.; Liu, X.et al. Imparting Functionality to a Metal–Organic Framework Material by Controlled Nanoparticle Encapsulation. *Nature Chem.* **2012,** *4*, 310-316.
(27) Dolgopolova, E. A.; Berseneva, A. A.; Faillace, M. S.; Ejegbavwo, O. A.; Leith, G. A.; Choi, S. W.; Gregory, H. N.; Rice, A. M.; Smith, M. D.; Chruszcz, M.et al. Confinement-Driven Photophysics in Cages, Covalent−Organic Frameworks, Metal–Organic Frameworks, and DNA. *J. Am. Chem. Soc.* **2020,** *142*, 4769-4783.
(28) Dolgopolova, E. A.; Moore, T. M.; Ejegbavwo, O. A.; Pellechia, P. J.; Smith, M. D.; Shustova, N. B. A Metal–Organic Framework as a Flask: Photophysics of Confined Chromophores with a Benzylidene Imidazolinone Core. *Chem. Commun.* **2017,** *53*, 7361-7364.

(29) Wang, C.; Xie, Z.; deKrafft, K. E.; Lin, W. Doping Metal–Organic Frameworks for Water Oxidation, Carbon Dioxide Reduction, and Organic Photocatalysis. *J. Am. Chem. Soc.* **2011,** *133*, 13445-13454.
(30) Feng, D.; Gu, Z.-Y.; Li, J.-R.; Jiang, H.-L.; Wei, Z.; Zhou, H.-C. Zirconium-Metalloporphyrin Pcn-222: Mesoporous Metal–Organic Frameworks with Ultrahigh Stability as Biomimetic Catalysts. *Angew. Chem., Int. Ed.* **2012,** *51*, 10307-10310.
(31) Feng, D.; Chung, W.-C.; Wei, Z.; Gu, Z.-Y.; Jiang, H.-L.; Chen, Y.-P.; Darensbourg, D. J.; Zhou, H.-C. Construction of Ultrastable Porphyrin Zr Metal–Organic Frameworks through Linker Elimination. *J. Am. Chem. Soc.* **2013,** *135*, 17105-17110.
(32) Manzoni, C.; Cerullo, G. Design Criteria for Ultrafast Optical Parametric Amplifiers. *J. Opt.* **2016,** *18*, 103501-103533.
(33) Neu, J.; Rahm, M. Terahertz Time Domain Spectroscopy for Carrier Lifetime Mapping in the Picosecond to Microsecond Regime. *Opt. Express* **2015,** *23*, 12900-12909.
(34) Barker, A. J.; Chen, K.; Hodgkiss, J. M. Distance Distributions of Photogenerated Charge Pairs in Organic Photovoltaic Cells. *J Am Chem Soc* **2014,** *136*, 12018-12026.
(35) Gerecke, M.; Bierhance, G.; Gutmann, M.; Ernsting, N. P.; Rosspeintner, A. Femtosecond Broadband Fluorescence Upconversion Spectroscopy: Spectral Coverage Versus Efficiency. *Rev. Sci. Instrum.* **2016,** *87*, 053115-053120.
(36) Berera, R.; van Grondelle, R.; Kennis, J. T. M. Ultrafast Transient Absorption Spectroscopy: Principles and Application to Photosynthetic Systems. *Photosynth. Res.* **2009,** *101*, 105-118.
(37) Alfano, R. R.; Shapiro, S. L. Emission in the Region 4000 to 7000 Å Via Four-Photon Coupling in Glass. *Phys. Rev. Lett.* **1970,** *24*, 584-587.
(38) Brodeur, A.; Chin, S. L. Ultrafast White-Light Continuum Generation and Self-Focusing in Transparent Condensed Media. *J. Opt. Soc. Am. B* **1999,** *16*, 637-650.
(39) Chen, M. C.; Arpin, P.; Popmintchev, T.; Gerrity, M.; Zhang, B.; Seaberg, M.; Popmintchev, D.; Murnane, M. M.; Kapteyn, H. C. Bright, Coherent, Ultrafast Soft X-Ray Harmonics Spanning the Water Window from a Tabletop Light Source. *Phys. Rev. Lett.* **2010,** *105*, 173901-173904.
(40) Huang, Z.; Lindau, I. Sacla Hard-X-Ray Compact Fel. *Nat. Photonics* **2012,** *6*, 505-506.
(41) Chollet, M.; Alonso-Mori, R.; Cammarata, M.; Damiani, D.; Defever, J.; Delor, J. T.; Feng, Y.; Glownia, J. M.; Langton, J. B.; Nelson, S.et al. The X-Ray Pump-Probe Instrument at the Linac Coherent Light Source. *J. Synchrotron Radiat.* **2015,** *22*, 503-507.
(42) Chen, L. X.; Zhang, X. Photochemical Processes Revealed by X-Ray Transient Absorption Spectroscopy. *J. Phys. Chem. Lett.* **2013,** *4*, 4000-4013.
(43) Pattengale, B.; Neu, J.; Tada, A.; Hu, G.; Karpovich, C. J.; Brudvig, G. W. Cation-Exchanged Conductive Mn_2DSBDC Metal–Organic Frameworks: Synthesis, Structure, and Thz Conductivity. *Polyhedron* **2021,** *203,* 185112-185122.
(44) Pattengale, B.; Liu, Q.; Hu, W.; Yang, S.; He, P.; Tender, S. L.; Wang, Y.; Zhang, X.; Zhou, Z.; Zhang, J.et al. Selective Excited-State Dynamics in a Unique Set of Rationally Designed Ni Porphyrins. *J. Phys. Chem. C* **2019,** *123*, 17994-18000.
(45) Mara, M. W.; Fransted, K. A.; Chen, L. X. Interplays of Excited State Structures and Dynamics in Copper(I) Diimine Complexes: Implications and Perspectives. *Coord. Chem. Rev.* **2015,** *282-283*, 2-18.
(46) Hunt, N. T. 2d-Ir Spectroscopy: Ultrafast Insights into Biomolecule Structure and Function. *Chem. Soc. Rev.* **2009,** *38*, 1837-1848.
(47) Zheng, J.; Kwak, K.; Fayer, M. D. Ultrafast 2d Ir Vibrational Echo Spectroscopy. *Acc. Chem. Res.* **2007,** *40*, 75-83.
(48) Ryder, M. R.; Civalleri, B.; Bennett, T. D.; Henke, S.; Rudić, S.; Cinque, G.; Fernandez-Alonso, F.; Tan, J.-C. Identifying the Role of Terahertz Vibrations in Metal-Organic Frameworks: From Gate-

Opening Phenomenon to Shear-Driven Structural Destabilization. *Phys. Rev. Lett.* **2014,** *113*, 215502.
(49) Neu, J.; Schmuttenmaer, C. A. Tutorial: An Introduction to Terahertz Time Domain Spectroscopy (THz-TDS). *J. Appl. Phys.* **2018,** *124*, 231101-231114.
(50) Beard, M. C.; Turner, G. M.; Schmuttenmaer, C. A. Transient Photoconductivity in Gaas as Measured by Time-Resolved Terahertz Spectroscopy. *Phys. Rev. B* **2000,** *62*, 15764-15777.
(51) Zarifi, M. H.; Mohammadpour, A.; Farsinezhad, S.; Wiltshire, B. D.; Nosrati, M.; Askar, A. M.; Daneshmand, M.; Shankar, K. Time-Resolved Microwave Photoconductivity (Trmc) Using Planar Microwave Resonators: Application to the Study of Long-Lived Charge Pairs in Photoexcited Titania Nanotube Arrays. *J. Phys. Chem. C* **2015,** *119*, 14358-14365.
(52) Bai, S.; Zhang, P.; Antoniou, P.; Skourtis, S. S.; Beratan, D. N. Quantum Interferences among Dexter Energy Transfer Pathways. *Faraday Discuss.* **2019,** *216*, 301-318.
(53) Zhu, J.; Shaikh, S.; Mayhall, N. J.; Morris, A. J. In *Elaboration and Applications of Metal-Organic Frameworks*, World Scientific, 2018, 1-732.
(54) Kent, C. A.; Liu, D.; Ma, L.; Papanikolas, J. M.; Meyer, T. J.; Lin, W. Light Harvesting in Microscale Metal–Organic Frameworks by Energy Migration and Interfacial Electron Transfer Quenching. *J. Am. Chem. Soc.* **2011,** *133*, 12940-12943.
(55) Choi, J. R.; Tachikawa, T.; Fujitsuka, M.; Majima, T. Europium-Based Metal–Organic Framework as a Photocatalyst for the One-Electron Oxidation of Organic Compounds. *Langmuir* **2010,** *26*, 10437-10443.
(56) Kent, C. A.; Liu, D.; Ito, A.; Zhang, T.; Brennaman, M. K.; Meyer, T. J.; Lin, W. Rapid Energy Transfer in Non-Porous Metal–Organic Frameworks with Caged Ru(Bpy)32+ Chromophores: Oxygen Trapping and Luminescence Quenching. *J. Mater. Chem. A* **2013,** *1*, 14982-14989.
(57) Cavka, J. H.; Jakobsen, S.; Olsbye, U.; Guillou, N.; Lamberti, C.; Bordiga, S.; Lillerud, K. P. A New Zirconium Inorganic Building Brick Forming Metal Organic Frameworks with Exceptional Stability. *J. Am. Chem. Soc.* **2008,** *130*, 13850-13851.
(58) Bock, C. R.; Connor, J. A.; Gutierrez, A. R.; Meyer, T. J.; Whitten, D. G.; Sullivan, B. P.; Nagle, J. K. Estimation of Excited-State Redox Potentials by Electron-Transfer Quenching. Application of Electron-Transfer Theory to Excited-State Redox Processes. *J. Am. Chem. Soc.* **2002,** *101*, 4815-4824.
(59) Maza, W. A.; Padilla, R.; Morris, A. J. Concentration Dependent Dimensionality of Resonance Energy Transfer in a Postsynthetically Doped Morphologically Homologous Analogue of Uio-67 Mof with a Ruthenium(Ii) Polypyridyl Complex. *J. Am. Chem. Soc.* **2015,** *137*, 8161-8168.
(60) Maza, W. A.; Morris, A. J. Photophysical Characterization of a Ruthenium(Ii) Tris(2,2′-Bipyridine)-Doped Zirconium Uio-67 Metal–Organic Framework. *J. Phys. Chem. C* **2014,** *118*, 8803-8817.
(61) Lin, J.; Hu, X.; Zhang, P.; Van Rynbach, A.; Beratan, D. N.; Kent, C. A.; Mehl, B. P.; Papanikolas, J. M.; Meyer, T. J.; Lin, W.et al. Triplet Excitation Energy Dynamics in Metal–Organic Frameworks. *J. Phys. Chem. C* **2013,** *117*, 22250-22259.
(62) Kent, C. A.; Mehl, B. P.; Ma, L.; Papanikolas, J. M.; Meyer, T. J.; Lin, W. Energy Transfer Dynamics in Metal-Organic Frameworks. *J. Am. Chem. Soc.* **2010,** *132*, 12767-12769.
(63) Lee, C. Y.; Farha, O. K.; Hong, B. J.; Sarjeant, A. A.; Nguyen, S. T.; Hupp, J. T. Light-Harvesting Metal–Organic Frameworks (Mofs): Efficient Strut-to-Strut Energy Transfer in Bodipy and Porphyrin-Based Mofs. *J. Am. Chem. Soc.* **2011,** *133*, 15858-15861.
(64) Son, H. J.; Jin, S.; Patwardhan, S.; Wezenberg, S. J.; Jeong, N. C.; So, M.; Wilmer, C. E.; Sarjeant, A. A.; Schatz, G. C.; Snurr, R. Q.et al. Light-Harvesting and Ultrafast Energy Migration in Porphyrin-Based Metal-Organic Frameworks. *J. Am. Chem. Soc.* **2013,** *135*, 862-869.
(65) Adams, M.; Kozlowska, M.; Baroni, N.; Oldenburg, M.; Ma, R.; Busko, D.; Turshatov, A.; Emandi, G.; Senge, M. O.; Haldar, R.et al. Highly Efficient One-Dimensional Triplet Exciton Transport in a

Palladium–Porphyrin-Based Surface-Anchored Metal–Organic Framework. *ACS Appl. Mater. Interfaces* **2019,** *11*, 15688-15697.

(66) Li, X.; Gurzadyan, G. G.; Gelin, M. F.; Domcke, W.; Gong, C.; Liu, J.; Sun, L. Enhanced S2 Fluorescence from a Free-Base Tetraphenylporphyrin Surface-Mounted Metal Organic Framework. *J. Phys. Chem. C* **2018,** *122*, 23321-23328.

(67) Li, X. X.; Gong, C. H.; Gurzadyan, G. G.; Gelin, M. F.; Liu, J. X.; Sun, L. C. Ultrafast Relaxation Dynamics in Zinc Tetraphenylporphyrin Surface-Mounted Metal Organic Framework. *J. Phys. Chem. C* **2018,** *122*, 50-61.

(68) Shaikh, Shaunak M.; Chakraborty, A.; Alatis, J.; Cai, M.; Danilov, E.; Morris, A. J. Light Harvesting and Energy Transfer in a Porphyrin-Based Metal Organic Framework. *Faraday Discuss.* **2019,** *216*, 174-190.

(69) Li, X.; Yu, J.; Gosztola, D. J.; Fry, H. C.; Deria, P. Wavelength-Dependent Energy and Charge Transfer in Mof: A Step toward Artificial Porous Light-Harvesting System. *J. Am. Chem. Soc.* **2019,** *141*, 16849-16857.

(70) Van Wyk, A.; Smith, T.; Park, J.; Deria, P. Charge-Transfer within Zr-Based Metal–Organic Framework: The Role of Polar Node. *J. Am. Chem. Soc.* **2018,** *140*, 2756-2760.

(71) Yu, J.; Park, J.; Van Wyk, A.; Rumbles, G.; Deria, P. Excited-State Electronic Properties in Zr-Based Metal–Organic Frameworks as a Function of a Topological Network. *J. Am. Chem. Soc.* **2018,** *140*, 10488-10496.

(72) Gutierrez, M.; Sanchez, F.; Douhal, A. Competitive Excimer Formation and Energy Transfer in Zr-Based Heterolinker Metal-Organic Frameworks. *Chem. Eur. J.* **2016,** *22*, 13072-13082.

(73) Gutierrez, M.; Cohen, B.; Sanchez, F.; Douhal, A. Photochemistry of Zr-Based Mofs: Ligand-to-Cluster Charge Transfer, Energy Transfer and Excimer Formation, What Else Is There? *Phys. Chem. Chem. Phys.* **2016,** *18*, 27761-27774.

(74) Caballero-Mancebo, E.; Cohen, B.; Moreno, J. M.; Corma, A.; Diaz, U.; Douhal, A. Exploring the Photodynamics of a New 2d-Mof Composite: Nile Red@Al-Itq-Hb. *Acs Omega* **2018,** *3*, 1600-1608.

(75) Deria, P.; Yu, J.; Smith, T.; Balaraman, R. P. Ground-State Versus Excited-State Interchromophoric Interaction: Topology Dependent Excimer Contribution in Metal–Organic Framework Photophysics. *J. Am. Chem. Soc.* **2017,** *139*, 5973-5983.

(76) Capano, G.; Ambrosio, F.; Kampouri, S.; Stylianou, K. C.; Pasquarello, A.; Smit, B. On the Electronic and Optical Properties of Metal–Organic Frameworks: Case Study of Mil-125 and Mil-125-Nh2. *J. Phys. Chem. C* **2020,** *124*, 4065-4072.

(77) de Miguel, M.; Ragon, F.; Devic, T.; Serre, C.; Horcajada, P.; García, H. Evidence of Photoinduced Charge Separation in the Metal–Organic Framework Mil-125(Ti)-Nh2. *ChemPhysChem* **2012,** *13*, 3651-3654.

(78) Santaclara, J. G.; Nasalevich, M. A.; Castellanos, S.; Evers, W. H.; Spoor, F. C. M.; Rock, K.; Siebbeles, L. D. A.; Kapteijn, F.; Grozema, F.; Houtepen, A.et al. Organic Linker Defines the Excited-State Decay of Photocatalytic Mil-125(Ti)-Type Materials. *ChemSusChem* **2016,** *9*, 388-395.

(79) Nasalevich, M. A.; Hendon, C. H.; Santaclara, J. G.; Svane, K.; van der Linden, B.; Veber, S. L.; Fedin, M. V.; Houtepen, A. J.; van der Veen, M. A.; Kapteijn, F.et al. Electronic Origins of Photocatalytic Activity in D0 Metal Organic Frameworks. *Sci. Rep.* **2016,** *6*, 23676-23685.

(80) Santaclara, J. G.; Olivos-Suarez, A. I.; du Fossé, I.; Houtepen, A.; Hunger, J.; Kapteijn, F.; Gascon, J.; van der Veen, M. A. Harvesting the Photoexcited Holes on a Photocatalytic Proton Reduction Metal–Organic Framework. *Faraday Discuss.* **2017,** *201*, 71-86.

(81) Wang, D.; Albero, J.; García, H.; Li, Z. Visible-Light-Induced Tandem Reaction of O-Aminothiophenols and Alcohols to Benzothiazoles over Fe-Based Mofs: Influence of the Structure Elucidated by Transient Absorption Spectroscopy. *J. Catal.* **2017,** *349*, 156-162.
(82) Guo, F.; Yang, S.; Liu, Y.; Wang, P.; Huang, J.; Sun, W.-Y. Size Engineering of Metal–Organic Framework Mil-101(Cr)–Ag Hybrids for Photocatalytic Co2 Reduction. *ACS Catal.* **2019,** *9*, 8464-8470.
(83) Chen, X.; Xiao, S.; Wang, H.; Wang, W.; Cai, Y.; Li, G.; Qiao, M.; Zhu, J.; Li, H.; Zhang, D.et al. Mofs Conferred with Transient Metal Centers for Enhanced Photocatalytic Activity. *Angew. Chem., Int. Ed.* **2020,** *59*, 17182-17186.
(84) Deng, X. Y.; Albero, J.; Xu, L. Z.; Garcia, H.; Li, Z. H. Construction of a Stable Ru-Re Hybrid System Based on Multifunctional Mof-253 for Efficient Photocatalytic Co2 Reduction. *Inorg. Chem.* **2018,** *57*, 8276-8286.
(85) Goswami, S.; Miller, C. E.; Logsdon, J. L.; Buru, C. T.; Wu, Y.-L.; Bowman, D. N.; Islamoglu, T.; Asiri, A. M.; Cramer, C. J.; Wasielewski, M. R.et al. Atomistic Approach toward Selective Photocatalytic Oxidation of a Mustard-Gas Simulant: A Case Study with Heavy-Chalcogen-Containing Pcn-57 Analogues. *ACS Appl. Mater. Interfaces* **2017,** *9*, 19535-19540.
(86) Xu, H.-Q.; Hu, J.; Wang, D.; Li, Z.; Zhang, Q.; Luo, Y.; Yu, S.-H.; Jiang, H.-L. Visible-Light Photoreduction of Co2 in a Metal–Organic Framework: Boosting Electron–Hole Separation Via Electron Trap States. *J. Am. Chem. Soc.* **2015,** *137*, 13440-13443.
(87) Yan, Z. H.; Du, M. H.; Liu, J. X.; Jin, S. Y.; Wang, C.; Zhuang, G. L.; Kong, X. J.; Long, L. S.; Zheng, L. S. Photo-Generated Dinuclear {Eu(Ii)}(2) Active Sites for Selective Co2 Reduction in a Photosensitizing Metal-Organic Framework. *Nat. Commun.* **2018,** *9*.
(88) Yang, S.; Pattengale, B.; Lee, S.; Huang, J. Real-Time Visualization of Active Species in a Single-Site Metal–Organic Framework Photocatalyst. *ACS Energy Lett.* **2018,** *3*, 532-539.
(89) Zeng, L. Z.; Wang, Z. Y.; Wang, Y. K.; Wang, J.; Guo, Y.; Hu, H. H.; He, X. F.; Wang, C.; Lin, W. B. Photoactivation of Cu Centers in Metal-Organic Frameworks for Selective Co2 Conversion to Ethanol. *J. Am. Chem. Soc.* **2020,** *142*, 75-79.
(90) Liu, J.; Jiang, S.-l.; Zhang, Q. Doping Copper Ions in a Metal-Organic Framework (Uio-66-Nh2): Location Effect Examined by Ultrafast Spectroscopy. *Chin. J. Chem. Phys.* **2020,** *33*, 394-400.
(91) Gutiérrez, L.; Mondal, S. S.; Bucci, A.; Kandoth, N.; Escudero-Adán, E. C.; Shafir, A.; Lloret-Fillol, J. Crystal-to-Crystal Synthesis of Photocatalytic Metal–Organic Frameworks for Visible-Light Reductive Coupling and Mechanistic Investigations. *ChemSusChem* **2020,** *13*, 3418-3428.
(92) Wei, Y.-P.; Yang, S.; Wang, P.; Guo, J.-H.; Huang, J.; Sun, W.-Y. Iron(Iii)-Bipyridine Incorporated Metal–Organic Frameworks for Photocatalytic Reduction of Co2 with Improved Performance. *Dalton Trans.* **2021,** *50*, 384-390.
(93) Mahringer, A.; Jakowetz, A. C.; Rotter, J. M.; Bohn, B. J.; Stolarczyk, J. K.; Feldman, J.; Bein, T.; Medina, D. D. Oriented Thin Films of Electroactive Triphenylene Catecholate-Based Two-Dimensional Metal-Organic Frameworks. *Acs Nano* **2019,** *13*, 6711-6719.
(94) Santiago Portillo, A.; Baldoví, H. G.; García Fernandez, M. T.; Navalón, S.; Atienzar, P.; Ferrer, B.; Alvaro, M.; Garcia, H.; Li, Z. Ti as Mediator in the Photoinduced Electron Transfer of Mixed-Metal Nh2–Uio-66(Zr/Ti): Transient Absorption Spectroscopy Study and Application in Photovoltaic Cell. *J. Phys. Chem. C* **2017,** *121*, 7015-7024.
(95) Milichko, V. A.; Makarov, S. V.; Yulin, A. V.; Vinogradov, A. V.; Krasilin, A. A.; Ushakova, E.; Dzyuba, V. P.; Hey-Hawkins, E.; Pidko, E. A.; Belov, P. A. Van Der Waals Metal-Organic Framework as an Excitonic Material for Advanced Photonics. *Adv. Mater* **2017,** *29*.
(96) Pattengale, B.; Freeze, J. G.; Guberman-Pfeffer, M. J.; Okabe, R.; Ostresh, S.; Chaudhuri, S.; Batista, V. S.; Schmuttenmaer, C. A. A Conductive Metal–Organic Framework Photoanode. *Chem. Sci.* **2020,** *11*, 9593-9603.

(97) Eads, C. N.; Bandak, D.; Neupane, M. R.; Nordlund, D.; Monti, O. L. A. Anisotropic Attosecond Charge Carrier Dynamics and Layer Decoupling in Quasi-2d Layered Sns2. *Nat. Commun.* **2017,** *8*, 1369.

(98) Pattengale, B.; Huang, J. Photoinduced Interfacial Charge Separation Dynamics in Zeolitic Imidazolate Framework. *Phys. Chem. Chem. Phys.* **2018,** *20*, 14884-14888.

(99) Yang, S.; Pattengale, B.; Kovrigin, E. L.; Huang, J. Photoactive Zeolitic Imidazolate Framework as Intrinsic Heterogeneous Catalysts for Light-Driven Hydrogen Generation. *ACS Energy Lett.* **2017,** *2*, 75-80.

(100) Pattengale, B.; SantaLucia, D. J.; Yang, S.; Hu, W.; Liu, C.; Zhang, X.; Berry, J. F.; Huang, J. Direct Observation of Node-to-Node Communication in Zeolitic Imidazolate Frameworks. *J. Am. Chem. Soc.* **2018,** *140*, 11573-11576.

(101) Hanna, L.; Kucheryavy, P.; Liu, C.; Zhang, X.; Lockard, J. V. Long-Lived Photoinduced Charge Separation in a Trinuclear Iron-M3-Oxo-Based Metal–Organic Framework. *J. Phys. Chem. C* **2017,** *121*, 13570-13576.

(102) Hanna, L.; Long, C. L.; Zhang, X.; Lockard, J. V. Heterometal Incorporation in Nh2-Mil-125(Ti) and Its Participation in the Photoinduced Charge-Separated Excited State. *Chem. Commun.* **2020,** *56*, 11597-11600.

(103) García-Sánchez, A.; Gomez-Mendoza, M.; Barawi, M.; Villar-Garcia, I. J.; Liras, M.; Gándara, F.; de la Peña O'Shea, V. A. Fundamental Insights into Photoelectrocatalytic Hydrogen Production with a Hole-Transport Bismuth Metal–Organic Framework. *J. Am. Chem. Soc.* **2020,** *142*, 318-326.

(104) Yang, S.; Hu, W.; Nyakuchena, J.; Fiankor, C.; Liu, C.; Kinigstein, E. D.; Zhang, J.; Zhang, X.; Huang, J. Unravelling the Long-Lived Ligand-to-Metal Cluster Charge Transfer State in Ce-Tcpp Metal Organic Frameworks. *Chem. Commun.* **2020,** *56*, 13971-13974.

(105) Yang, S.; Fan, D.; Hu, W.; Pattengale, B.; Liu, C.; Zhang, X.; Huang, J. Elucidating Charge Separation Dynamics in a Hybrid Metal–Organic Framework Photocatalyst for Light-Driven H2 Evolution. *J. Phys. Chem. C* **2018,** *122*, 3305-3311.

(106) Xie, L. S.; Skorupskii, G.; Dincă, M. Electrically Conductive Metal–Organic Frameworks. *Chem. Rev.* **2020,** *120*, 8536-8580.

(107) Sun, L.; Campbell, M. G.; Dincă, M. Electrically Conductive Porous Metal–Organic Frameworks. *Angew. Chem., Int. Ed.* **2016,** *55*, 3566-3579.

(108) Ko, M.; Mendecki, L.; Mirica, K. A. Conductive Two-Dimensional Metal–Organic Frameworks as Multifunctional Materials. *Chem. Commun.* **2018,** *54*, 7873-7891.

(109) Sun, L.; Miyakai, T.; Seki, S.; Dincă, M. Mn2(2,5-Disulfhydrylbenzene-1,4-Dicarboxylate): A Microporous Metal–Organic Framework with Infinite (−Mn–S−)∞ Chains and High Intrinsic Charge Mobility. *J. Am. Chem. Soc.* **2013,** *135*, 8185-8188.

(110) Sun, L.; Hendon, C. H.; Minier, M. A.; Walsh, A.; Dincă, M. Million-Fold Electrical Conductivity Enhancement in Fe2(Debdc) Versus Mn2(Debdc) (E = S, O). *J. Am. Chem. Soc.* **2015,** *137*, 6164-6167.

(111) Aubrey, M. L.; Wiers, B. M.; Andrews, S. C.; Sakurai, T.; Reyes-Lillo, S. E.; Hamed, S. M.; Yu, C.-J.; Darago, L. E.; Mason, J. A.; Baeg, J.-O.et al. Electron Delocalization and Charge Mobility as a Function of Reduction in a Metal–Organic Framework. *Nat. Mater.* **2018,** *17*, 625-632.

(112) Liu, J.; Zhou, W.; Liu, J.; Howard, I.; Kilibarda, G.; Schlabach, S.; Coupry, D.; Addicoat, M.; Yoneda, S.; Tsutsui, Y.et al. Photoinduced Charge-Carrier Generation in Epitaxial Mof Thin Films: High Efficiency as a Result of an Indirect Electronic Band Gap? *Angew. Chem., Int. Ed.* **2015,** *54*, 7441-7445.

(113) Narayan, T. C.; Miyakai, T.; Seki, S.; Dincă, M. High Charge Mobility in a Tetrathiafulvalene-Based Microporous Metal–Organic Framework. *J. Am. Chem. Soc.* **2012,** *134*, 12932-12935.

(114) Pattengale, B.; Neu, J.; Ostresh, S.; Hu, G. F.; Spies, J. A.; Okabe, R.; Brudvig, G. W.; Schmuttenmaer, C. A. Metal-Organic Framework Photoconductivity Via Time-Resolved Terahertz Spectroscopy. *J. Am. Chem. Soc.* **2019,** *141*, 9793-9797.
(115) Alberding, B.; Heilweil, E. *Time-Resolved Terahertz Spectroscopy of Electrically Conductive Metal-Organic Frameworks Doped with Redox Active Species*; SPIE, **2015,** *9567,* 1-11.
(116) Dong, R.; Han, P.; Arora, H.; Ballabio, M.; Karakus, M.; Zhang, Z.; Shekhar, C.; Adler, P.; Petkov, P. S.; Erbe, A.et al. High-Mobility Band-Like Charge Transport in a Semiconducting Two-Dimensional Metal–Organic Framework. *Nat. Mater.* **2018,** *17*, 1027-1032.
(117) Nyakuchena, J.; Ostresh, S.; Streater, D.; Pattengale, B.; Neu, J.; Fiankor, C.; Hu, W.; Kinigstein, E. D.; Zhang, J.; Zhang, X.et al. Direct Evidence of Photoinduced Charge Transport Mechanism in 2d Conductive Metal Organic Frameworks. *J. Am. Chem. Soc.* **2020,** *142*, 21050-21058.
(118) Park, J.; Hinckley, A. C.; Huang, Z.; Feng, D.; Yakovenko, A. A.; Lee, M.; Chen, S.; Zou, X.; Bao, Z. Synthetic Routes for a 2d Semiconductive Copper Hexahydroxybenzene Metal-Organic Framework. *J. Am. Chem. Soc.* **2018,** *140*, 14533-14537.
(119) Huang, J.; Huang, Z.; Jin, S.; Lian, T. Exciton Dissociation in Cdse Quantum Dots by Hole Transfer to Phenothiazine. *J. Phys. Chem. C* **2008,** *112*, 19734-19738.
(120) Grimaldi, G.; Geuchies, J. J.; van der Stam, W.; du Fossé, I.; Brynjarsson, B.; Kirkwood, N.; Kinge, S.; Siebbeles, L. D. A.; Houtepen, A. J. Spectroscopic Evidence for the Contribution of Holes to the Bleach of Cd-Chalcogenide Quantum Dots. *Nano Lett.* **2019,** *19*, 3002-3010.
(121) Zhang, C.; Do, T. N.; Ong, X.; Chan, Y.; Tan, H.-S. Understanding the Features in the Ultrafast Transient Absorption Spectra of Cdse Quantum Dots. *Chem. Phys.* **2016,** *481*, 157-164.
(122) Redfern, L. R.; Farha, O. K. Mechanical Properties of Metal–Organic Frameworks. *Chem. Sci.* **2019,** *10*, 10666-10679.
(123) Sheveleva, A. M.; Kolokolov, D. I.; Gabrienko, A. A.; Stepanov, A. G.; Gromilov, S. A.; Shundrina, I. K.; Sagdeev, R. Z.; Fedin, M. V.; Bagryanskaya, E. G. Structural Dynamics in a "Breathing" Metal–Organic Framework Studied by Electron Paramagnetic Resonance of Nitroxide Spin Probes. *J. Phys. Chem. Lett.* **2014,** *5*, 20-24.
(124) Blake, A. J.; Champness, N. R.; Easun, T. L.; Allan, D. R.; Nowell, H.; George, M. W.; Jia, J.; Sun, X.-Z. Photoreactivity Examined through Incorporation in Metal−Organic Frameworks. *Nat. Chem.* **2010,** *2*, 688-694.
(125) Nishida, J.; Tamimi, A.; Fei, H.; Pullen, S.; Ott, S.; Cohen, S. M.; Fayer, M. D. Structural Dynamics inside a Functionalized Metal–Organic Framework Probed by Ultrafast 2d Ir Spectroscopy. *Proc. Natl. Acad. Sci.* **2014,** *111*, 18442-18447.
(126) Nishida, J.; Fayer, M. D. Guest Hydrogen Bond Dynamics and Interactions in the Metal–Organic Framework Mil-53(Al) Measured with Ultrafast Infrared Spectroscopy. *J. Phys. Chem. C* **2017,** *121*, 11880-11890.
(127) Neu, J.; Stone, E. A.; Spies, J. A.; Storch, G.; Hatano, A. S.; Mercado, B. Q.; Miller, S. J.; Schmuttenmaer, C. A. Terahertz Spectroscopy of Tetrameric Peptides. *J. Phys. Chem. Lett.* **2019,** *10*, 2624-2628.
(128) Neu, J.; Nikonow, H.; Schmuttenmaer, C. A. Terahertz Spectroscopy and Density Functional Theory Calculations of Dl-Norleucine and Dl-Methionine. *J. Phys. Chem. A* **2018,** *122*, 5978-5982.
(129) Tan, N. Y.; Ruggiero, M. T.; Orellana-Tavra, C.; Tian, T.; Bond, A. D.; Korter, T. M.; Fairen-Jimenez, D.; Axel Zeitler, J. Investigation of the Terahertz Vibrational Modes of Zif-8 and Zif-90 with Terahertz Time-Domain Spectroscopy. *Chem. Commun.* **2015,** *51*, 16037-16040.
(130) Li, Q.; Zaczek, A. J.; Korter, T. M.; Zeitler, J. A.; Ruggiero, M. T. Methyl-Rotation Dynamics in Metal–Organic Frameworks Probed with Terahertz Spectroscopy. *Chem. Commun.* **2018,** *54*, 5776-5779.

(131) Zhang, W.; Maul, J.; Vulpe, D.; Moghadam, P. Z.; Fairen-Jimenez, D.; Mittleman, D. M.; Zeitler, J. A.; Erba, A.; Ruggiero, M. T. Probing the Mechanochemistry of Metal–Organic Frameworks with Low-Frequency Vibrational Spectroscopy. *J. Phys. Chem. C* **2018,** *122*, 27442-27450.
(132) Tanno, T.; Watanabe, Y.; Umeno, K.; Matsuoka, A.; Matsumura, H.; Odaka, M.; Ogawa, N. In Situ Observation of Gas Adsorption onto Zif-8 Using Terahertz Waves. *J. Phys. Chem. C* **2017,** *121*, 17921-17924.